WARMINGUP

Innovatief Duurzaam Warmtecollectief

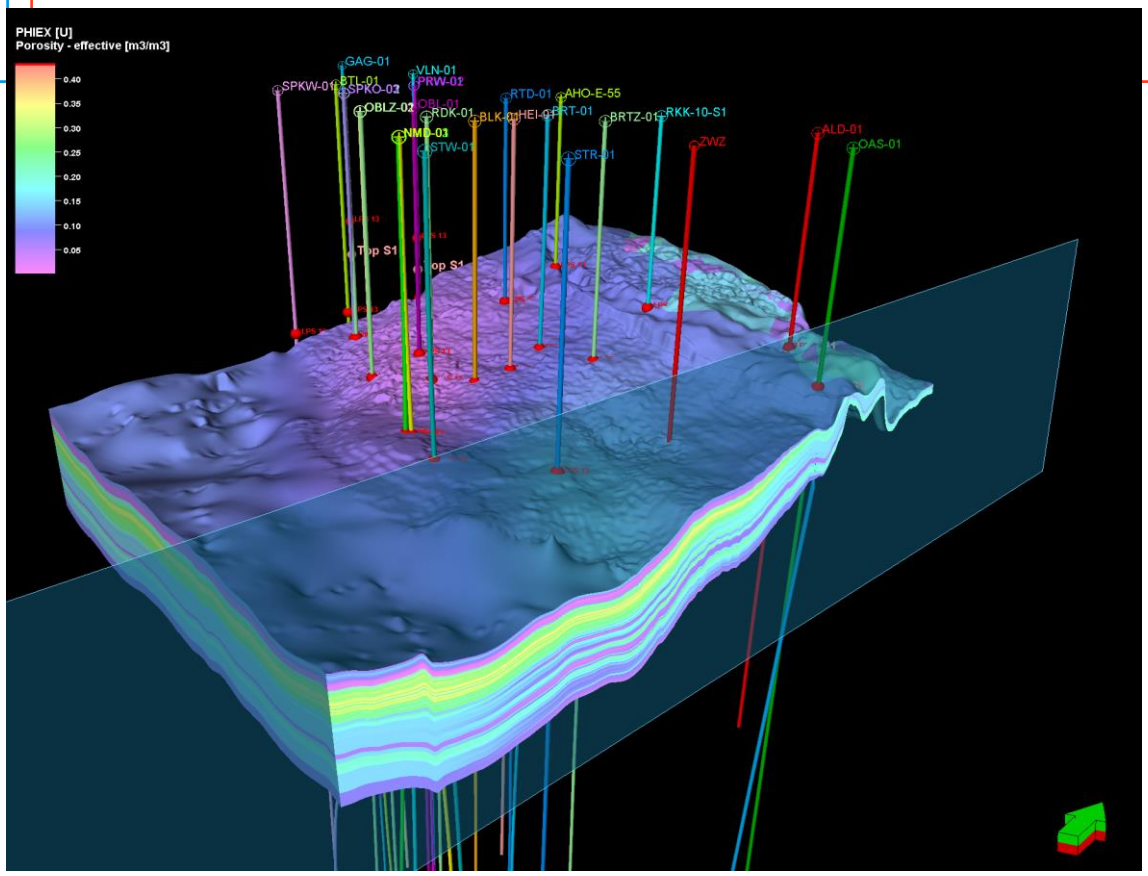

Characterisation and production of the Brussels Sand Member near Zwijndrecht Zuid

Characterisation and production of the Brussels Sand Member near Zwijndrecht Zuid

C.R. Geel, H.B. de Haan, E. Peters
25 mei 2022

Kwaliteitsborger
J.G. Veldkamp

Dit project is uitgevoerd als onderdeel van het Innovatieplan WarmingUP. Dit is mede mogelijk gemaakt door subsidie van de Rijksdienst voor Ondernemend Nederland (RVO) in het kader van de subsidieregeling Meerjarige Missiegedreven Innovatie Programma's (MMIP), bij RVO bekend onder projectnummer TEUE819001.
WarmingUP geeft invulling aan MMIP-4 – Duurzame warmte en koude in gebouwde omgeving en levert daarmee een bijdrage aan Missie B – Een CO_2-vrije gebouwde omgeving in 2050.

Projectnummer
060.43190/01.01.01

Keywords
Brussels Sand Mb, geological model, production simulation

Jaar van publicatie
2022

Meer informatie
Lies Peters
T +31611012687
E lies.peters@tno.nl

Inhoudsopgave

Samenvatting

In het WarmingUP-project wordt kennis ontwikkeld om collectieve warmtesystemen betrouwbaar, duurzaam en betaalbaar te maken. In Thema 4 van dit project, waar het gebruik van met name ondiepe en marginale geothermische bronnen als warmtebron voor stedelijke warmtenetten onderzocht wordt, worden drie regionale studies uitgevoerd. In dit rapport worden de resultaten van een van de drie regionale studies beschreven, namelijk van het Zand van Brussel Laagpakket (ZBL) uit het Eoceen in de regio Zwijndrecht. De verwachting is dat het ZBL hier goed ontwikkeld is

Om de reservoireigenschappen te schatten is een reservoirmodel gebouwd van 44 x 33 km. Voor de diepte en dikte van het ZBL is gebruik gemaakt van de opnieuw geprocesste Donkersloot seismische survey. The top van het ZBL is geïnterpreteerd op een “hard kick” (een toename in de akoestische impedantie), die de overgang tussen de schalies van de Asse Member en de top van het ZBL representeert. De top van het ZBL bevat veel dunne, massieve, calciet-gecementeerde lagen met een hoge akoestische snelheid. Een tweede, minder geprononceerde toename in de akoestische impedantie is geïnterpreteerd als de top van de onderste van drie “coarsening-up” sequenties in het ZBL (S1). De twee horizons zijn gefit aan de putten en gebruikt als input-oppervlakken voor het model. In de seismische survey zijn geen breuken gezien met een verzet groter dan de seismische resolutie en dus zijn er geen breuken meegenomen in het model. Het is onderzocht of in de seismische attributen een variatie in de aanwezigheid van de calciet-gecementeerde lagen te zien is, maar dit was niet het geval.

Op basis van de data van 37 putten is een stratigrafische onderverdeling gemaakt en een gedetailleerd reservoir model gecreëerd. Er zijn twee versies gemaakt: een grof model met 18 lagen en een gemiddelde laagdikte van ongeveer 11 m en een gedetailleerd model met een gemiddelde laagdikte van ongeveer 1 m. De reservoireigenschappen (kleigehalte, effectieve porositeit, permeabiliteit en de aanwezigheid van de calciet-gecementeerde lagen) zijn gemodelleerd door middel van interpolatie van de waarden in zes putten in het modelgebied.

Bij Zwijndrecht-Zuid wordt de top van het ZBL gevonden op een diepte van 620 m. Een cumulatief permeabiliteitslog laat zien dat 90% van de stroming uit de bovenste 60 m van het ZBL komt. De transmissiviteit (product van permeabiliteit en netto dikte) varieert van 35 tot 40 Dm en neemt toe in zuidelijke richting. Dunne calciet-gecementeerde lagen komen in het hele ZBL voor met een gemiddelde afstand van ongeveer 5 m, maar in de bovenste 30 m met een hogere frequentie. Deze laag-permeabele lagen zijn mogelijk continu of bijna continu en als dit zo is verdelen zij het ZBL in compartimenten van gemiddeld 5 m dik. De laterale uitgestrektheid van deze lagen is echter nog onzeker.

Reservoirsimulaties met het gedetailleerde model (met 1 m dikke lagen) laten een verwachte productiviteit/injectiviteit voor een doublet met verticale putten zien van 9 tot 11 m^3/uur/bar voor de productie put met een viscositeit van 0.9 cP en 6 tot 8 m^3/uur/bar voor de injector met viscositeit van 1.5 cP. Voor een doublet met gedevieerde putten, neemt dit met 20 tot 25% toe. Voor sub-horizontale putten is de toename ongeveer 50 tot 100% waarbij de onzekerheid een gevolg is van de onzekerheid in de horizontale en verticale permeabiliteit. Drukval in de putten zelf is niet meegenomen in deze berekeningen. Het is ook onderzocht hoe de verticale permeabiliteit het beste opgeschaald zou kunnen worden voor reservoirmodellen met grotere laagdikte. Geen van de onderzochte methoden, waaronder “flow-based upscaling”, was in staat om de resultaten van het model met dunne lagen goed weer te geven voor alle putconfiguraties. Daarom wordt aanbevolen om deze formatie altijd met een hoge verticale resolutie te modelleren in de omgeving van de put (maximaal een paar meter dik).

Summary

The WarmingUp project aims to increase the use of urban heat networks to replace gas. Within Theme 4 of this project which studies the use of geothermal energy in urban heating and in particular the development of shallow and marginal resources, three detailed regional studies are performed. This report describes the results of the first regional study, for which the Eocene Brussels Sand in the region Zwijndrecht was selected. The Brussels Sand Member is expected to be well developed in the Zwijndrecht area and is therefore a suitable target for shallow geothermal development.

To predict the reservoir properties of the Brussels Sand, an area of 44 x 33 km was selected in which a reservoir model of the Brussels Sand was built. A reprocessed seismic survey, the Donkersloot survey, was interpreted to yield two seismic horizons that served to construct a reservoir model of the Brussels Sand. The top Brussels Sand was interpreted on a “hard kick” (an acoustic impedance increase) representing the boundary between the shales of the Asse Member and the top part of the Brussel sands in which high velocity, tight, calcite-cemented streaks are abundant. A second less pronounced acoustic impedance increase was interpreted close to the top of the lowest of three “coarsening-up” sequences identified in the Brussels Sand (S1). The two horizons were tied to the wells and used as guiding surfaces in the modelling. No faults with a throw beyond seismic resolution were seen on the seismic data in the Zwijndrecht area, hence no faults were included in the modelling. It was investigated whether the presence of many high-velocity streaks could be seen in the seismic attributes, but this proved impossible.

Stratigraphic subdivision and correlation of the well logs from 37 wells resulted in a detailed reservoir model. Two versions were created: a coarse one consisting of 18 layers with an average layer thickness of 11 m, and a detailed one with an average layer thickness of 1 m. The models were populated by interpolating reservoir properties (clay content, effective porosity, permeability, and the occurrence of calcite-cemented streaks) from 6 wells in the area.

Near Zwijndrecht-Zuid, the top of the Brussels Sand can be found at 620 m depth. A cumulative permeability log showed that 90% of the flow will come from the uppermost 60 m of the Brussels Sand. Net thickness is ~80 m. The transmissivity (product of permeability and net thickness) ranges from 35 to 40 Dm and increases in southerly direction. Thin carbonate-cemented streaks occur throughout the Brussels sand, on average every 5 m, but are especially frequent in the upper 30 m of the Brussels Sand. These low-permeable streaks are thought to be continuous or nearly continuous over the area of interest and in that case divide the Brussels Sand into vertical compartments of some 5 m thick. However, the lateral extent is still uncertain.

Using the detailed reservoir model with 1 m thick layers, simulation showed an expected productivity/injectivity for a vertical doublet of 9 to 11 m^3/hr/bar for the producer with viscosity 0.9 cP and 6 to 8 m^3/hr/bar for the injector with viscosity 1.5 cP. For a deviated doublet, this increased around 20 to 25%. For the sub-horizontal doublet, the increase was around 50 to 100% with the uncertainty due to the uncertainty in the horizontal and vertical permeability. No pressure drop inside the wells was included in the calculations. In addition to the productivity of potential wells in the Brussels Sand, it was also investigated, how the vertical permeability might best be upscaled for coarser simulation grids. It was found that none of the investigated approaches which included flow-based upscaling could accurately represent the results from the fine scale models. Therefore, it is advised to use detailed vertical resolution in the higher permeable layers (few metres thickness at most).

1 Introduction

In the Climate Agreement, it has been agreed that 1.5M houses need to be heated sustainably in 2030. Heating of these houses is currently done using natural gas. Part of these houses will be heated using collective heat networks and geothermal energy is an important source of heat for such networks. Within the WarmingUP project Theme 4, the goal is to accelerate the development and use of geothermal sources for use in urban heat networks. The following 3 main aspects are addressed:

1. Reduction of the geological risk through improved characterisation of the relatively poorly studied shallow subsurface and of marginal reservoirs, fit-for-purpose well designs and integration in heat networks
2. Quantification and control of the risk of induced seismicity and other effects on the environment.
3. Improved performance through optimisation of the production process.

The improved characterisation will primarily be made available via ThermoGIS (www.thermogis.nl). The goal of ThermoGIS is to present a regional geothermal resource assessment (Vrijlandt et al., 2019) to facilitate the use of geothermal resources. In addition to the characterization at a national level, three local areas are studied in more detail. The first of these is the area around Zwijndrecht (Figure 1-1), with the Brussels Sand Member as potential target. Of the shallow formations of Cenozoic age, The Brussels Sand Member is expected to be the most prolific reservoir and therefore a prime focus in the project. It is expected to be well developed in the Zwijndrecht area and is therefore the subject of the present study. The possible location for a geothermal doublet targeting the Brussels Sand the southern part of Zwijndrecht is shown in Figure 1-1.

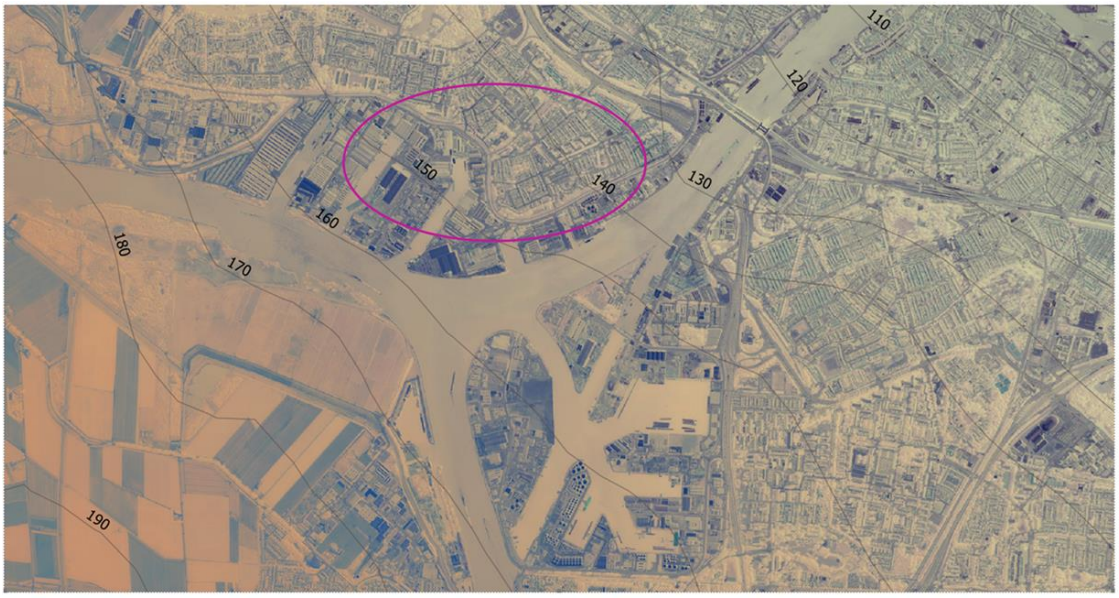

Figure 1-1 Zwijndrecht-Zuid, a possible location for a doublet in the Brussels Sand Mb.

The study reported here describes the regional geological modelling and reservoir simulation for the Zwijndrecht location. A 3D geocellular reservoir model was built in which the reservoir properties (thickness, net to gross ratio, porosity, permeability, shale content) are derived from neighbouring wells in a geologically sound and consistent way.
The first part of the report (Chapter 2) describes the seismic interpretation of the top and base of the Brussels Sand. These horizons constitute the foundation for the 3D geocellular reservoir model. The

second part (Chapter 3) describes of the building of the model. In the last part (Chapter 4), the dynamic modelling and potential production of a doublet near Zwijndrecht is given.
The current study relies heavily on previous WarmingUP studies:

- The seismic interpretation is in line with the earlier mapping of the Brussels Sand for the Netherlands as described in (Haan et al., 2020).
- Some of the wells in the vicinity of the Zwijndrecht-Zuid location were analysed in an earlier WarmingUp petrophysical study. For a detailed description of this petrophysical study the reader is referred to the report (Geel & Foeken, 2021). In the current report, the results of that study are concisely incorporated.

2 Seismic interpretation Brussels Sand Member in the area of Zwijndrecht Zuid

2.1 Data and data quality near Zwijndrecht-Zuid location

The area around Zwijndrecht is covered by a large 3D PreSDM (pre-Stack Depth Migration) survey which is a reprocessing of multiple vintage 3D surveys that have been merged in the pre-processing phase (referred to as the Donkersloot survey). Both depth and time cubes are available for this survey. The quality of the survey is generally good and there are many wells to constrain the depth of the survey. Southwest of the location where the potential project is planned the seismic data show a zone in which data quality is deteriorated. This is probably due to acquisition problems near the water of the "Oude Maas". In Figure 2-1 a seismic line crossing the Zwijndrecht-Zuid location is displayed. Directly beneath the seismic section a Google Maps image is scaled and rotated to match the seismic line. In the disturbed zone the frequency content is lower and the amplitudes around the top Brussels Sand Member are brighter. It is likely that this brightening is caused by amplitude balancing in the seismic processing.

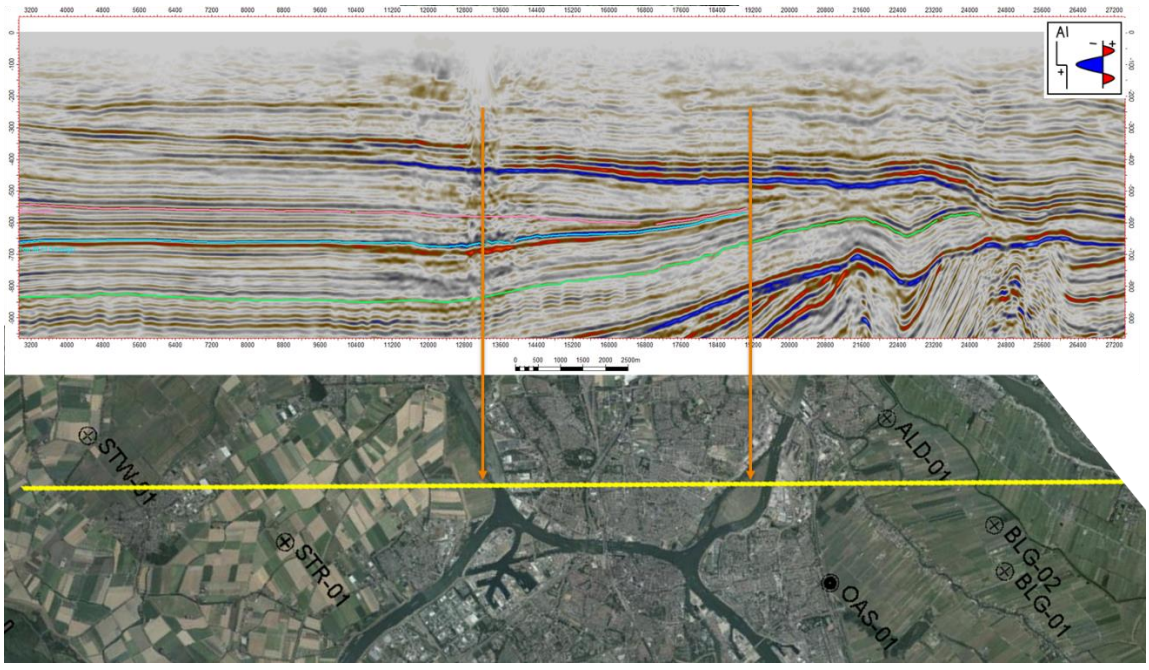

Figure 2-1 Seismic section over the Zwijndrecht Zuid location showing the top and near base BSM as the blue and green horizons. The pink horizon represents the base Rupel unconformity that erodes into the top of the BSM. At the location of the left orange arrow the seismic data quality is poorer probably as the result of data acquisition problems at the "Oude Maas" river.

2.2 Seismic character of the Brussels Sand Member and interpreted horizons

The Brussels Sand Member (BSM) is subdivided into three cycles (from base to top S1 to S3) described in paragraph 3.2. The top of the BSM (corresponding to the top of the S3 cycle) approximately coincides with the top of an interval with a higher acoustic impedance (AI) caused by the occurrence of cemented streaks that have a higher velocity and density that show up as spikes on the sonic and density well logs. The polarity of the seismic survey is such that an impedance increase corresponds to a trough, being a negative amplitude. This trough is mostly followed by a peak which more or less coincides with the base

of the uppermost Brussels Sand Member where the cemented streaks are most frequent. This is illustrated in Figure 2-2 showing a synthetic seismogram at the location of the Barendrecht-1 (BRT-01) well. Below this doublet the BSM is relatively transparent although significant acoustic impedance changes are present as a result of the high velocity/density streaks. These are less frequent than in the upper part of the BSM and they are thin and therefore below seismic resolution and not picked up by the seismic (and synthetic). The synthetic seismogram shows that only thicker zones with AI different from surrounding zones are coinciding with reflectors. It is mainly at the top and around the BSM cycle closest to the base (S1) where the reflectivity is increased. The top of the S1 cycle gives a sharper impedance contrast (increase) and hence a more continuous reflector (trough) than the base which shows a more gradual decrease in impedance. Besides the top of the BSM this “near top S1” reflector is the second reflector that has been picked in this study. In Figure 2-3 the two picked BSM reflectors are shown against the GR and Sonic log around the BRT-01 well. Northeast of the Zwijndrecht-Zuid location the top of the BSM is eroded by the base of the Rupel Formation. In this area the base Rupel reflector is picked on a peak that is locally the top of the part of the BSM that is preserved below the unconformity.

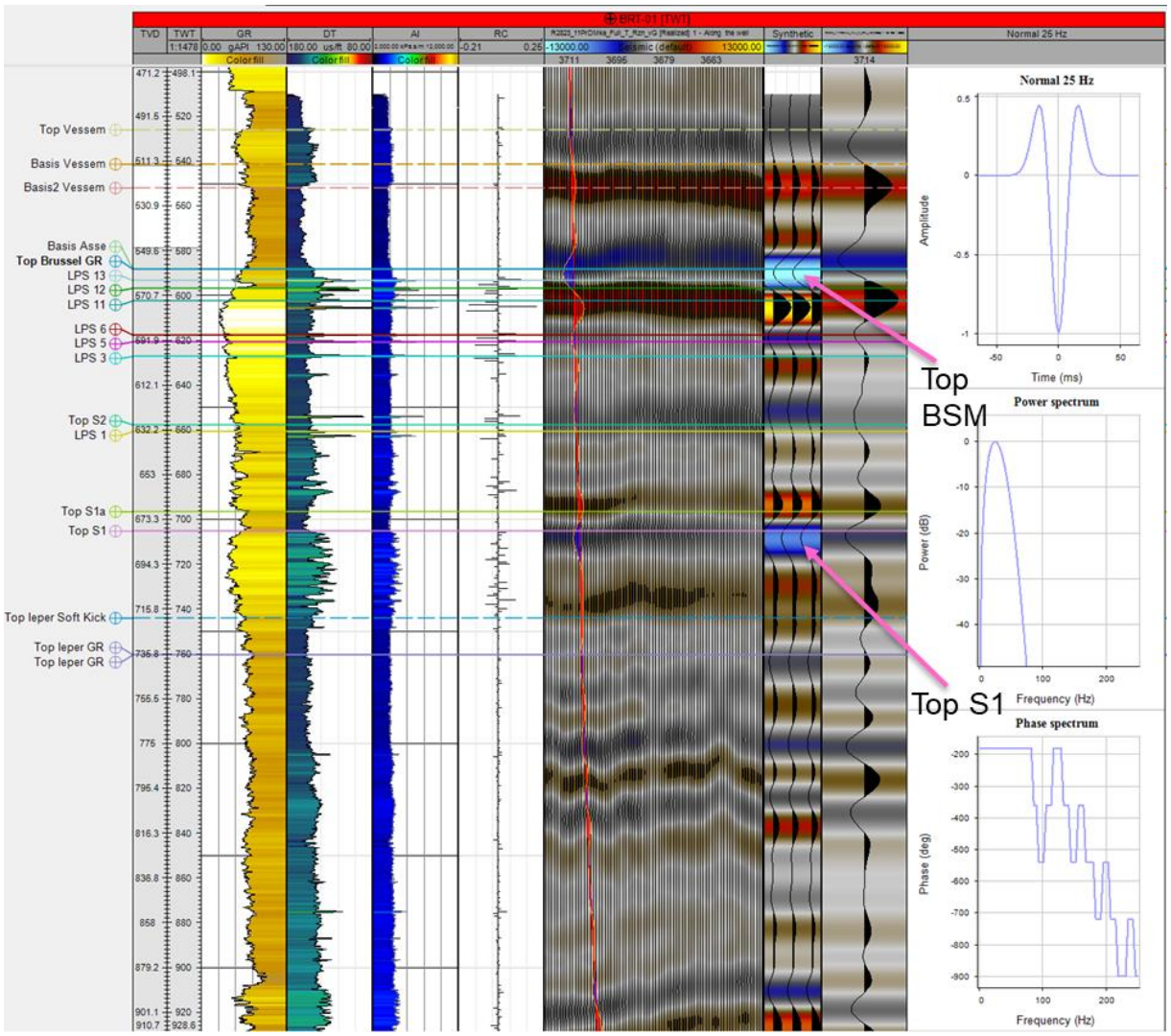

Figure 2-2 Synthetic seismogram of the BRT-01 well showing a rather good match between synthetic seismogram and seismic sections. The synthetic seismogram was made using a Ricker wavelet of 25 Hz as simplified estimation of the real wavelet.

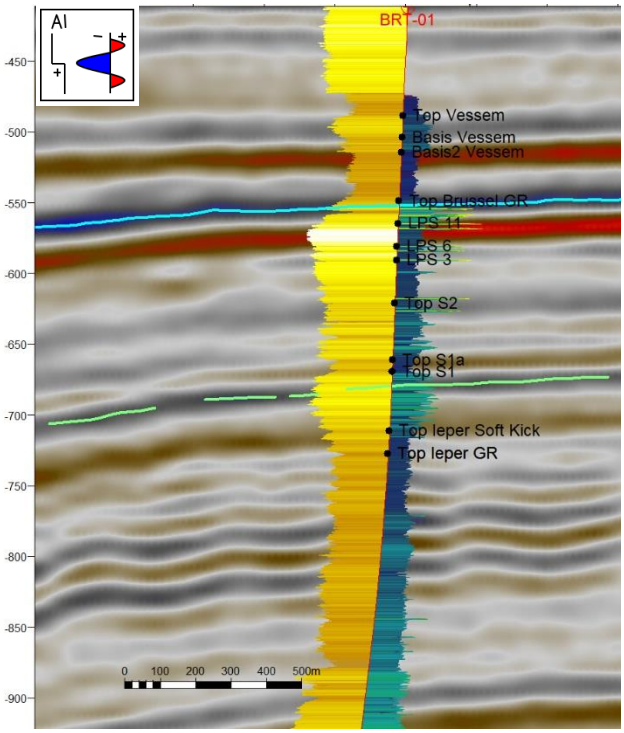

Figure 2-3 Picked top BSM and intra BSM (top S1) reflectors in blue and green with the GR (left) and sonic log (right) indicating which events were correlated on the seismic data

2.3 Local mapping of the BSM and input depth surfaces to the static model

The two interpreted BSM horizons were mapped on the depth cube of the PreSDM cube. Both reflectors are truncated by the base Rupel unconformity in the North-eastern part of the study area. The erosion of the top starts approximately 5 km northeast of the Zwijndrecht-Zuid location and about 10 km northeast of the location the complete Brussels Sand Member is eroded. The Top BSM interpretation is merged with the Base Rupel interpretation at places where the top is eroded but the basal part is still preserved. In these areas the base Rupel unconformity is the top of the remaining BSM interval. The seismic interpretation of both BSM reflectors is done by making use of 3D autotracking resulting in a very dense picking on the 3D cube. Only in areas where autotracking did not work caused by poorer quality seismic data manual interpretation was done on a coarser grid (every 50th inline). This only applies to small areas of the near top S1 BSM reflector and the Rupel reflector that is quite hard to trace in the areas where the top of the BSM is eroded. In Figure 2-4 the seismic interpretation of the three horizons is displayed.

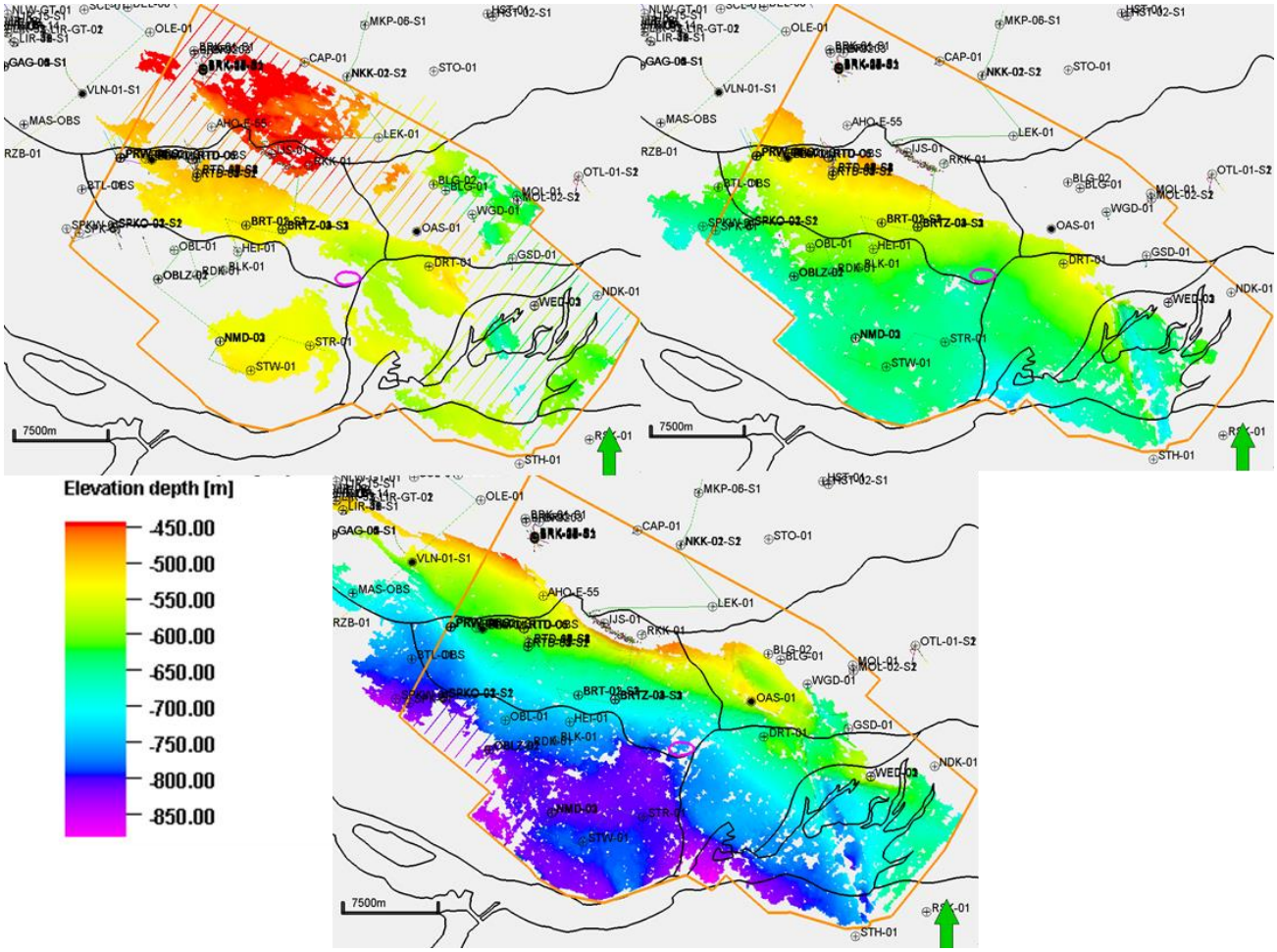

Figure 2-4 Seismic interpretation data of (clockwise) base Rupel, top BSM and near top S1 (intra BSM).

The seismic interpretation is transformed into a 50 x 50 m grid using the Petrel convergent gridding algorithm. The top BSM grid is tied to the well top LPS13 (Low Permeability Streak 13, see Section 3.2) within a radius of 2000 m. This well top represents the uppermost low permeability streak within the BSM picked and correlated on well logs which is thought to coincide with the trough picked on seismic data. The tying results in a residual surface that is depicted in Figure 2-5. The picked near-top S1 horizon was tied to the top S1 well top by first applying a bulk shift of 12.5 m (upward; being the average of the residuals) and then tying the residual that is left after the bulk shift with a radius of 2000 m (Figure 2-6). The residuals are tabulated in Table 2-1. The residuals of top BSM show an average of -2 m and a standard deviation of 10 m. The main uncertainty is in the area where the base Rupel cuts away the top of the BSM, this reflector is less pronounced and the picking less dense and reliable. If only the wells are considered in which the complete BSM is present the average mis-tie is +2 m and the standard deviation reduced to only 5 m. The residual of the top S1 grid shows (after bulk shift of 12.5 m) a standard deviation of 8 m.

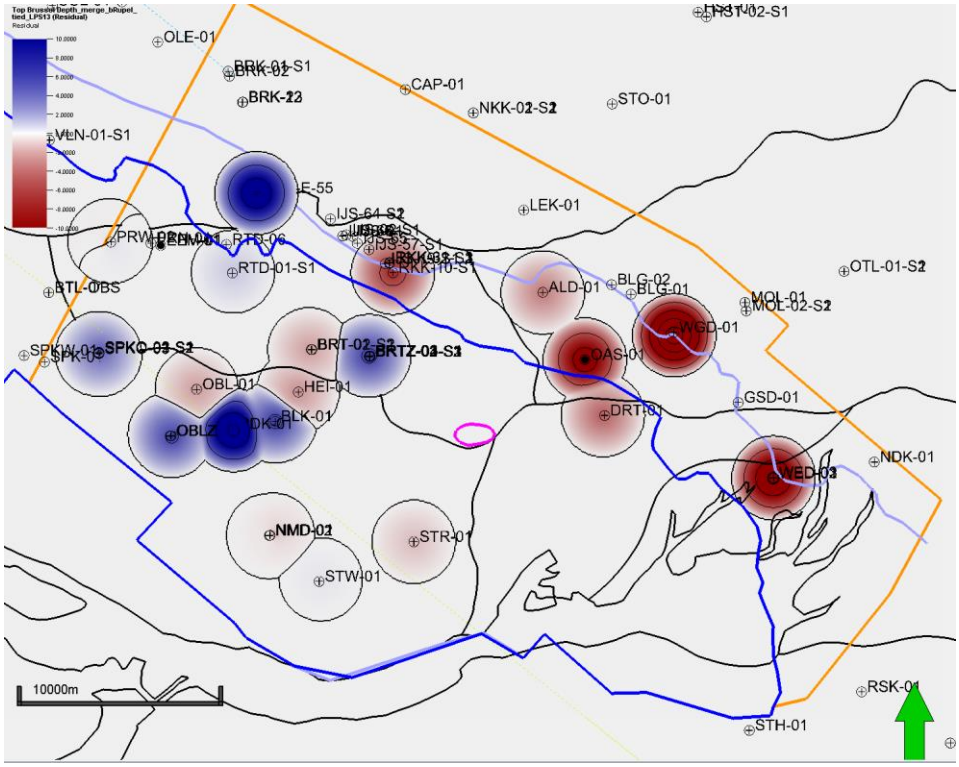

Figure 2-5 Depth difference (residual (in m)) between top BSM grid and the LPS13 well top. At places where the LPS 13 is eroded the top BSM is tied to base Rupel. Contour increment 5m. Most residuals are within +-10 m. A radius of 2000 m was used to tie grids to wells.

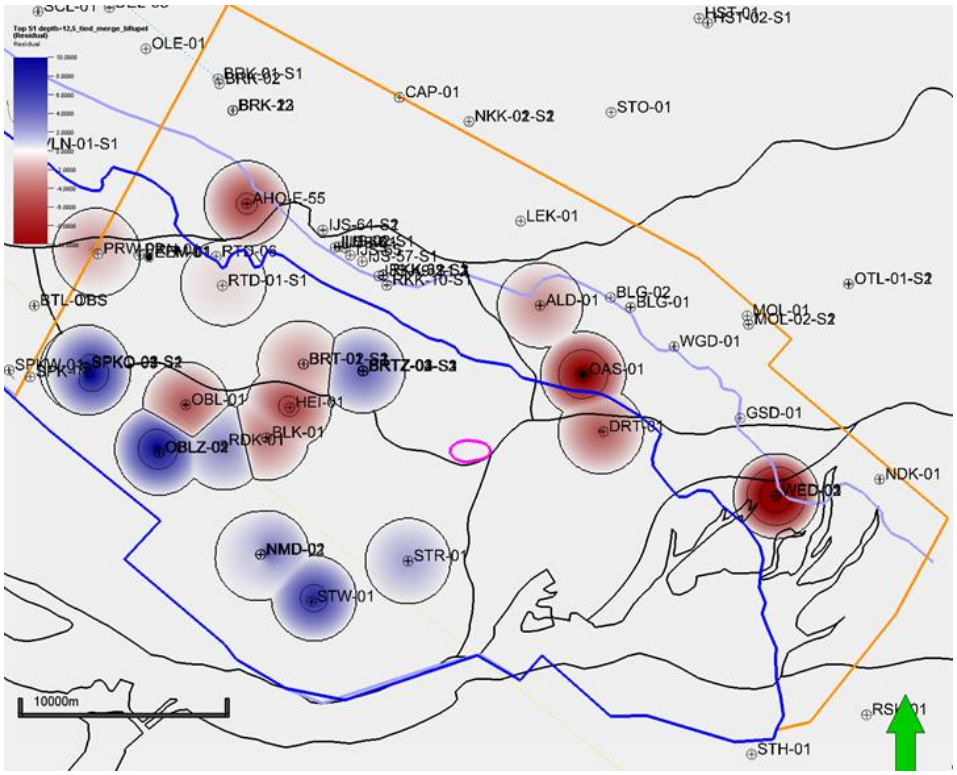

Figure 2-6 Depth difference (residual (in m)) between near top S1 grid and the top S1 well top. Contour increment 5m. Most residuals are within +-10 m. A radius of 2000 m was used to tie grids to wells.

Top BSM all wells	
Well	**residual (m)**
AHO-E-55	15.7
ALD-01	-3.3
BLK-01	6.1
BRT-01	-2.1
BRTZ-01	6.1
DRT-01	-4.4
HEI-01	-2.5
NMD-01	-1.3
NMD-02	-0.1
NMD-03	-0.2
OAS-01	-14.1
OBL-01	-2.1
OBLZ-01	7.1
OBLZ-02	4.5
PRW-01	-0.7
PRW-02	0.8
RDK-01	17.3
RKK-10-S1	-7.3
RTD-01	0.9
SPKO-01	7.1
SPKO-02	3.1
SPKO-03	2.0
STR-01	-1.3
STW-01	0.2
WED-01	-16.9
WED-02	-18.7
WED-03	-17.1
WGD-01	-25.3
Average	**-1.7**
StDev	**9.7**

Wells complete BSM	
Well	**residual (m)**
BLK-01	6.1
BRT-01	-2.1
BRTZ-01	6.1
DRT-01	-4.4
HEI-01	-2.5
NMD-01	-1.3
NMD-02	-0.1
NMD-03	-0.2
OBL-01	-2.1
OBLZ-01	7.1
OBLZ-02	4.5
PRW-01	-0.7
PRW-02	0.8
RDK-01	17.3
RTD-01	0.9
SPKO-01	7.1
SPKO-02	3.1
SPKO-03	2.0
STR-01	-1.3
STW-01	0.2
Average	**2.0**
StDev	**5.0**

Top S1	
Well	**residual (m)**
AHO-E-55	-6.7
ALD-01	-2.9
BLK-01	-3.7
BRT-01	-2.7
BRTZ-01	4.4
DRT-01	-5.2
HEI-01	-6.7
NMD-01	4.9
NMD-02	0.6
NMD-03	1.3
OAS-01	-12.1
OBL-01	-5.2
OBLZ-01	7.7
OBLZ-02	10.9
PRW-01	-4.8
PRW-02	0.0
RDK-01	3.0
RTD-01	-0.7
SPKO-01	9.4
SPKO-02	14.1
SPKO-03	-0.1
STR-01	2.0
STW-01	7.4
WED-01	-16.1
WED-02	-16.5
Average	**-0.7**
StDev	**7.7**

Table 2-1 Difference (residual (in m)) between grid and well top before well tie for top BSM and top S1. A positive number (blue) means that the grid is deeper than the well top.

2.4 Seismic attributes

Seismic attributes have the potential to show lateral changes in aquifer properties. In principal the seismic attributes will respond in changes in acoustic impedance but these can be interpreted as changes in certain properties. In this study seismic attributes were extracted hoping that these would give indications of areas in which the calcite streaks observed in wells would be more abundant than in other areas.

The sonic logs in wells show that especially the calcite-cemented streaks (low permeability streaks (LPS)) stand out having a higher velocity than surrounding lithology. Also the density in these zones is higher, resulting in higher acoustic impedance values in these zones. Individual streaks are too thin to be seen on seismic data (below seismic resolution), but possibly areas with a higher abundance of these streaks could result in higher reflectivity than areas with a low number of streaks. To this end amplitudes were extracted from seismic data. The top part of the BSM contains most of the streaks and is expected to show most of the amplitude variation caused by the streaks.

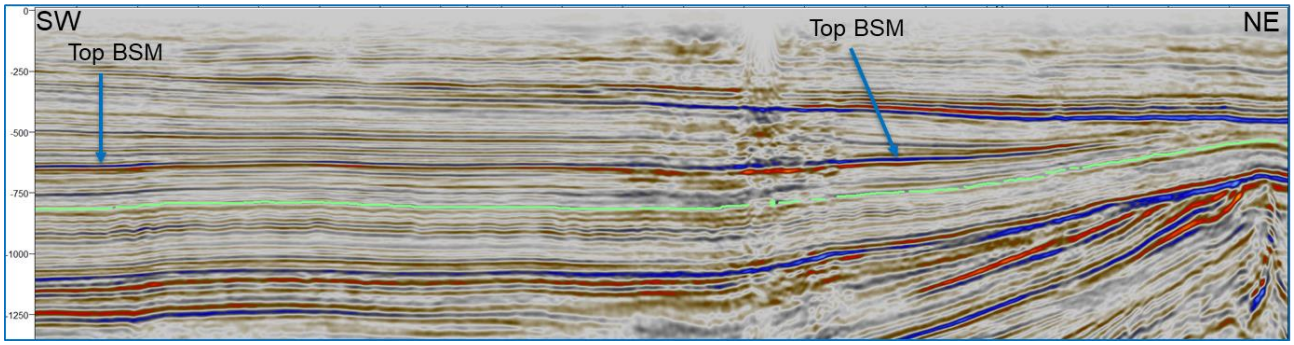

Figure 2-7 NW-SE seismic section (location see Figure 7). Top BSM is picked on the blue trough indicated by the arrow. The main amplitude change of top BSM seems to take place in the "disturbed" area just left of the arrow at the right hand side. The amplitude is quite constant but dims at the NE side where the top BSM is eroded by the base Rupel.

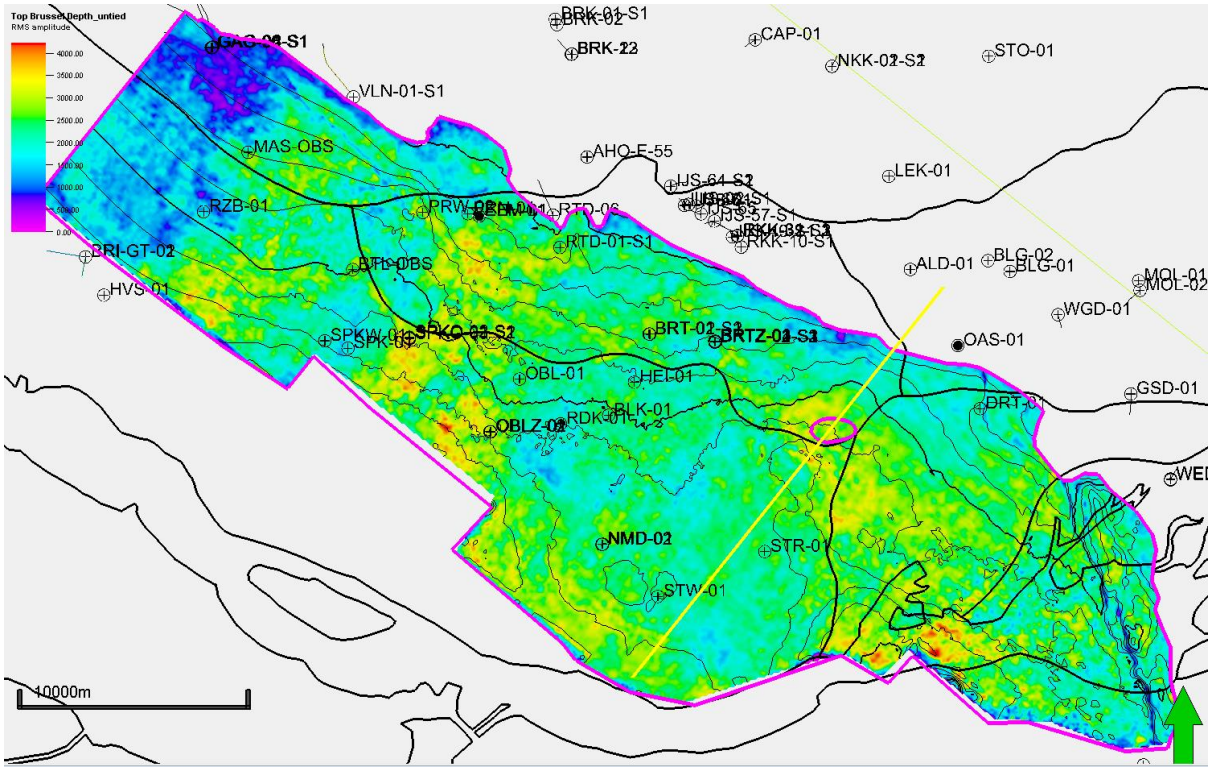

Figure 2-8 RMS amplitude of double loop (trough and peak) of the top BSM. The Zwijndrecht Zuid location is indicated by the purple ellipse. The yellow line refers to the seismic section of Figure 2-7.

In Figure 2-7 a seismic section is shown on which the lateral variation can be seen along the top Brussels reflector. In *Figure 2-8* a map is shown where the Root Mean Square (RMS) amplitude is extracted around the top Brussels trough and subsequent peak. In the subsequent Figure 2-9 the extracted amplitudes along the top BSM trough and the peak below it are displayed. It is hard to read any coherent amplitude information from these amplitude maps. It is however clear that the amplitude is dimmer towards the area where the top Brussels is eroded by the Rupel unconformity as a consequence of negative interference. The amplitudes in the area close to the Zwijndrecht Zuid location are somewhat higher but as discussed in the data quality paragraph (paragraph 2.1) this is probably due to seismic data quality and amplitude balancing of the poorer zones. The Donkersloot reprocessed survey is a pre-stack merge of several individual surveys with independent acquisition parameters. As a result, amplitudes may vary laterally. Another complication is that the beds that are lying directly on top of the BSM are varying. As shown in *Figure 2-10* the Asse Member is on top of the BSM in the SW, while the Rupel Member is on top in the rest of the section. The Asse shows an onlap pattern onto the BSM. The Rupel thins to the NE and

at the base also an onlap configuration can be seen. As a result of this the acoustic impedance will vary along the top of the BSM. Moreover, at the places where this onlap takes place local dimming or brightening(tuning) is observed in the seismic data.

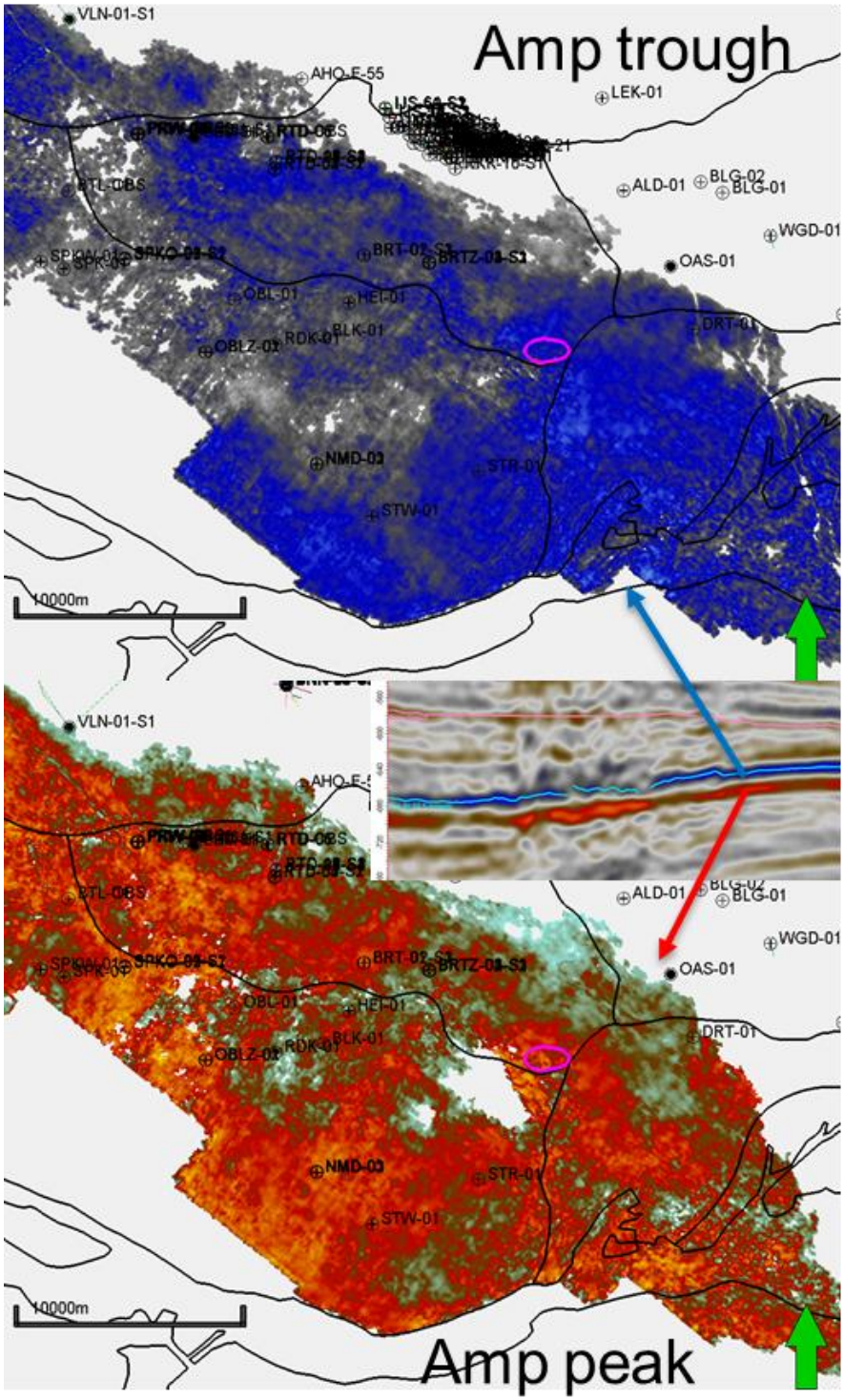

Figure 2-9 Amplitude maps of the top BSM trough (upper) and subsequent peak (lower).

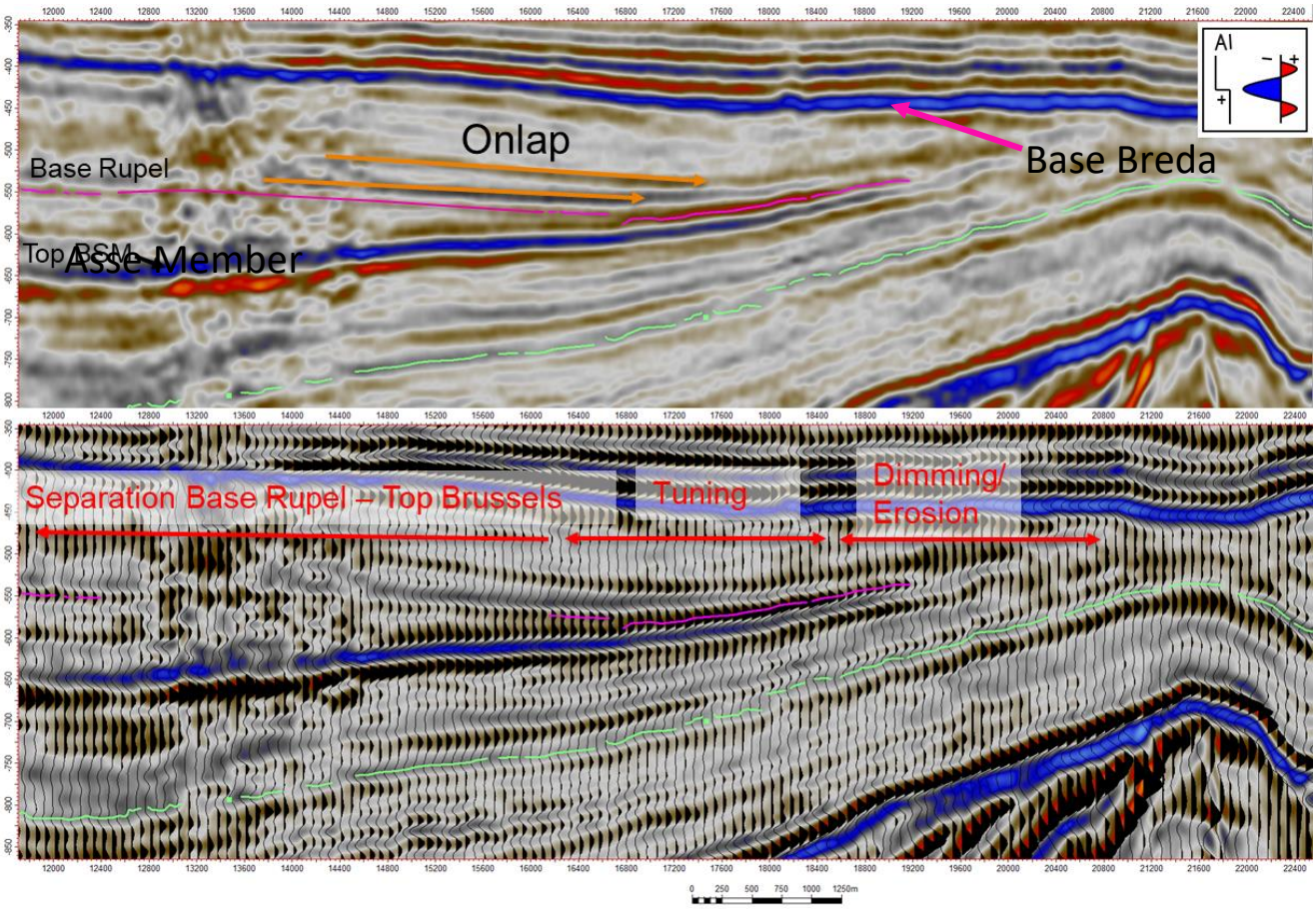

Figure 2-10 Detail of SW-NE seismic section at the location where the top BSM is eroded by the base Rupel (pink). Top BSM amplitudes brighten (tuning) just SW from the area where the top BSM is eroded. The amplitudes dim where the top is eroded.

This point is nicely demonstrated in Figure 2-11 where the amplitudes are extracted along the base Rupel reflector. At places where this reflector gets close to top BSM the sidelobe of the top BSM and the main peak of the base Rupel positively interfere (tune) and cause a zone of higher amplitude parallel to the erosional edge of top BSM. Further to the south a clear change in amplitude value can be seen likely to be caused by different acquisition of the input seismic surveys.

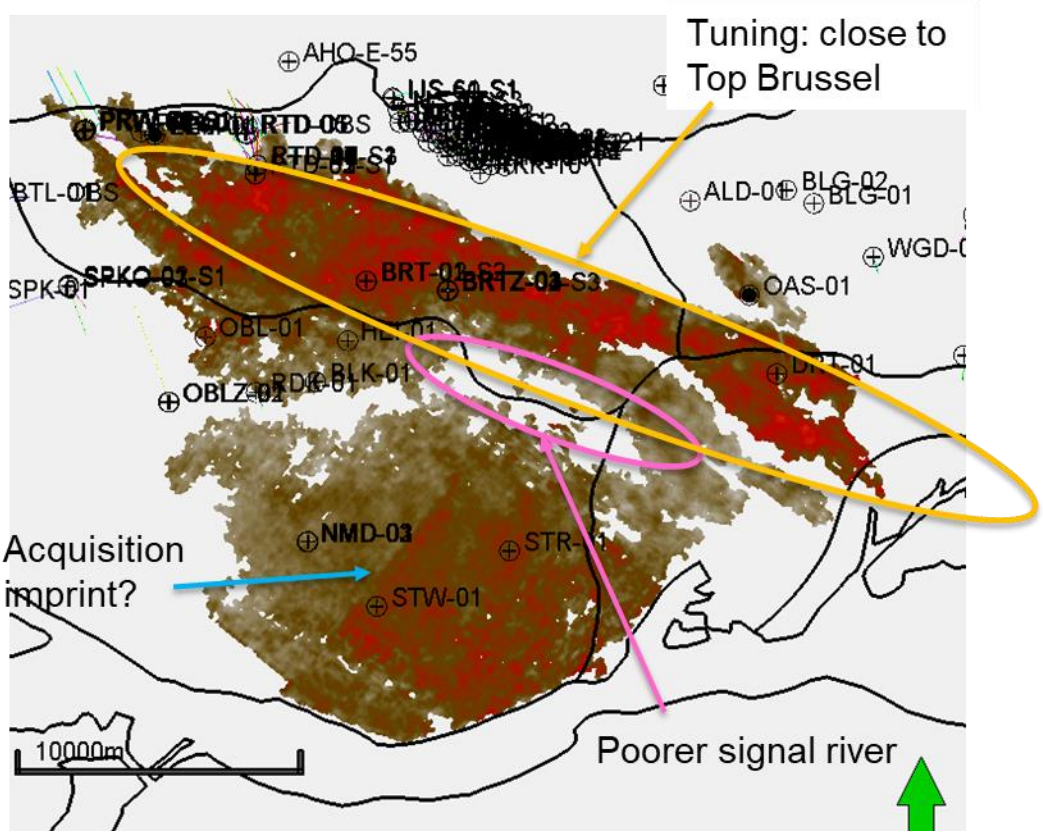

Figure 2-11 Amplitude along the base Rupel reflector. Brightening (tuning; orange ellipse) takes place just SW of where the top BSM is eroded. The area of poor data quality below the "Oude Maas" river is not tracked (pink). There is an abrupt amplitude change visible indicated by the blue arrow, probably caused by differences in acquisition of the data.

There are some higher RMS amplitudes seen around the SPKO and OBLZ wells. Unfortunately, none of these well have sonic (or density) data making it impossible to check the frequency of occurrence of the LPS intervals. As a conclusion it seems impossible to predict the frequency of occurrence (or total thickness) of the LPS intervals from seismic data. There is a variation of acoustic impedance contrast along the top of the BSM caused by variation in acoustic impedance of the overlying beds as a result of the onlap geometry of these beds and dimming and brightening along the top as a consequence of interference. On top of this the amplitude content is also subject to the acquisition of the original input seismic surveys.

To detect potential faults transecting the BSM the variance attribute has been extracted from the seismic time cube. This attribute shows changes in continuity of the seismic waveform along reflectors. Disruptions like faults will cause discontinuous events that will line up. In most of the area no faults are observed in the BSM interval. There are some discontinuities observed around the Zwijndrecht Zuid location, but these are caused by the disturbed seismic signal beneath the "Oude Maas" river. In Figure 2-12 a seismic section showing the variance attribute is shown and the BSM shows up as a transparent interval, except around the bad data area. Only deeper (below the North Sea Group) disruptions line up and can be interpreted as faults. The transparency of the interval means that no faults with a seismically detectable throw can be expected in the Zwijndrecht Zuid area.

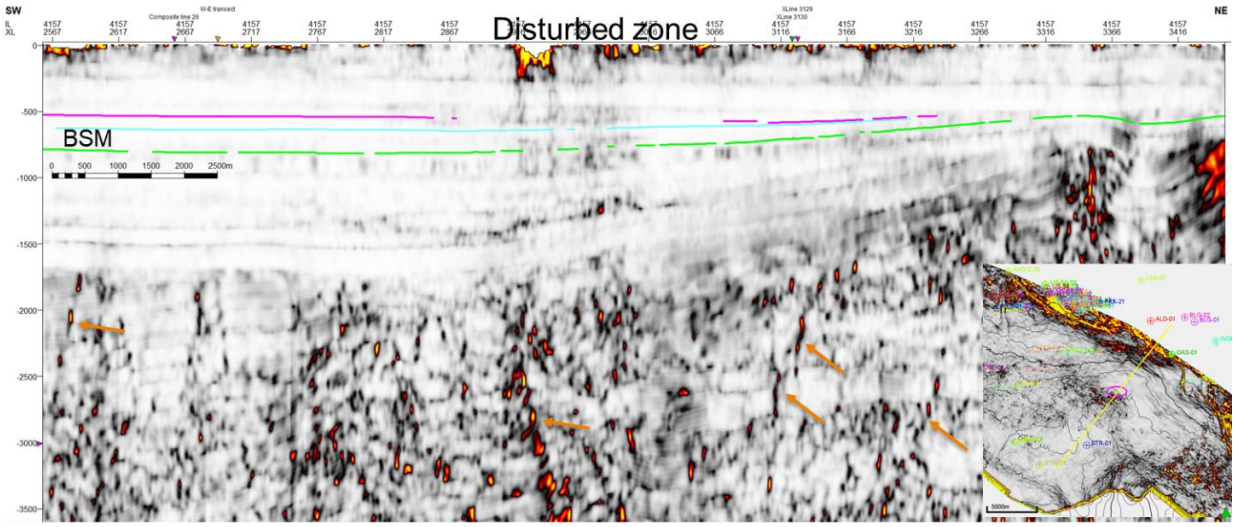

Figure 2-12 Seismic section showing the “variance” attribute. Within the BSM no discontinuities are observed indicating that no faults with throw exceeding seismic resolution are present. In the deeper part of the section faults are recognized (indicated by orange arrows. The inset map shows the variance attribute along top BSM. In both the section and the map, the “disturbed” zone with poorer data quality can be recognised.

3 Static Reservoir Modelling

3.1 Data and methods

The input data for building the reservoir model consisted of the following:

- Two interpreted horizons from 3D seismic: one near Top Brussels Sand, and one at the Top S1, the lowermost unit of the Brussels Sand;
- Wells in the area: publicly released wells (all data from www.nlog.nl) and the Zevenbergen geothermal wells that were not publicly released at the moment of writing;
- End-of-well reports (confidential) on the Zevenbergen geothermal wells;
- A petrophysical study done by TNO on 32 wells in the Netherlands on the Brussels Sand, amongst which 6 wells in the Zwijndrecht area (Geel and Foeken, 2021).

Figure 3-1 shows wells that are located near Zwijndrecht. There is a cluster of wells in the Ridderkerk and IJsselmonde Fields.

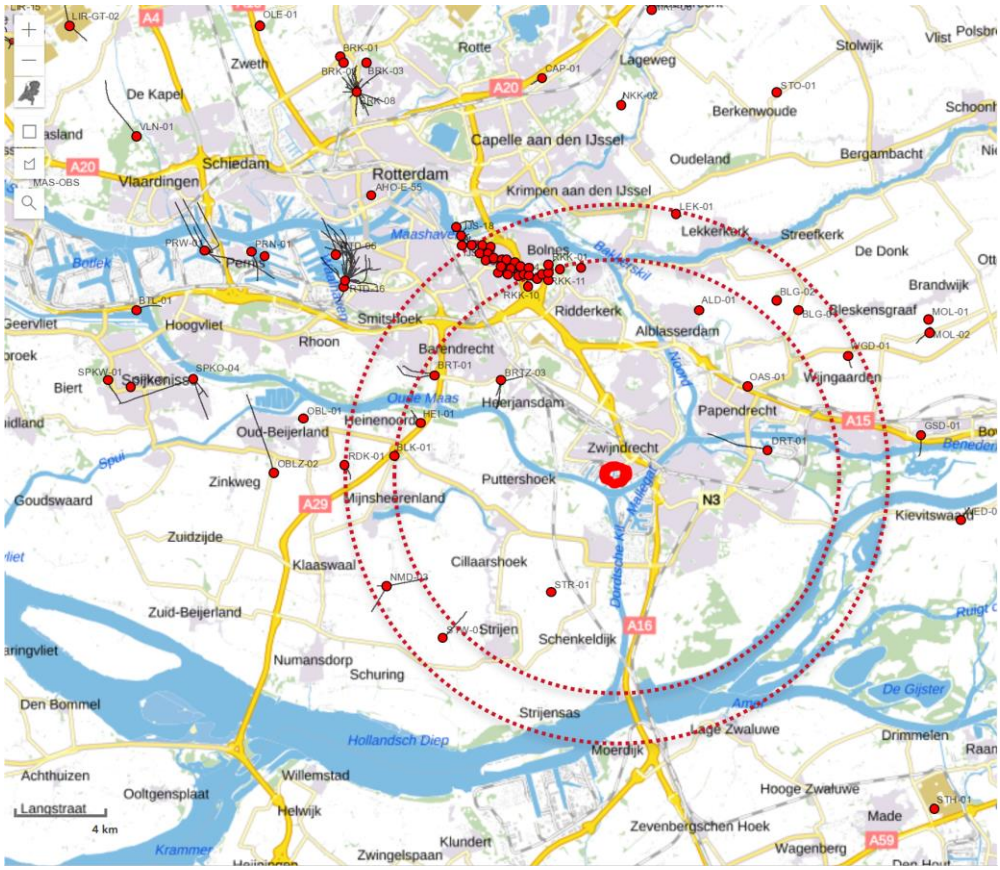

Figure 3-1 Wells within a radius of 10 and 12 km (from nlog.nl) from the proposed location of the Zwijndrecht-Zuid doublet.

There are 16 wells within a radius of 10 kilometres, of which only STR-01 and BRT-01 have porosity logs (Table 3-1). Additionally, a large number of wells, mostly from the IJsselmonde and Ridderkerk oil fields, are located at a distance between 10 and 12 kilometres (Table 3-1).

Table 3-1 Wells in the vicinity of the Zwijndrecht Zuid location

Well name	Location	Distance from Zwijndrecht Zuid location	Porosity log
STR-01	Strijen	< 10 km	STR-01
ALD-01	Alblasserdam		no
BLK-01	Blaaksedijk		no
BRT-01 and -02	Barendrecht		BRT-01
BRTZ-01 through -04	Barendrecht Zuid		no
DRT-01	Dordrecht		no
HEI-01	Heinenoord		no
NMD-03	Numansdorp		no
OAS-01	Oud Alblas		no
RKK-10	Ridderkerk		no
RKK-11	Ridderkerk		no
STW-01	Strijen West		no
NMD-01 and -02	Numansdorp	< 12 km	no
BLG-01 and -02	Bleskensgraaf		no
IJS-01 through -67	IJsselmonde		no
LEK-01	Lekkerkerk		no
RDK-01	Reedijk		RDK-01
RKK-01-09;12-32	Ridderkerk		no
WGD-01	Wijngaarden		no
ZVB-GT-01	Zevenbergen	> 12 km	ZVB-GT-01
SPK-01	Spijkenisse	-	-
STH-01	Steelhoven		STH-01
RTD-01 through -21	Rotterdam		RTD-01
SPKO-01 through-04	Spijkenisse-Oost	-	-
SPKW-01	Spijkenisse-West	-	-
GAG-01	Gaag	-	-

The ZVB-GT-01 well, although at more than 12 kilometres distance, is also very important for the current project. This pilot well, and the two injection/production wells were specifically drilled with the aim to produce from the Brussels Sand. Therefore, a wealth of information was available for the project, kindly provided by the operator, Visser & Smit Hanab. A few other wells, outside the model area, were incorporated into the project because they were located within the area of the Donkersloot seismic survey. They were used for correlation purposes and well tying (Table 3-1).

All wells were used to build the geological model, except for those belonging to the Ridderkerk, Rotterdam and IJsselmonde oil fields. A single representative well was selected to represent those fields. Only six of the wells had porosity logs in the Brussels Sand which could be used to populate the model with reservoir properties. Table 3-2 lists the wells that were used.

Table 3-2 List of wells used in the present study. Indicated are which well logs were available for the Brussels Sand. Wells that have GR or SP were used for correlation, while wells that have Phie (effective porosity), Perm (permeability), VCL (clay volume), and LPS (low-permeability streak) were used for reservoir properties. Well ZWZ (lowermost row) is a proposed well at the Zwijndrecht-Zuid location.

Name	RD X [m]	RD Y [m]	KB elev [m]	GR	SP	DT	PHIE	PERM	VCL	LPS
AHO-E-55	92014	436468	0.1		●					
ALD-01	105930	431640	3.8		●					
BLK-01	92939	425371	7.5	●						
BRT-01	94682	428862	8.4	●		●	●	●	●	●
BRTZ-01	97501	428547	9.4	●						
BTL-01	81928	431631	13.4	●						
DRT-01	108933	425656	12.6	●						
GAG-01	75888	441184	6	●						
GSD-01	115419	426290	5	●						
HEI-01	94051	426796	9.1	●						
NDK-01	122036	423395	8.5	●						
NMD-01	92683	419834	8.3	●						
NMD-02	92649	419823	8.3	●						
NMD-03	92650	419838	8.2	●						
OAS-01	107974	428370	4.2	●	●					
OBL-01	89109	426927	10.6	●						
OBLZ-01	87869	424664	9.3	●						
OBLZ-02	87833	424667	9.7	●						
PRW-01	84914	434083	12.1	●						
PRW-02	84944	434088	12.1	●						
RDK-01	90875	425003	9.3	●		●	●	●	●	●
RKK-10-S1	98651	432597	2.9	●						
RTD-01	90846	432582	12	●		●	●	●	●	●
SPKO-01	84366	428691	16	●						
SPKO-02	84368	428721	16.1	●						
SPKO-03	84362	428658	15.6	●						
SPKW-01	80727	428571	8.4	●						
STH-01	115960	410350	9	●		●	●	●	●	●
STR-01	99659	419516	4.9	●		●	●	●	●	●
STW-01	95064	417589	9	●						
VLN-01	81957	439047	11	●						
WED-01	117128	422596	6		●					
WED-02	117124	422603	7	●						
WED-03	117127	422634	11	●						
WGD-01	112284	429695	6.1	●						
ZVB-GT-01	102251	405433	6	●		●	●	●	●	●
ZWZ	102780	424150	12							

Data availability

As is apparent from Table 3-2, most wells only have a gamma-ray (GR) or spontaneous potential (SP) log in the Brussels Sand. Six of the wells also have a porosity log (mostly derived from the sonic log). In three wells (RTD-01, BRT-01, ZVB-GT-01) density and/or neutron logs were available.

Gamma ray logs are required for the determination of the shale content, which in turn is necessary for the determination of porosity and permeability. Gamma ray logs cannot be used straight away either for correlation or for shale volume determinations, because they were acquired under widely differing borehole conditions that significantly influenced the readings. Factors that influence the gamma ray log response are:

- Drilling muds with varying densities and additives (e.g. KCl)
- Varying borehole size
- Centred or uncentered tools
- Tool run through casing

- The newest wells (NMD-01 and DRT-01) have Measurement While Drilling (MWD) logs where the resolution and amount of detail is far larger than the other ones.

In order to use the gamma ray logs for correlation and shale volume calculations they should be normalized. This can be done using borehole corrections, or histogram matching with other wells but these techniques are usually time consuming, if applicable at all. It was therefore decided to do the gamma ray normalization in Petrel. In short, this works as follows: first, a well-known, trusted well is assigned the role of standard well that contains the gamma-ray log that all other wells should adhere to. Well BRT-01 was chosen to be this standard well. Then for each well the minimum GR value (so the 100% sand point) is adjusted to match the minimum GR value from BRT-01. This process is repeated for the maximum GR value (the 100% shale point). The result is that within the study area, and within the Brussels Sand, all gamma-ray logs are scaled to match the GR log of BRT-01. The assumption is of course that there are no big facies changes in the area of investigation. We believe that this the case because the AOI is relatively small. Furthermore, the environment of deposition of the Brussels Sand, a marine shelf sand, is not known for its rapid later facies changes. Figure 3-2 illustrates the effect of normalisation of the gamma-ray log on the correlation process.

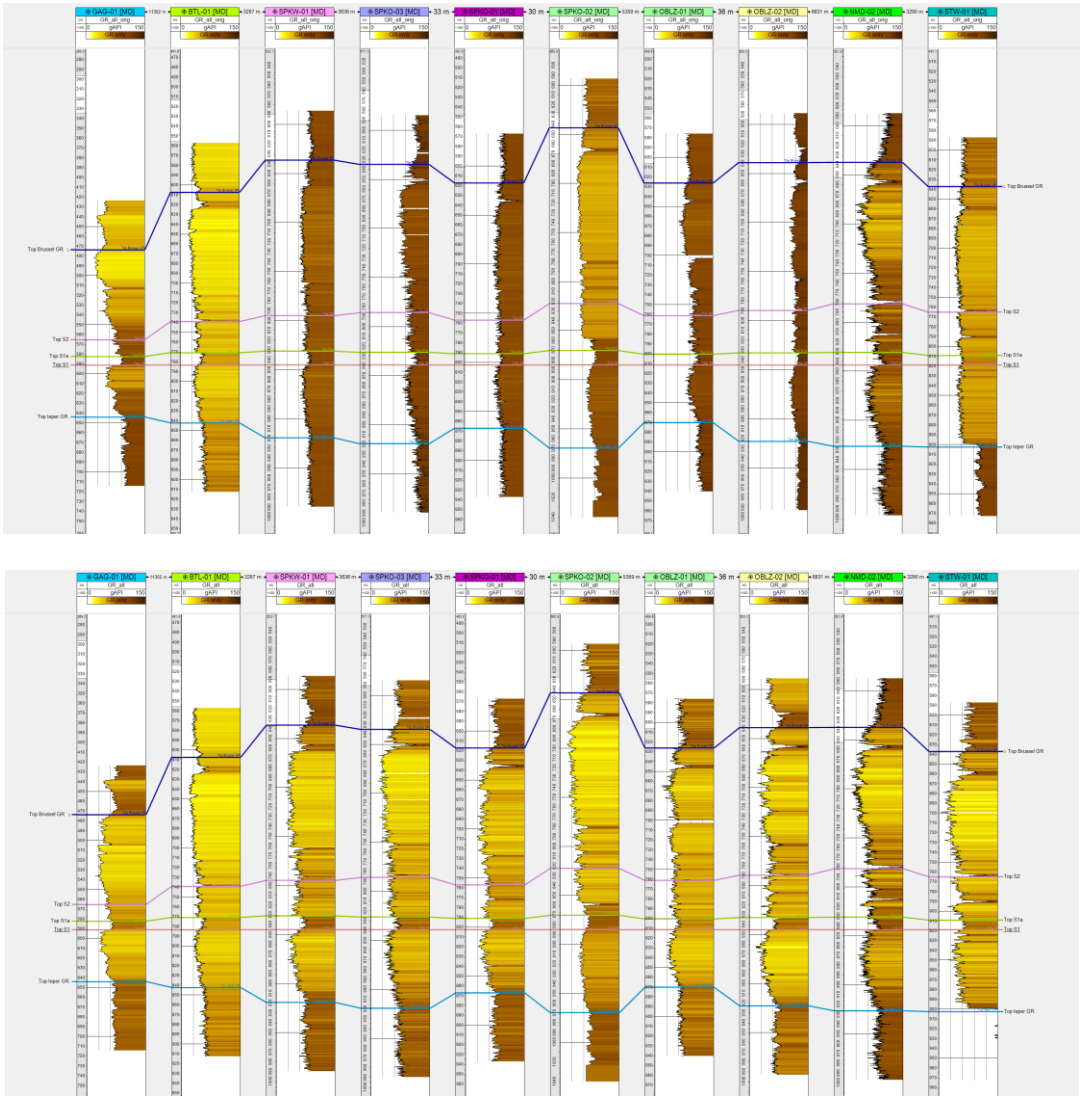

Figure 3-2 Illustration of the effect of normalisation of the gamma-ray log on the correlation process. Upper: GR logs as downloaded from nlog.nl, showing various effects of drilling mud, hole size, type of tool, running through casing, and MWD. Lower: GR logs were normalised by adjusting the ranges and in case of MWD (NMD-02) the resolution of the GR logs.

3.2 Reservoir modelling

Top and base of reservoir

Two seismic horizons were available to base the reservoir model on. The top is defined by a seismic hard kick (see above) that coincides with the first calcite-cemented tight streak, named here LPS13. Unfortunately, the Donkersloot seismic survey does not sufficiently extend southward to include the ZVB-GT-01 well, so some cut-and-paste activities were included. Figure 3-3 shows a merged surface with a wide gap: the newly mapped LPS13 horizon and the previously mapped Top Brussels Sand (de Haan et al, 2020) that covers the ZVB-GT-01 well. The merged surface was in Petrel tied to the LPS13 well top. By creating a wide gap, a smooth transition was ensured in the final model.

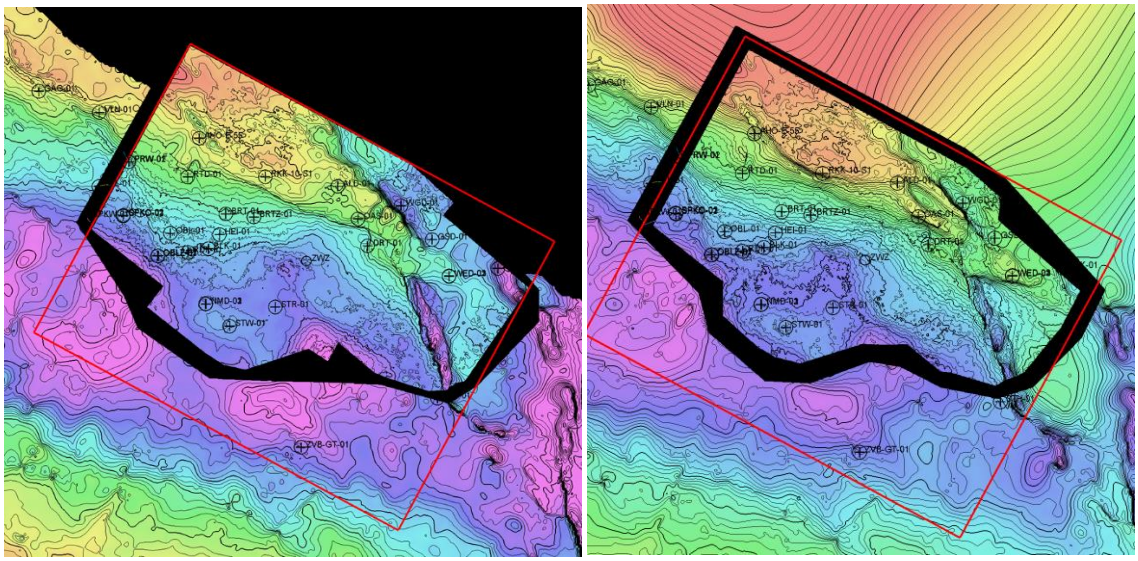

Figure 3-3 Input horizons for the reservoir model. Left: Merged surface of the LPS13 horizon from the Donkersloot survey and the larger Top Brussels Sand horizon from Haan et al (2020). Right: Merged surface of the S2 horizon from the Donkersloot survey and the larger Base S2 horizon from de Haan et al (2020).

The base of the Brussels Sand is not well visible on seismic because the boundary between the Ieper Clay and the Brussels Sand is defined by a gradual increase in sand content. On the both the GR and sonic logs it is often arguable where to put it. In order to create a consistent framework for the reservoir model, the base of S1 was in each well picked at the depth point where the GR log stopped increasing and a stable, high GR value marks the presence of the Ieper Clay. It should be noted that in most wells this base S1 does not coincide with the previously established base S1 (Haan et al, 2020). Gross thickness of the Brussels Sand is in the study area therefore larger than shown in Haan et al (2022). For the net thickness there is hardly any difference, since S1 contains hardly any net reservoir.

The regional reservoir model was eventually built using the seismically interpreted horizons LPS13 and Top S1. The actual base of the Brussels Sand was created by isopaching down from the Top S1 using the isopach S1 from the wells, and in the same way the top of the model was isopached upward from LPS13.

Subdivision and correlation

From the WarmingUp sub-project on the mapping of the Brussels Sand (Haan et al., 2020) a subdivision into four units was made: S3, S2, S1a, and S1. Each of these units can be easily recognized on well logs

throughout the Netherlands. However, this subdivision proved to be too coarse to make a good prediction of the reservoir properties in the Zwijndrecht Zuid well location, so a finer (local) subdivision was created for the area, resulting in 18 units (Figure 3-4). These units were based on log patterns, expressing mostly coarsening-up sequences that are overlain by a thin mica-rich layer, easily recognisable as a high GR peak. This way a good prediction can be made of the reservoir properties of the Brussels Sand at the Zwijndrecht-Zuid location.

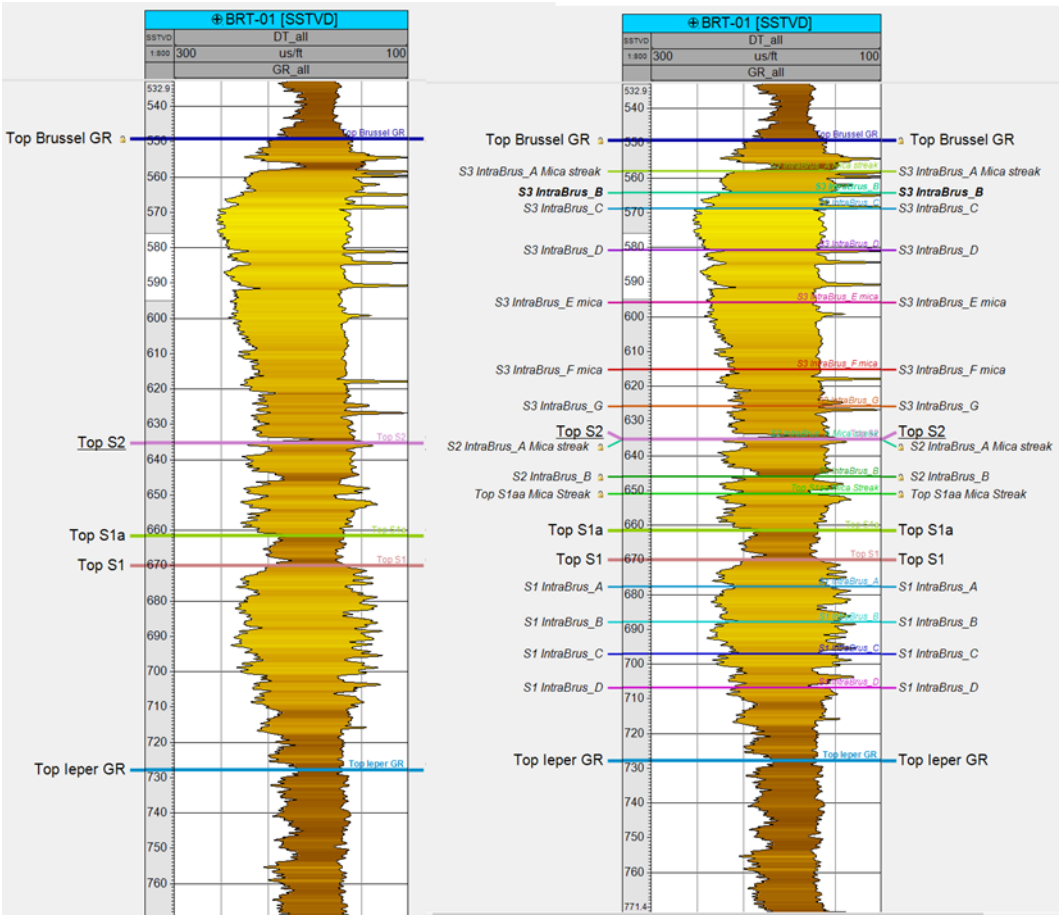

Figure 3-4 Original subdivision of the Brussels Sand as described in Haan et al (2020), left, and further local subdivision as used in the current study (right).

Lithological characteristics of the Brussels Sand

A potential well drilled at the location Zwijndrecht-Zuid (coined ZWZ) will geologically be fairly similar to BRT-01 as it is only 10 km away along strike, is roughly at the same depth, and has the same thickness. The subdivision shown in Figure 3-4 proves to be a robust stratigraphic framework, where especially in an East-West direction (i.e. along strike) individual units can be easily correlated over tens of kilometres (see Figure 3-6). Moreover, because BRT-01 had a lithodensity tool run in the Brussels Sand, providing density, neutron, and photo-electric effect (PEF) logs we consider this well a key well for the prediction of the properties at the Zwijndrecht-Zuid location.

The Brussels Sand contains some glauconite and mica. Glauconite is found throughout the formation in small quantities, usually a few percent. In the study area mica is found concentrated in thin streaks. Another conspicuous constituent is the presence of small carbonate-rich fossils, such as nummulites, green algae, and tube worms. The number of fossils increases toward the top of the Brussels Sand.

The lithological characteristics of BRT-01 can be summarised as follows (see Figure 3-4 and Figure 3-5):

- S3: Coarsening-up sequence. Highest porosity but also many Low-Perm Streaks (LPS), especially near the top. This carbonate-rich interval (LPS13-LPS8) can sometimes be seen on seismic, at least the topmost carbonate (LPS13).
- S2: Shaly sand, largely non-reservoir.
- S1A: Shale interval. Non-reservoir.
- S1: Coarsening-up sequence, reservoir, but with much lower porosity than S3. Analysis of sonic and resistivity logs indicates a much higher compaction than the overlying sequences. Contains many thin LPS's.

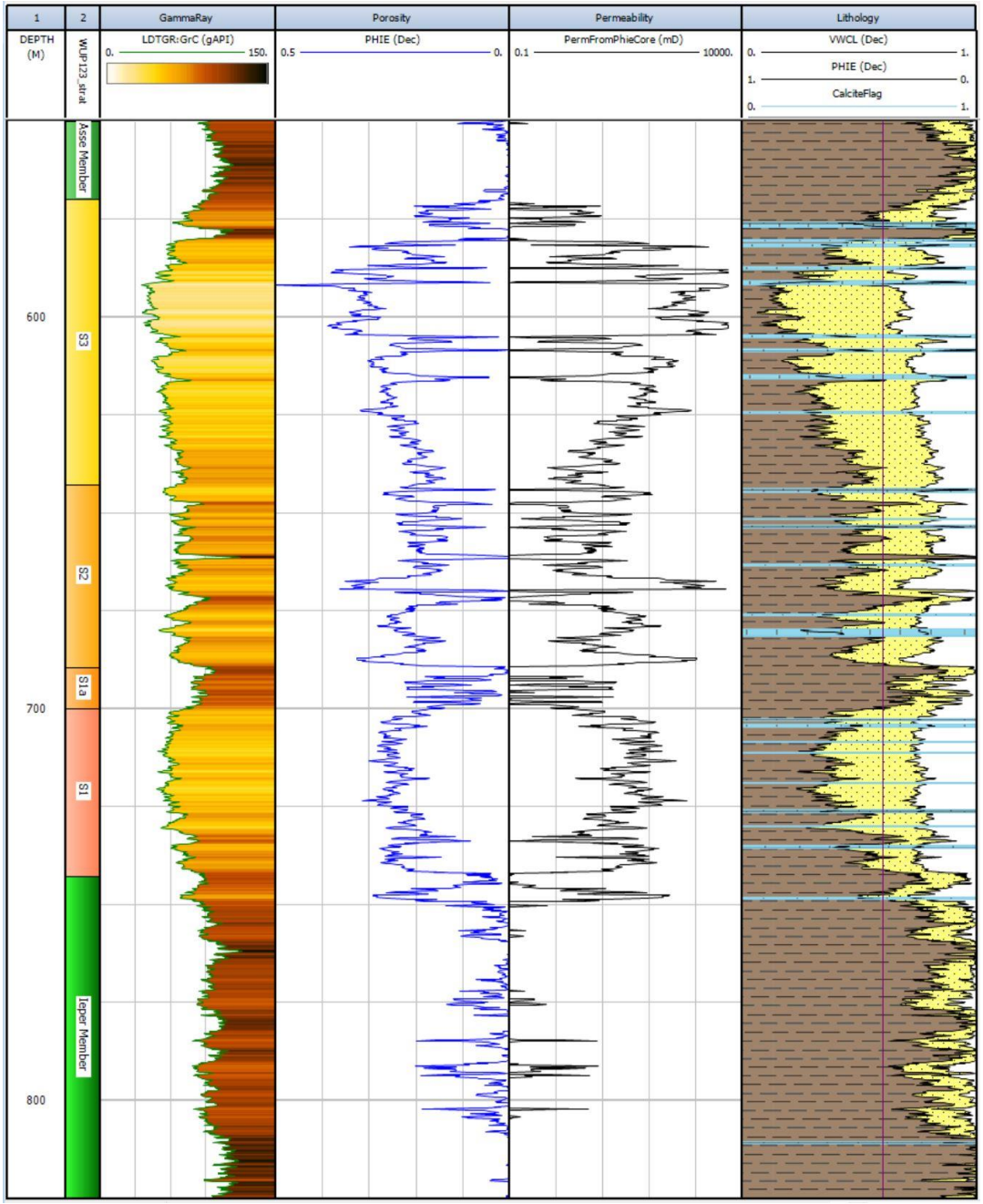

Figure 3-5 Reservoir properties of well BRT-01: Effective porosity (PHIE), permeability (PermfromPhieCore), and lithological composition: clay, sandstone, effective porosity, and carbonate-cemented low-perm streaks.

Internal correlation of the Brussels Sand

The Brussels Sand sequences can be correlated very well in the area (see well correlation panel in Figure 3-6). The thicknesses of the individual units vary only slightly between wells, although all units thin towards the North. Close to the northern limit of occurrence the uppermost units have been eroded. That means that the most permeable and therefore profitable S3 unit is absent close to the northern limit, which gives rise to low average reservoir permeabilities. Reservoir properties as seen in the logs vary only slightly from well to well within correlatable units. This means that the reservoir properties at the Zwijndrecht-Zuid location can be predicted with a reasonable degree of confidence from those observed at surrounding wells.

Appendix B shows well correlation panels for different cross-sections in the area for more detail.

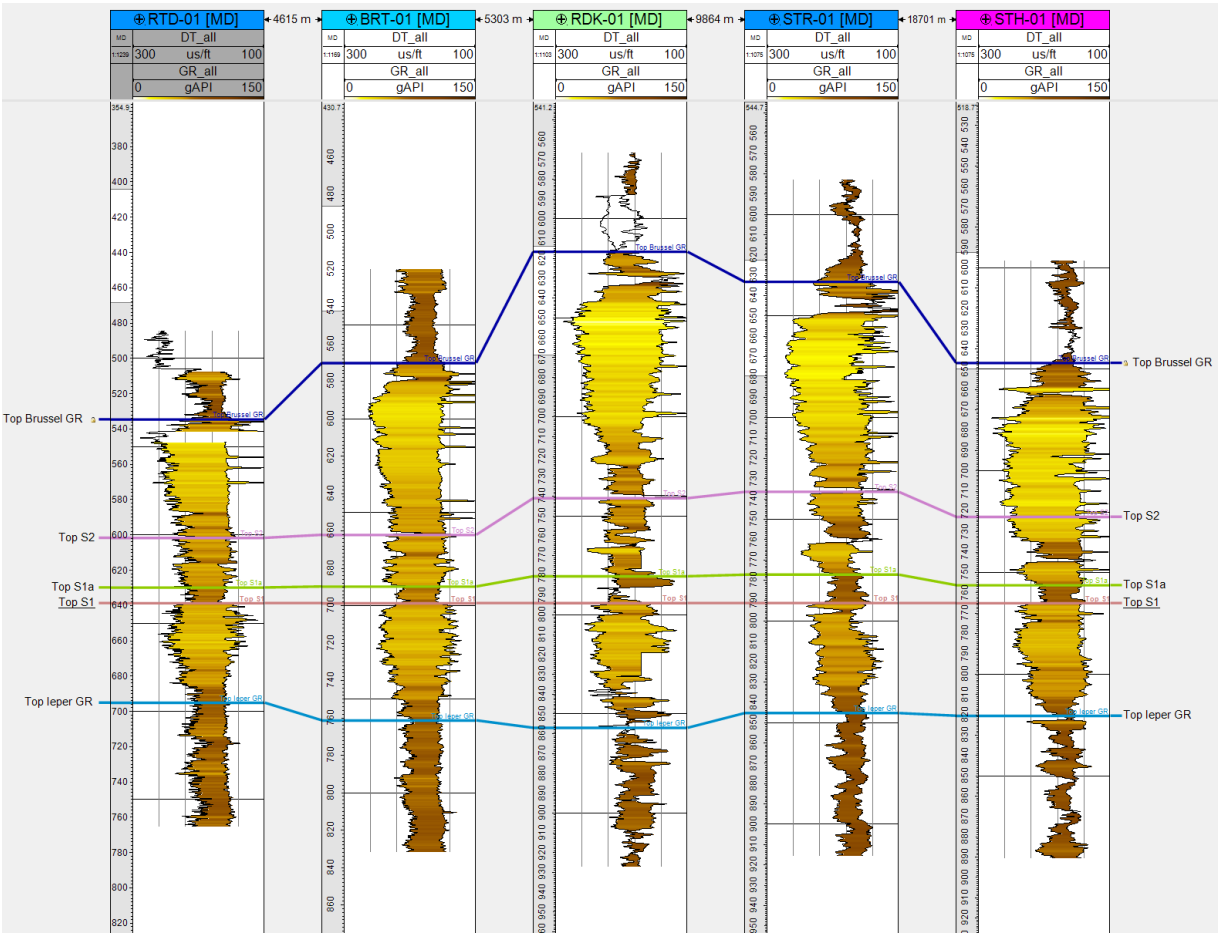

Figure 3-6 Well correlation panel through all the wells in the Zwijndrecht area that have a porosity log. Panel is flattened on Top S1. Location is shown in Figure 3-7.

Figure 3-7 Location of the well panel of Figure 3-6

3.3 3D geocellular reservoir model

Based on a subdivision of the Brussels Sand Mb into 18 units (or zones) of 10-20 m each, a 3D geocellular model was built. Figure 3-8 shows the outline of the model area. The model dimensions are 44 x 33 kilometres. As stated above, it was chosen such to include all 6 wells for which VCL (clay volume), porosity, and permeability are available: RTD-01, BRT-01, RDK-01, STR-01, ZVB-GT-01, and STH-01. With an average grid cell size of 50 x 50 x 1 m, the grid contains around 108 million cells (832 x 658 x 198).

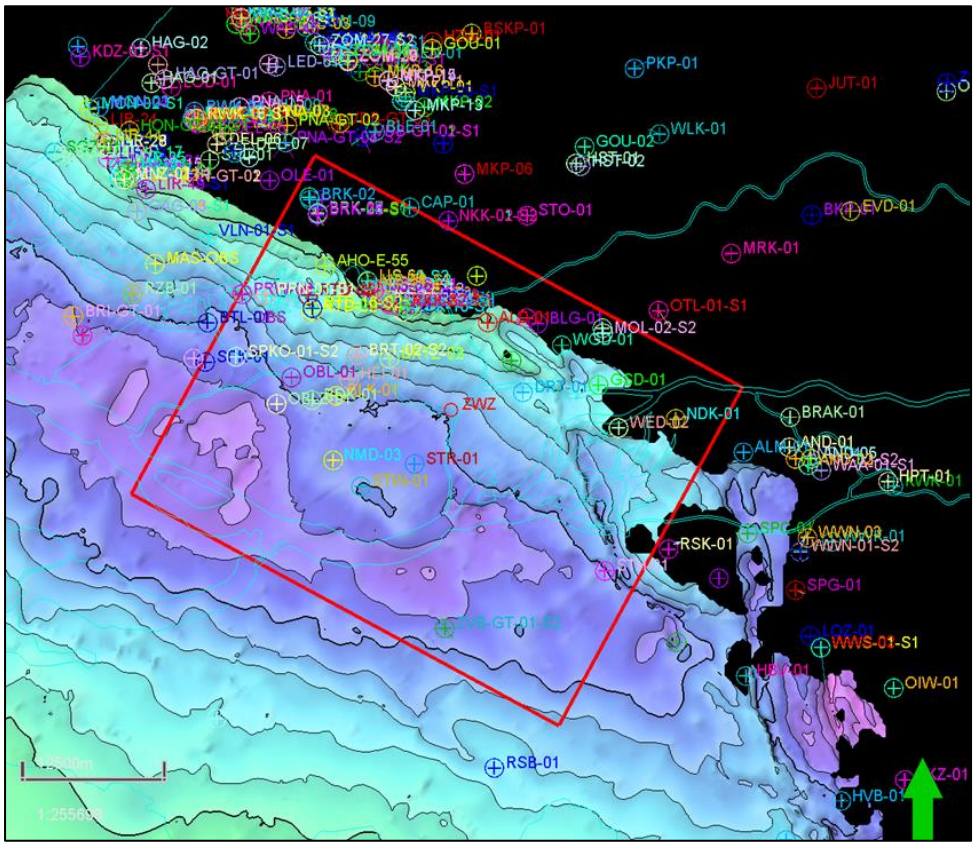

Figure 3-8 Boundary of the model area. Presence (actually a depth map) of the Base S2 reflector is used as background to show the erosion/non-deposition of the Brussels Sand in the central part of The Netherlands in late Eocene times. ZWZ indicates the location of Zwijndrecht-Zuid.

Appendix A contains the details of how the geocellular model was built. The main aspects are as follows:

- The top of the model is a seismic horizon tied to LPS13 (topmost low-perm streak); the base is the base of unit S2, tied to Base S2.
- The layers are modelled with proportional thickness per zone. The number of layers is chosen such that the average grid cell thickness is 1 meter.
- Properties modelled: gamma-ray GR, clay volume VCL, effective porosity PHIE and permeability PERM. Also the presence of calcite-cemented streaks (LPS) is modelled. This is discussed separately below.
- The properties are modelled as continuous variables with Kriging, with a NW-SE elongated variogram and strike NW-SE, in accordance with the geology: both paleo-coastline and basin axis strike NW-SE. Correlation ranges were 24 km in SW-NE direction and 10 km SW-NE direction (Figure 3-9). The correlation ranges are taken large because changes are expected to be gradual for a shallow marine shelf sand. For the permeability the distribution was log transformed as is commonly done for permeability. In additional the data were 'normal scored' to improve the representation of the well log data. After simulation, the permeability was maximized on 5000 mD to avoid unrealistic spikes in the permeability.

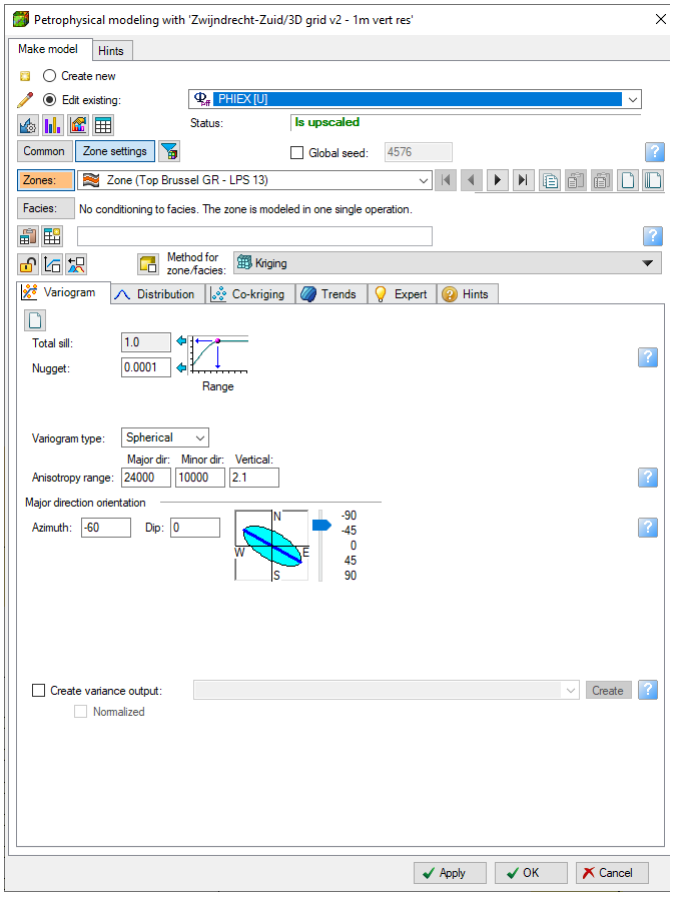

Figure 3-9 Example of the population of the reservoir model. The Gamma Ray property was distributed in the model using Kriging with a NW-SE elongated variogram with correlation ranges 24 and 10 km.

The calcite-cemented low perm streaks

Apart from the gamma ray, porosity and permeability one additional property was modelled: the presence of thin calcite cemented layers as Low Perm Streaks (LPS). As illustrated in Figure 3-5, calcite-cemented, low permeability streaks are abundant throughout the Brussels Sand. As shown in Geel and Foeken (2021), the average interval thickness between streaks is about 5 m in the Zuid-Holland - Zeeland region, while the average LPS thickness is 0.2 m. If these streaks are laterally continuous, they form effective barriers to vertical flow. A more detailed discussion on these calcite-cemented low perm streaks is given in Geel & Foeken (2021).

The streaks are modelled in two ways: as a continuous variable (LPSC) and as a binary variable (LPSX). The continuous variable LPSC is upscaled from the integer well log property "CalciteFlag", which indicates the presence of calcite, to the 1 m vertical scale using "arithmetic averaging" upscaling. The integer variable LPSX is upscaled using "maximum" upscaling, meaning that it will be 1 as soon as some calcite is present. Thus LPSX indicates the presence of a tight calcite cement layer as 1 (present) or 0 (not present). For modelling the property in the 3D geocellular reservoir model indicator kriging was used. The variogram chosen was the same as for the other properties. The choice for kriging as modelling method means that far away from the wells (i.e. further than the correlation range), the value of any property tends to the average value. For LPSX this is 0 (no calcite present). Thus the LPSX property can only be used in the vicinity of the wells. For the Zwijndrecht area this condition is met, since the location is surrounded by wells. South of Zwijndrecht however, where wells are almost absent, both variables (LPSC and LPSX) predict the complete absence of calcite-cemented streaks, a highly unlikely scenario (see Figure 3-13). Care should therefore be taken with the use of these properties in the southern part of the model area.

To account for the uncertainty in the lateral extent of the calcite-cemented layers, additional (10) realizations were created for the production estimation. This was done using sequential indicator simulation with different variogram settings. In this case, simulation was chosen rather than kriging, because with simulation different realizations can be created by changing the seed used in the simulation. The ranges of the variogram were reduced by a factor 4 compared to the other simulations, resulting in 3000 m, 1325 m and 2 m in x, y and z-direction respectively with an azimuth of -60° (same as before). The reason for this is to allow for more variability in the presence of the layers, to better represent the uncertainty.

3.4 Results

Figure 3-10 to Figure 3-13 show 3D views of the modelled properties. The modelled properties are spatially distributed with very gradual changes, in accordance with the expectations for a shallow marine shelf sand. From the 3D model a series of synthetic logs were generated for the future well "ZWZ". Figure 3-14 shows the gamma-ray and porosity logs in a well panel with neighbouring wells. The logs shown in these wells are actually upscaled versions of the real well logs.
The permeability log in well ZWZ was integrated to produce a (pseudo-) cumulative flow profile for the well. Figure 3-15 shows synthetic GR, LPS, PHIE, PERM, and cumulative PERM logs.
From the permeability log, but especially from the cumulative permeability log, it is clear that:

- 90% of the flow is delivered by unit S3;
- The upper 40 m of S3 delivers 70% of the flow;
- The contribution of unit S1 is negligible.

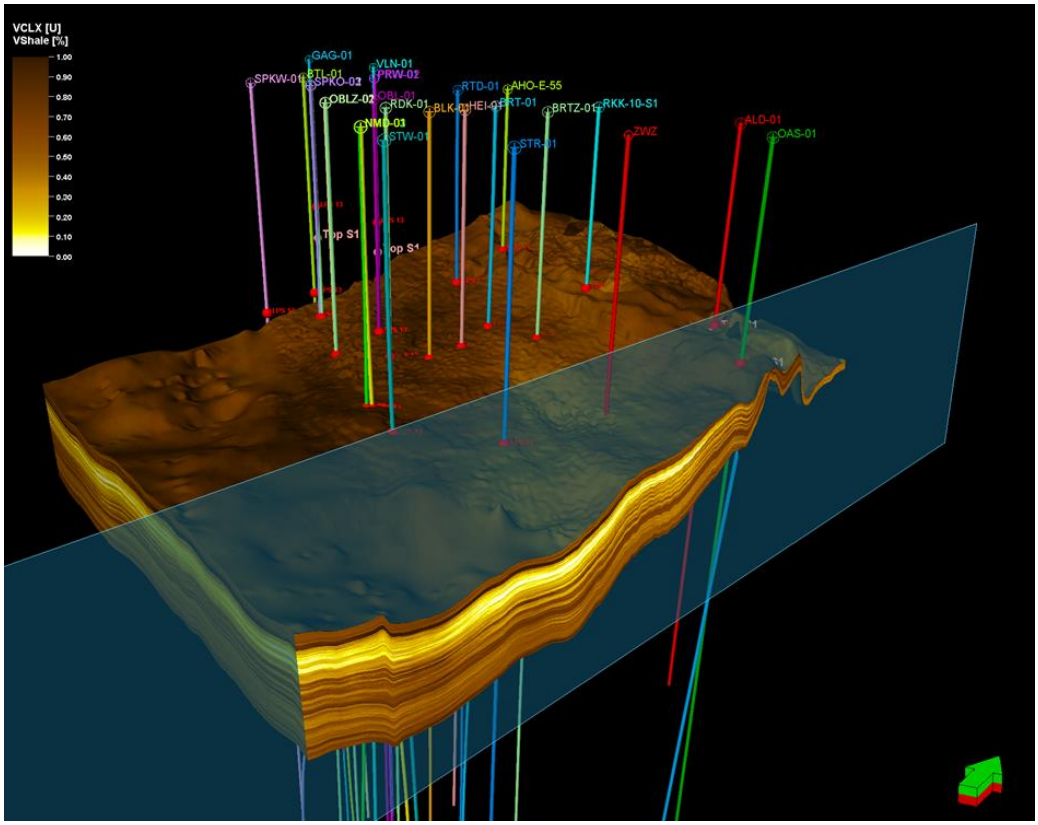

Figure 3-10 3D view of the reservoir model. The property shown is the Clay content (VCL). The proposed doublet location is indicated by the red well labelled “ZWZ”

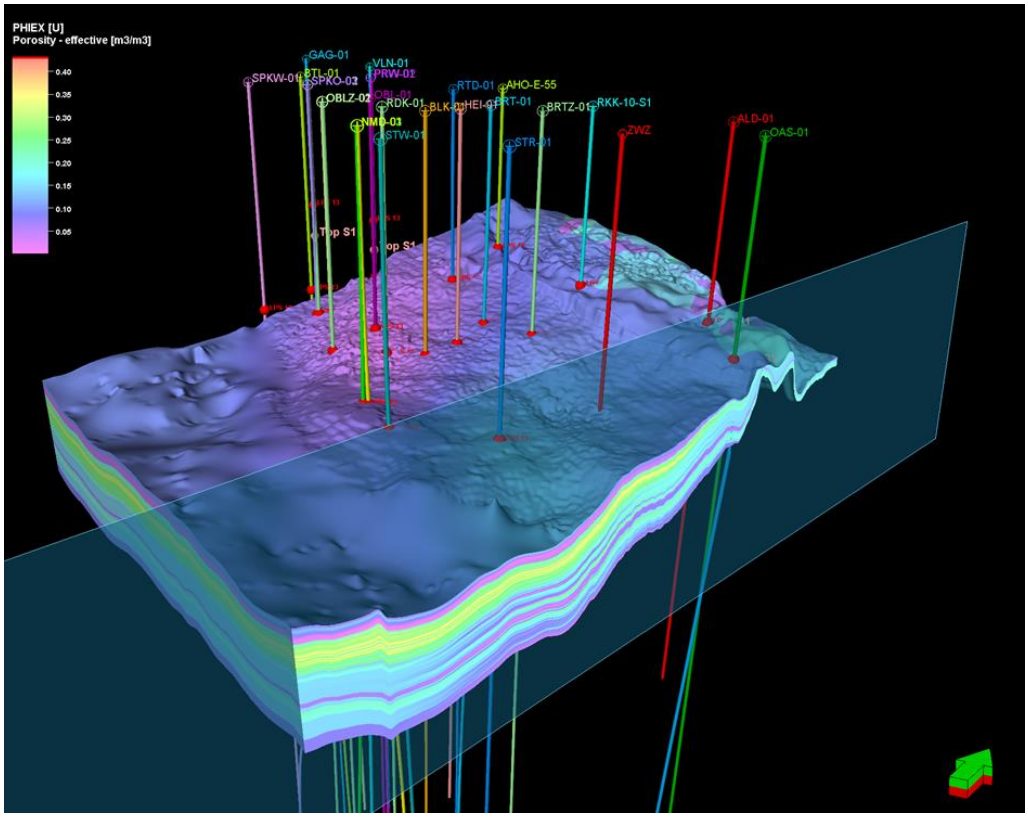

Figure 3-11 3D view of the reservoir model. The property shown is the effective (clay-free) porosity (PHIE).

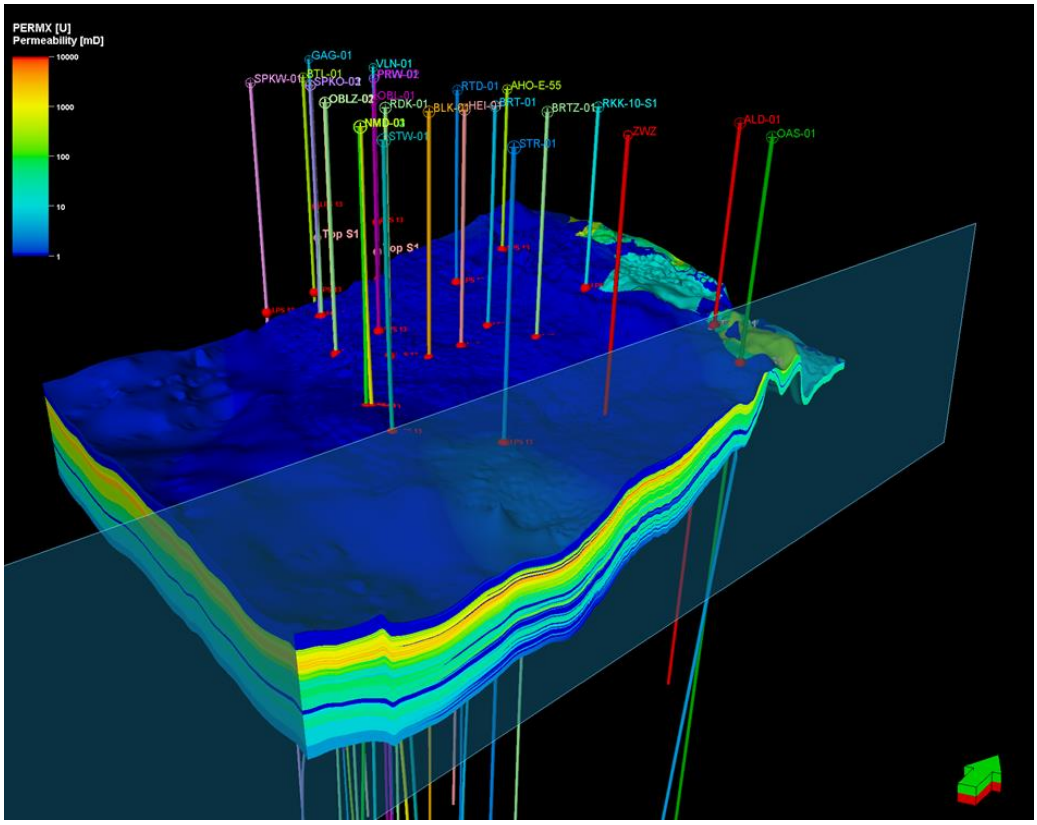

Figure 3-12 3D view of the reservoir model. The property shown is the permeability (PERM).

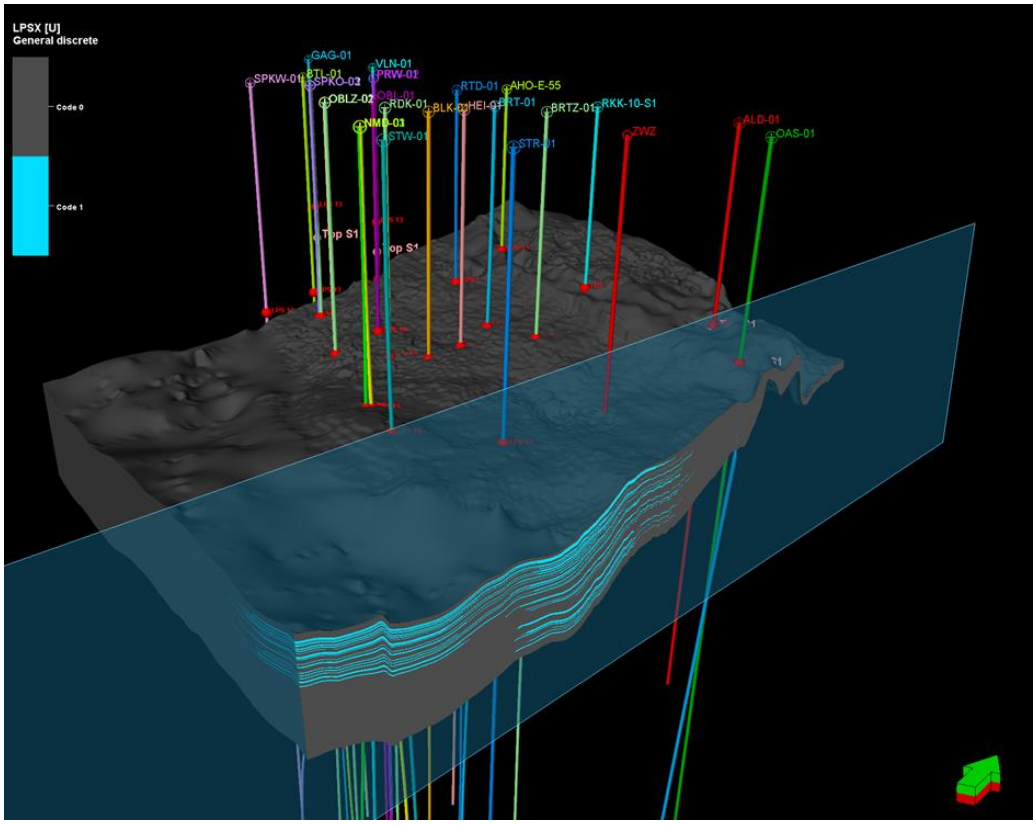

Figure 3-13 3D view of the reservoir model. The property shown is the presence of calcite-cemented streaks (low-permeable streaks or LPS).

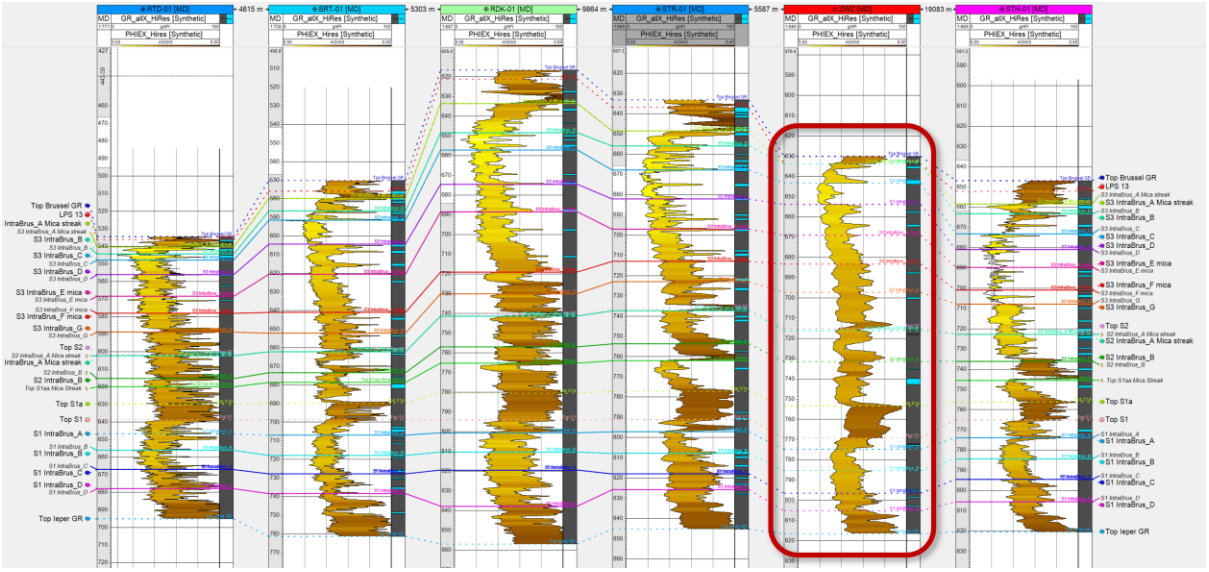

Figure 3-14 East-West well panel with synthetic GR, PHIE, and LPS logs extracted from the geocellular reservoir model. Potential well ZWZ is indicated by a red rounded rectangle.

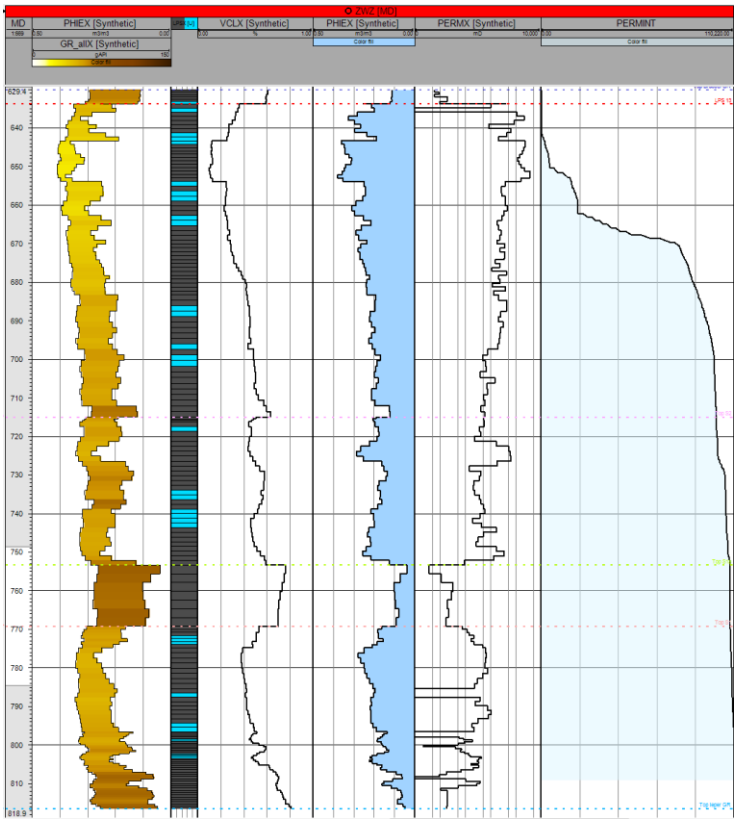

Figure 3-15 Potential well ZWZ with synthetic GR, LPS, VCL, PHIE, PERM, and cumulative permeability (PERMINT) logs extracted from the reservoir model.

Figure 3-16 shows the gross thickness (A) and net transmissivity (product of net thickness and permeability) (B) maps of the regional model. Also indicated are the wells used for the property modelling of the permeability. The maps show the largest thickness in the west of the model. This thickness is well constrained by the seismic interpretation and the wells in Table 3-2. The best transmissivity is found in the area around STR-01, which is due to the higher permeability in this well. The distribution of the permeability is much more uncertain than that of the thickness, as the thickness is

based on continuous seismic data whereas the permeability is interpolated from only a few wells. The transmissivity map shows that the permeability outside of the wells is underestimated (see the bull's eyes around the wells). This is also visible in the histogram in Figure 3-17 A. The two bars at the highest values (which determine most of the good quality reservoir) are clearly underrepresented in the modelled (Kriged) results (in blue) compared to the original well logs (in red). For the reservoir simulations, it was therefore decided not to use the log transform for modelling the permeability. The histogram in Figure 3-17 B (right side) and the transmissivity in Figure 3-18 show the resulting distribution without the log transform.

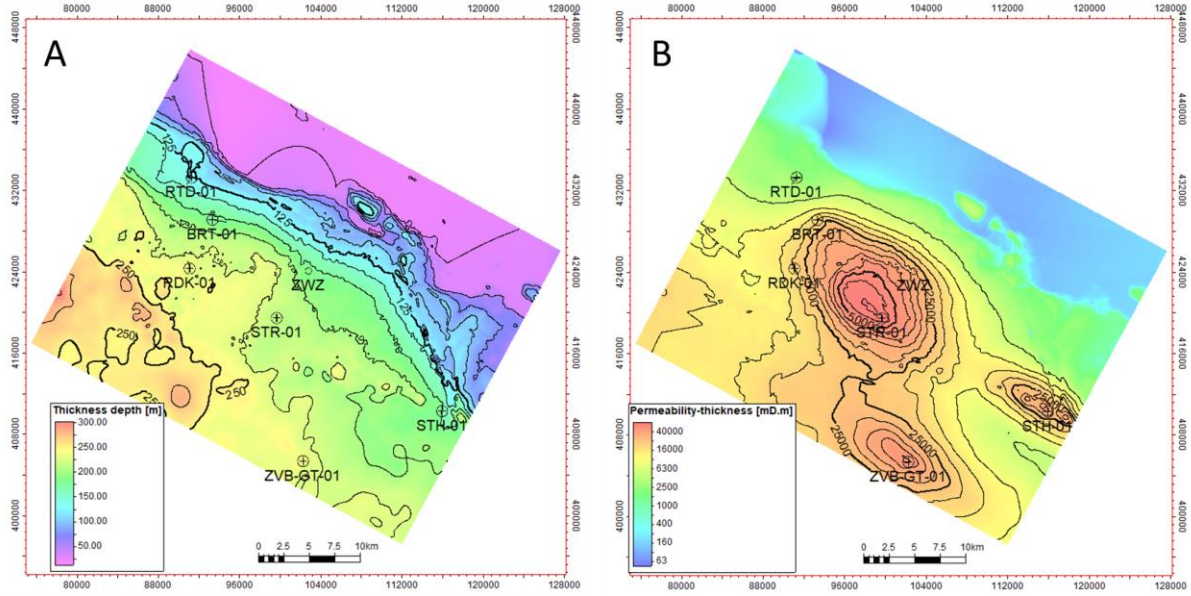

Figure 3-16 Gross thickness (m, left) and net transmissivity (permeability x net thickness) (KH in mDm, right) of the regional model. Wells with permeability logs are indicated. ZWZ indicates the location of the potential well at Zwijndrecht Zuid.

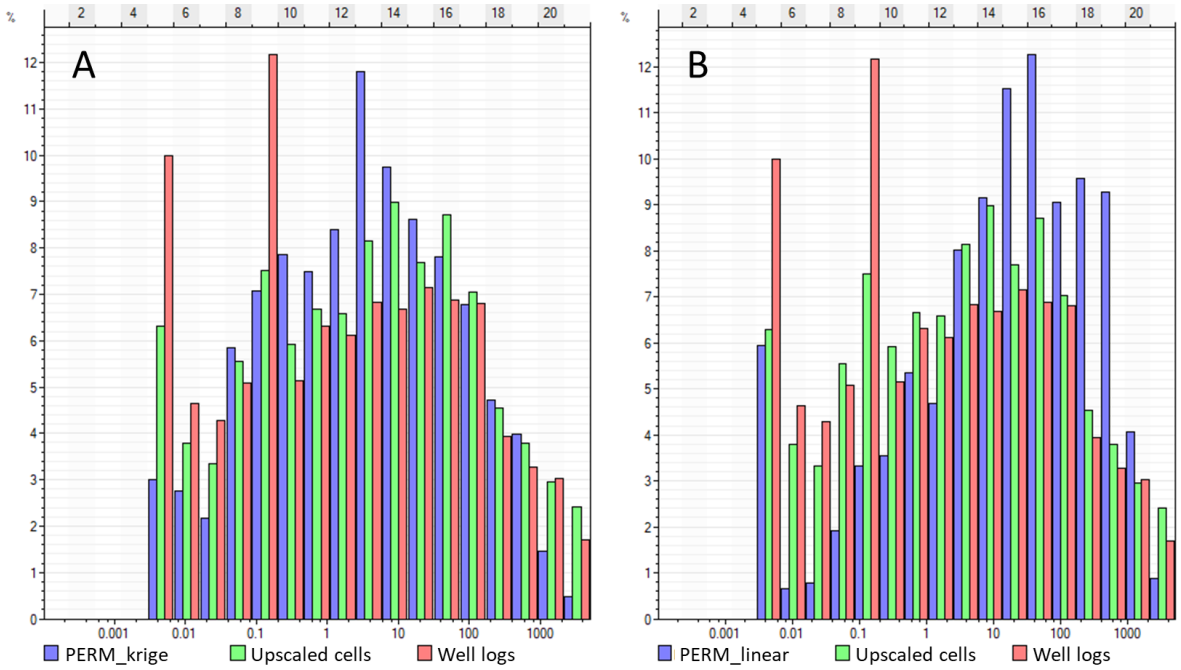

Figure 3-17 Histogram of the kriged permeability with log transform (A) and without (B). In red are the well logs, green the upscaled well logs and in blue the kriged values

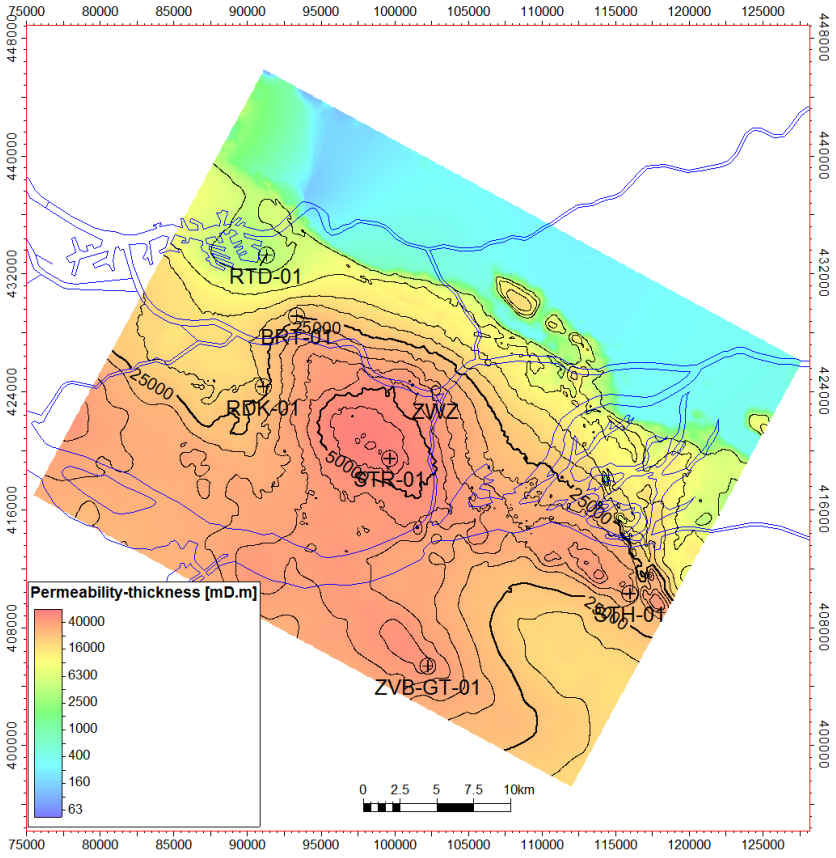

Figure 3-18 Net transmissivity (permeability x net thickness) (KH in mDm) of the regional model including the wells with permeability logs with permeability kriged as a linear property. Blue lines indicate water ways. ZWZ indicates the location of the potential well at Zwijndrecht Zuid.

3.5 Discussion and conclusions

A regional geological reservoir model of the Brussels Sand Member has been created for the region around Zwijndrecht with dimensions 44 x 33 km x 300 m. Due to good quality seismic data and well correlatable units, the residuals of the tie of the surfaces interpreted on the seismic data and the well tops was generally below 10 m. Also, faults with an offset above the seismic resolution were not observed. Therefore, the uncertainty in the depth and thickness of the model is relatively small. The number of wells with logs suitable for the estimation of the reservoir properties is only 6 in the entire model area. Thus, the uncertainty in the properties is considerable. The spatial variation of the transmissivity in Figure 3-16 shows that at STR-01 a higher value of permeability is estimated than in the other 5 wells. This is due to a 10-m thick layer of very high porosity which contains only 1 calcite-cemented streak. This results in a transmissivity which is more than 50% higher than in any of the other wells (64 Dm). Because the quality of the logs in STR-01 is moderate (Geel and Foeken, 2021), this permeability is possibly overestimated. On the other hand, the well RDK-01 seems to lack such a layer and has an estimated transmissivity of only 22 Dm. The transmissivity of the wells BRT-01, STH-01 and ZVB-GT-01 is in between. Well RTD-01 has poor reservoir quality because it is located too far to the North-West, where the Brussels Sand becomes thinner and the good quality top layer has been eroded. The transmissivity at the potential well location in Zwijndrecht Zuid is 38 Dm, which is close to the average of the other wells (excl. RTD-01).

4 Dynamic Reservoir Simulation

In this chapter, the inflow performance of different well designs is investigated. The goal is to understand the performance of the reservoir given the uncertainty in the reservoir properties for different well orientations rather than estimate the optimal well design for a specific location.

4.1 Dynamic input data

Based on the regional static model, local reservoir simulation models can be made with the required size, which is generally smaller than the regional model. In this study only a single doublet will be simulated and therefore the reservoir size was chosen as 6 by 6 km. This size is sufficient to have negligible impact of the boundary on the doublet performance. Since no barriers to horizontal flow have been identified in the seismic data (Chapter 2), model boundaries should not affect the performance of the doublet. First a more general analysis is done with basic well designs which do not consider drillability of the well path, next more realistic well designs created by WEP (Blinovs and van Og, 2022) are simulated.

Most properties of the grid blocks (porosity, net to gross (N/G) and horizontal permeability) were taken from the static model described in Chapter 3, except for the vertical permeability. Estimating the vertical permeability is challenging because of the calcite-cemented streaks. This will be discussed in the next paragraph. The horizontal permeability for the basic well designs is the permeability estimated using kriging from Chapter 3. For the WEP designs, the horizontal permeability is simulated using Gaussian simulation. Kriging results in a smooth, interpolated permeability distribution with average permeability outside of the range if influence of the measurements. Gaussian simulation results in a property distribution which reproduces the complete distribution (or histogram) of the measurements, resulting in a far less smooth distribution of the properties (see Figure 3-17 for the impact of kriging on the histogram). More details are given in Section 4.3.3. Table 4-1 gives an overview of the additional input values for the reservoir model.

Table 4-1. Input for the reservoir simulation model of a potential doublet near Zwijndrecht

Variable	Value
Model size	6 x 6 km
Horizontal grid resolution	50 x 50 m
Fluid density and viscosity @ salinity = 38 g/kg	(Batzle and Wang, 1992)
Rock heat capacity	2700 kJ/m^3/K (Robertson, 1988)
Fluid heat capacity	4 kJ/kg/K (Grunberg, 1970)
Thermal conductivity of the saturated rock	180 kJ/m/d/K (Eppelbaum et al., 2014; Clauser, 2011)
Reservoir temperature	10 °C + 0.032 °C/m * depth [m]
Reservoir pressure	60 bar @ 600 m TVD
Well diameter	0.19 m
Length of inflow section	Vertical and deviated: entire reservoir depth of unit S3 (sub-)horizontal wells: variable
Well distance at reservoir depth	Basic designs: 1250 m ; WEP designs: variable
Max injection pressure	Basic designs: 14.5 bar ; WEP designs: 16 bar

Max drawdown @ producer	Basic designs: 10 bar ; WEP designs: 14 bar
Max. flow rate	Basic designs: 150 m^3/hr; WEP designs: 200 m^3/hr
Injection temperature	8 °C

All simulations are done with Eclipse (E100) with the TEMPERATURE option. This is a simplified thermal modelling approach, which does not solve the fully-coupled hydrothermal equations, but deals with temperature as if it is a tracer. This means that the properties depending on temperature are updated the next time step. Only viscosity is changing as a function of temperature and not density. If time steps are taken reasonably small (10 to 20 days), this approach achieves acceptable results for low-enthalpy geothermal systems.

The horizontal resolution is relatively coarse at 50 x 50 m. The horizontal resolution affects the transient behaviour of the wells more than the steady state behaviour which we are interested in here. Sensitivity runs indicated that the steady-state behaviour changes a few percent at most, with the largest changes observed for the deviated well.

The pressure constraints for the injector are based on the protocol by State Supervision of Mines (SodM) for determining the maximum injection pressure. The top depth of the formation is 620 m TVDSS. Using the gradient of 0.135 bar/m, maximum injection pressure would be 83.7 bar. Since the bottom hole pressure without flow is 62 bar, this would results in an allowable overpressure at reservoir depth of 21.7 (less at the well head). The Zevenbergen doublet using a maximum value of 17 bar at the wellhead (Geobrothers BV and Visser & Smit Hanab BV, 2020). For the Brussels Sand Mb, the seal is mostly the Asse Mb, which is unconsolidated to poorly consolidated clay and expected to be approximately 35 to 40 m thick (see well Barendrecht-01 in Figure 2-2). A little to the north-east of Zwijndrecht, the Asse Mb has been eroded and the bottom of the Rupel Fm is on top of the Brussels Sand Mb. The lower part of the Rupel Fm in this area is the Berg Mb (formerly Vessem Mb), which is mostly sandy. For the basic designs, a large safety margin was assumed and a maximum injection pressure of 14.5 bar (downhole) was taken. For the producer a maximum drawdown of 10 bar was used. These choices are very conservative and larger values may be possible, however they only affect the absolute flow rate and not the productivity/injectivity index estimates. For the more detailed well designs in Section 4.3.2, less conservative values were used, namely 16 and 14 bar respectively for the injector and producer. The results in this report are mostly presented as productivity or injectivity index, which is calculated as:

$$PI = \mathrm{abs}\left(\frac{Q}{BHP - BHP_{ini}}\right)$$

Where
Q : rate (m^3/hr)
BHP : bottom hole pressure (bar)
BHP_{ini} : initial BHP without production (bar)

For the simulations in this report, the pressure drop inside the well was not included. This means that only the pressure drop in the reservoir is accounted for.

To ensure that all pressure constraints are met and that the entire produced volume can be re-injected, the well constraints were taken as follows. If the injector was the most constraining (which it usually is due to the impact of the high viscosity of cold water), the producer was run in production balancing mode (PRBL keyword in Eclipse). In this case, first the injectors are solved and this rate is used as constraint for the producer. In case the producer has the lowest productivity, the injector was run on a

re-injection constraint which forces a solution in which the produced volume is re-injected for each time step (GCONINJE keyword with option 8 set to NO (no freedom to respond to higher level targets)).

4.2 Vertical permeability and upscaling

For vertical wells, the permeability in vertical direction (k_v) has little impact on the flow. For deviated or horizontal wells on the other hand, the vertical permeability is also important. Therefore in this section, two questions are addressed:

- What is the impact of the calcite cemented layers on the productivity and how does the uncertainty about these layers affect the uncertainty in the production? This will be evaluated on a model with high vertical resolution.
- How can the calcite cemented layers be represented in models with coarse layers? Some workflows are described to estimate the vertical permeability at the coarser scale. This should lead to a more generic understanding of how the cemented layers can be accounted for in a simulation workflow.

The properties in the regional static model were simulated at three vertical scales: 0.2 m, 1 m and 1 layer per zone. The model with one layer per zone has a vertical grid resolution around 10 to 15 m. An important step towards estimating the vertical permeability is the realization that the vertical permeability k_v in a reservoir model is grid size dependent. The vertical permeability in the Brussels Sand is determined by an alternation of high permeability zones and thin zones with very low permeability. For simulations with a very high vertical resolution (0.2 m and 1 m vertical resolution) it is appropriate to take the thin low permeability layers into account in a simple way: if a calcite cemented streak is present (as indicated by the variable Low Permeable Streak X (LPSX, see Section 3.3)), k_v is low (in this case: 0.01 mD was taken), if no cemented layer is present $k_v = 0.5 * k_h$. This approach reproduced the initial productivity of the Zevenbergen doublet well, which is estimated at ~22 m^3/hr/bar (Geobrothers BV and Visser & Smit Hanab BV, 2020) from well tests. Later productivity/injectivity declined, but it is not clear at this point why.

As a first step the impact of upscaling from the very fine (0.2 m) to the fine (1 m) vertical resolution was tested for a highly deviated well (85°) to compare the impact of the difference in resolution. The results in Figure 4-1 show that the difference is minimal. Therefore in the following only the fine resolution (1 m) is used.

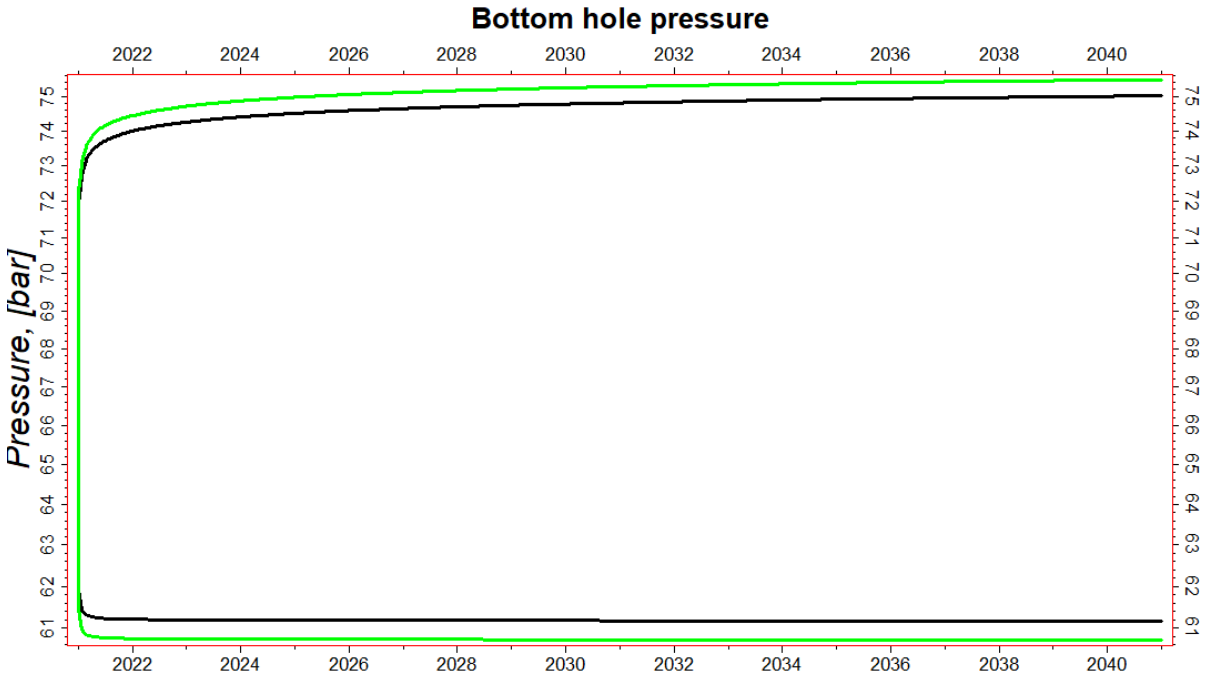

Figure 4-1 Bottom hole pressure for a deviated producer and injector well for fine (1 m, green) and ultra fine (0.2 m, black) layering.

The following workflows were used for estimating the vertical permeability for the coarse scale:

- Flow-based upscaling from the 1-m model. The disadvantage of this approach is that a detailed model has to be created first. Also flow-based upscaling is not easy to perform and not many tools for upscaling include it as an option. Here the implementation in Petrel (version 2020.2) is used.
- A constant anisotropy (k_h/k_v) factor. The value needs to be matched to the fine scale model
- Upscaling the presence of calcite-cemented layers from the well logs as an arithmetic average (LPSC=Low Permeable Streak continuous upscaled; LPSX is the integer property indicating presence of cementation. See section 3.3 for the description of these properties). LPSC values range from 0 to 0.44. An equation of the following shape can be fitted.

$$k_v = 0.2k_h(1 - a\mathrm{LPSC})^b$$

Where *a* and *b* can be fitted to the results from the fine scale model, with the condition that *a**LPSC_max < 1.

To compare the performance of these different approaches for vertical permeability, three well configurations are simulated with the fine scale model and the coarse scale model with the different approaches to k_v:

- A doublet of vertical wells perforated over the entire thickness of the Brussels Sand
- A doublet of highly deviated wells (75°) with a perforated length of 400 m
- A doublet of horizontal wells with a perforated length of 500 m located in the highest permeability layer.

Although the focus is on the upscaling in the vertical direction, the upscaling in the horizontal direction will also affect the results. Therefore first the results for the vertical wells are compared, since these indicate the fit from the upscaling of the horizontal permeability: vertical permeability doesn't influence inflow to a vertical well. The results in Figure 4-2 show the results of the 1-m model and a coarse model based on flow-based upscaling. All models with different vertical permeability have the same horizontal permeability and have the same results for the vertical wells. The productivity/injectivity for the fine

scale model is higher than the coarse model: an averaged permeability tends to underestimate the inflow compared to a detailed vertical resolution. The reduction in productivity is 10% In injectivity it is 9.6%.

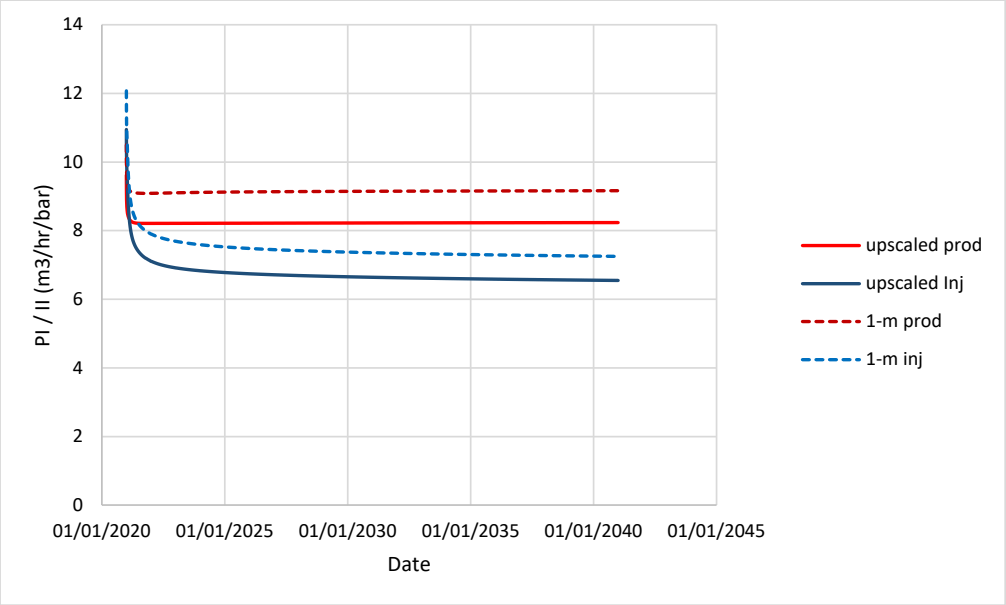

Figure 4-2 Productivity/injectivity for the fine scale 1-m model and an upscaled model for a doublet of vertical wells.

The values tested for the constant approach is $k_h/k_v = 30$ and $k_h/k_v = 50$.
For the approach based on LPSC (averaged presence of calcite-cemented layers) the fitted variable are:

$$k_v = 0.2k_h(1 - 3.5\text{LPSC})^4$$

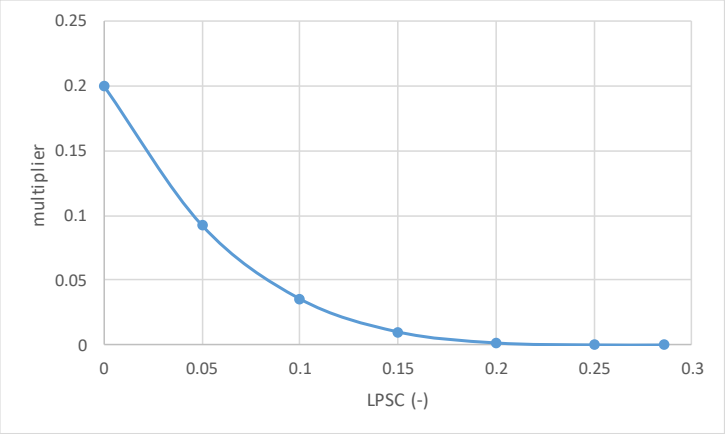

Figure 4-3 Multiplier to calculate kv from kh

For the doublet with deviated wells, all approaches to estimate the vertical permeability perform similar to each other (Figure 4-4), and all are underestimating the productivity/injectivity. The underestimation of productivity/injectivity is larger (18 to 30%) than was seen for the vertical wells (~10%). The results with flow-based upscaling are closest to the fine grid results, followed by the constant anisotropy of 30. The increase due to the deviation of the well is smaller in the coarse model than in the fine model. This suggests that the vertical permeability is under-estimated using the selected approaches. However, for the horizontal well the results are reversed (Figure 4-5). For the horizontal well, the fine scale model has the lowest productivity/injectivity. The results for the constant anisotropy of 50, LPSC and flow-based

upscaling are now very similar. Anisotropy of 30 overestimates productivity/injectivity a lot. From the sensitivity results for the fine scale model, it was clear however that the sensitivity of the horizontal wells to the simulation settings of the vertical permeability is largest. Nevertheless, the horizontal wells produce best in all the simulation approaches. This is the only setup for which the target flow rate of 3600 m^3/d (150 m^3/hr) is achieved.

The results in this section show that the coarser model with grid layer thickness of around 10 m cannot properly reproduce the behaviour of the fine scale model for all well configurations. This is expected to be the results of the high vertical heterogeneity in the horizontal and vertical permeability, which cannot be represented with a coarse grid. The results of the fine scale model are expected to be more accurate and therefore all further simulations were done using the model with a 1 m vertical resolution.

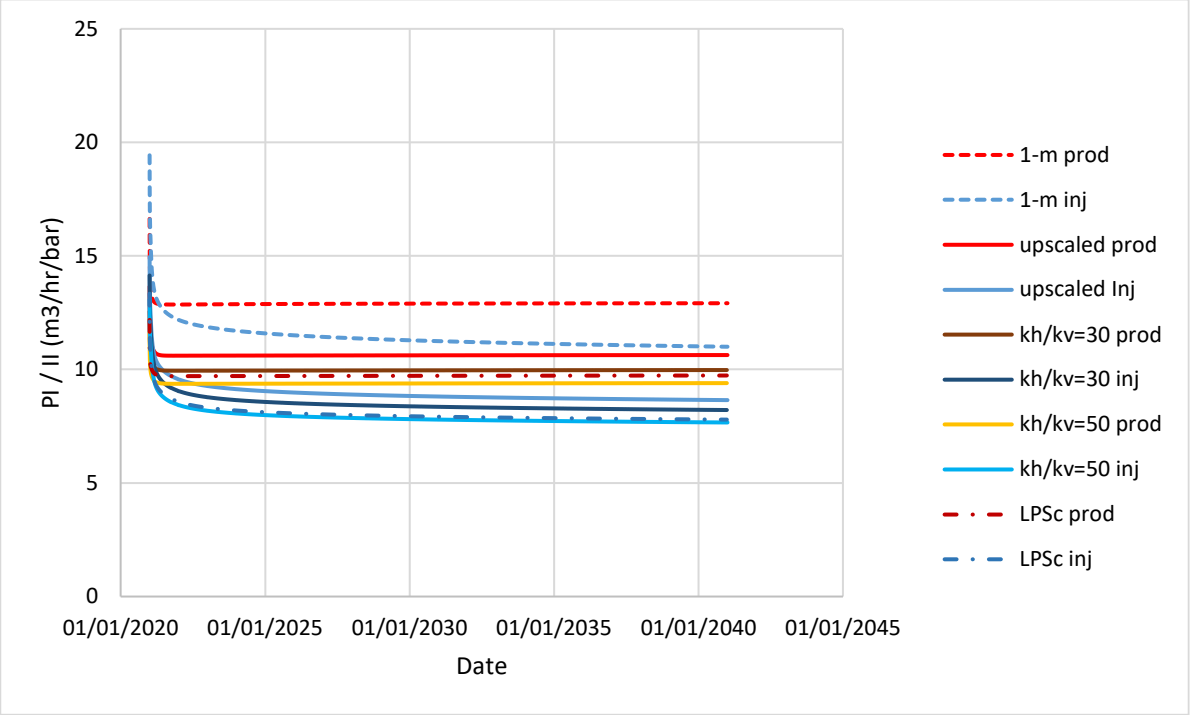

Figure 4-4 Productivity/injectivity for the fine scale model and the 4 approaches to the estimate the vertical permeability for a doublet of deviated wells.

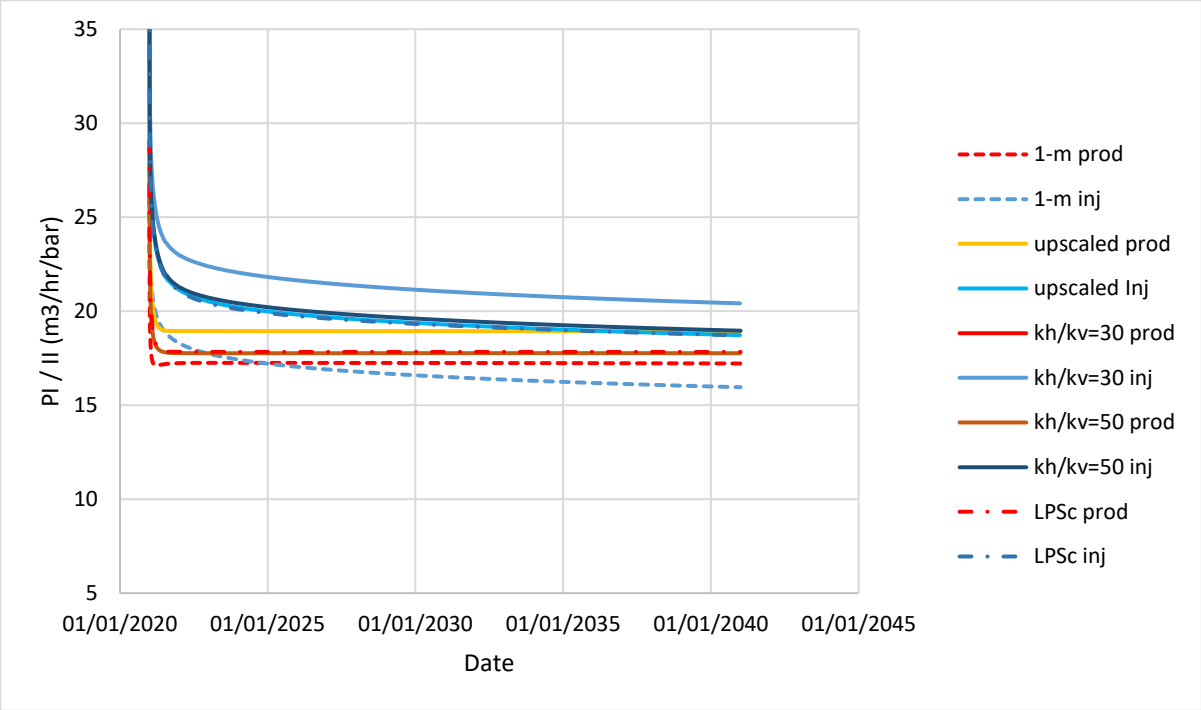

Figure 4-5 Productivity/injectivity for the fine scale model and the 4 approaches to the estimate the vertical permeability for a doublet of horizontal wells.

4.3 Results

In this section, the productivity is estimated for different well designs. First the productivity is estimated for the three general well designs from last section using the permeability estimated in the regional reservoir model (Figure 3-18). The impact of the uncertainty in the vertical permeability on the productivity of these well designs will be analysed in Section 4.3.2. In Section 4.3.3 a number of detailed well designs created by WEP (Blinovs and van Og, 2022) is evaluated, taking into account the uncertainty in both the horizontal and vertical permeability.

4.3.1 Basic well designs

In Figure 4-6, the simulated productivity and injectivity for the three doublets (with vertical, deviated and horizontal wells) for the 1-m model are presented. Although in all cases the injector was placed in the area with better reservoir quality (see Figure 4-7), the injectivity is lower due to the higher viscosity of the cooled water (1.4 cP versus 0.9 cP for the producer). Due to the low vertical permeability, the increase from vertical to horizontal wells is not very large. The productivity increases by 37% and 88% for deviated and horizontal producer respectively. The injectivity increases by 48% and 145% (Table 4-2). The production temperature is 31°C (average over 20 years) for the vertical well, 30.8°C for the deviated well and 30.5°C for the horizontal producer. No thermal breakthrough is observed during 20 years for the well distance of 1250 m for either of the well configurations.

It should be noted that for convenience here two well head locations were selected. In practice, the southerly location would be inconvenient, because it is on the other side of the Oude Maas. Such considerations have not been included in the current analysis.

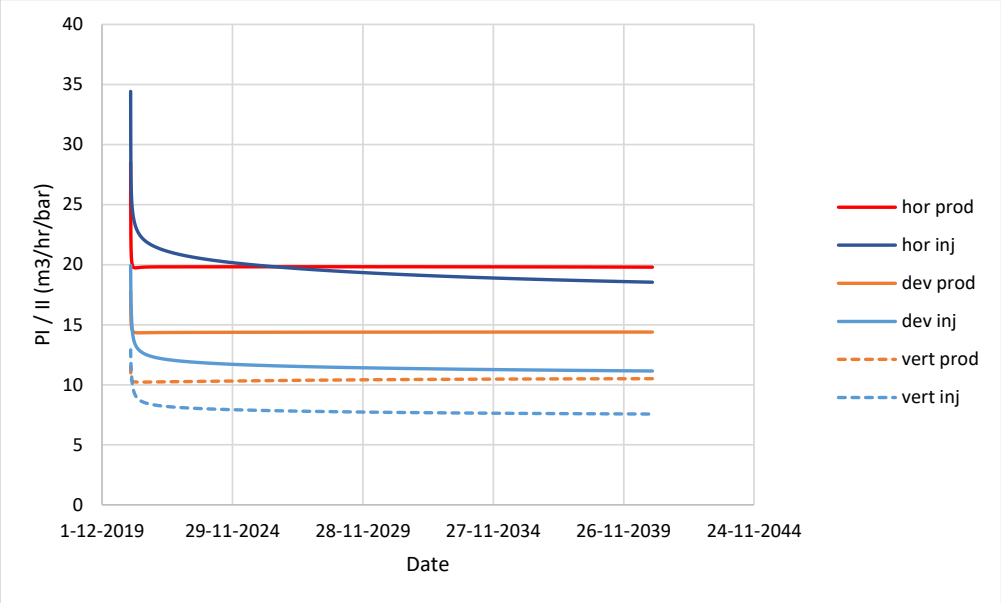

Figure 4-6 Productivity / Injectivity index (m^3/hr/bar) for a doublet with vertical, deviated or horizontal wells for a period of 20 years.

Table 4-2 Overview of the productivity/injectivity (m^3/hr/bar) for a doublet of vertical, deviated and horizontal wells after 20 years.

Well type	Producer	Injector (@ 8°C*)
Vertical	10.5 m^3/hr/bar	7.6 m^3/hr/bar
Deviated (400 m @ 75°)	14.4 m^3/hr/bar (37% increase)	11.2 m^3/hr/bar (48% increase)
Horizontal (500 m length)	19.8 m^3/hr/bar (88% increase)	18.5 m^3/hr/bar (145% increase)

* viscosity at 8°C is 1.4 cP and at 0.9 cP at the production temperature of 30°C.

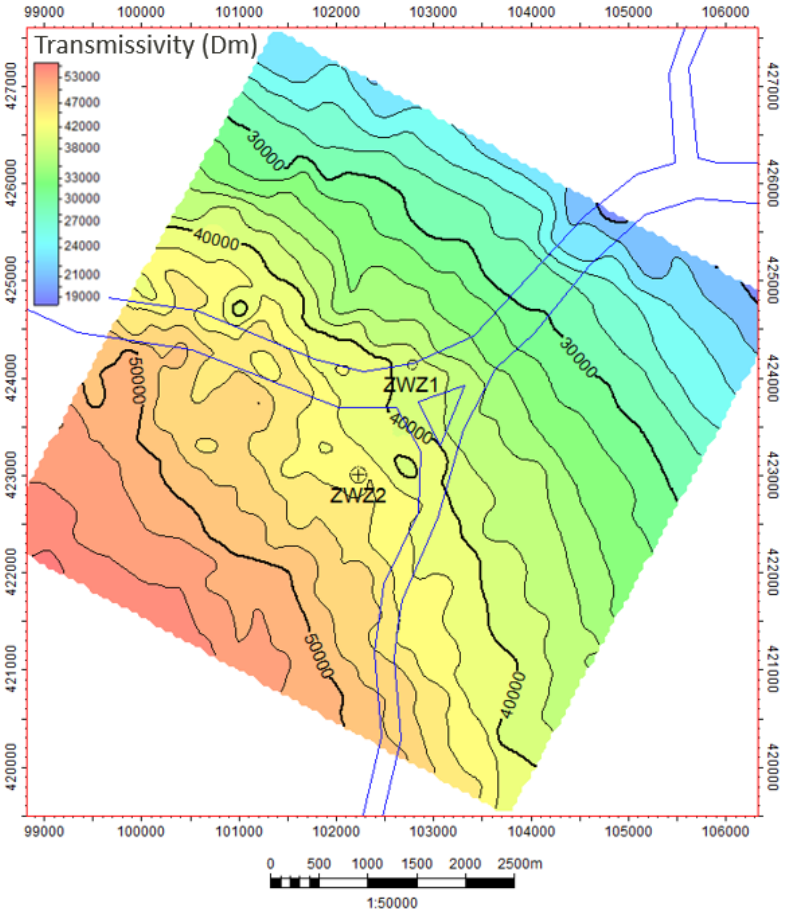

Figure 4-7 Well head position of the vertical producer (ZWZ1) and injector (ZWZ2) and the transmissivity (permeability x net reservoir height). Permeability kriged without using log transform. Thin blue lines indicate major waterways.

4.3.2 Uncertainty vertical permeability

The vertical permeability depends strongly on the interpolation of the presence of the calcite cemented layers. By selecting indicator kriging with a large range, the calcite cemented layers have a very large lateral extent. There is however considerable uncertainty about the lateral extent of these layers (see Section 3.3 and (Geel and Foeken, 2021)). To evaluate the impact of the uncertainty in the lateral extent of the calcite cemented layers, the integer property indicating the presence of these layers (LPSX) was simulated with indicator simulation with a smaller range than used for the base case as described in Section 3.3. The settings for the indicator simulation runs were the same as for the earlier indicator kriging application, but with the ranges of the variogram reduced by a factor 4, resulting in 3000 m, 1325 m and 2 m in x, y and z-direction respectively. One of the reasons for reducing the ranges was the fact that the calcite-cemented layers could not be correlated between wells. This means that their extent might be smaller.

The values of LPSX were translated to vertical permeability as described in Section 4.2: if a calcite cemented streak is present, k_v is low (in this case: 0.01 mD was taken), if no cemented layer is present $k_v = 0.5 * k_h$. For both the deviated and horizontal wells, 10 realisations were run. The resulting productivity and injectivity after 20 years are shown in Table 4-3. The variability in the productivity/injectivity of the deviated wells are modest. For the horizontal wells, the variability is large with a range in injectivity of almost 100% from only 10 realisations. These differences are caused by the variability in the vertical permeability only. The averaged productivity/injectivity of both the deviated and horizontal wells is lower with this workflow than for the kriging results (compare Table 4-2 and Table 4-3).

The transmissivity KH of the formation at the locations of the vertical wells near Zwijndrecht is around 40 Dm. Just south of this area the KH is larger (see Figure 3-16) reaching up to 57 Dm. So moving the wells further south could improve their performance. It should be taken into account however, that this higher transmissivity is determined mainly by the higher permeability in well STR-01. Since this is based on a single well, the uncertainty is large.

Table 4-3 Productivity/injectivity* (m^3/hr/bar) from 10 realizations of the vertical permeability based on of the distribution of the calcite cemented layers.

	Mean (m^3/hr/bar)	Standard dev. (m^3/hr/bar)	Min (m^3/hr/bar)	Max (m^3/hr/bar)
Deviated well productivity	12.7	0.5	11.9	13.4
Deviated well injectivity	10.7	0.6	10.0	11.6
Horizontal well productivity	15.7	2.9	11.7	19.2
Horizontal well injectivity	15.4	3.7	11.5	22.2

* Please not that these simulations were done with a slightly different version of the model (in particular NG) than used in the other simulations. However nothing was changed in the vertical permeability modelling.

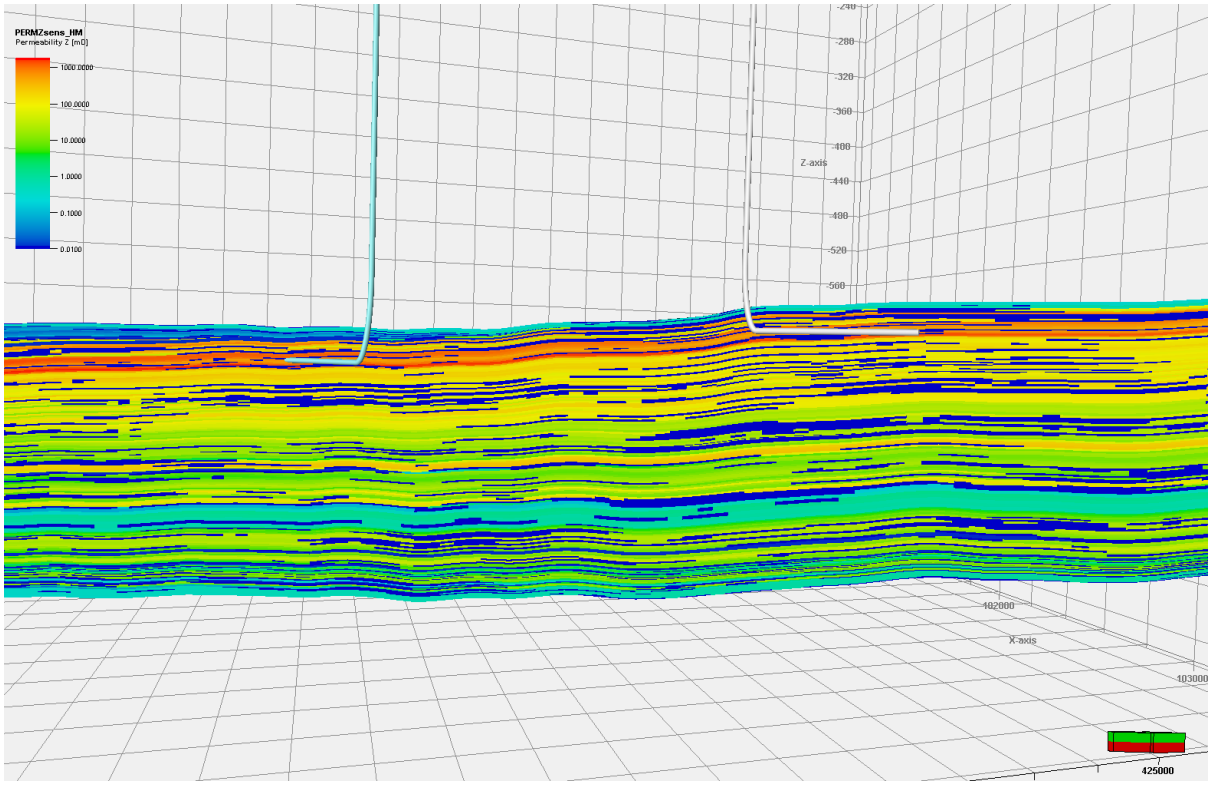

Figure 4-8 Position of the horizontal wells and a realization of the vertical permeability (vertical axis is exaggerated 5x).

4.3.3 Well designs from WEP

In this sections, the productivity and injectivity of the well designs as described in (Blinovs and van Og, 2022) are simulated. These designs take into account the limitations resulting from constraints on drilling.

The uncertainty in the permeability (both in horizontal and vertical direction) is taken into account by running 14 realizations. This relatively small ensemble size was selected to keep the simulation time manageable. This ensemble size is too small to reproduce the full uncertainty, but enough to provide

reasonable estimates. The uncertainty in the horizontal permeability is incorporated by using Gaussian simulation instead of kriging. The ranges of the variogram for the Gaussian simulation are taken identical to the ranges used for kriging of the properties (see Section 3.3), namely 24 km, 10 km and 2 m (Figure 3-9). The distribution (here: histogram) to be reproduced in the simulation is the distribution taken from the upscaled logs. The uncertainty in the vertical permeability is simulated in the same way as in Section 4.3.2. Please note that the simulation of the horizontal permeability and the LPSX property used for the vertical permeability are simulated on the regional model and not on the simulation model, because they are based on the well logs of the wells inside the model area. The 6 x 6 km simulation model does not contain any wells.

The production settings for determining these results were changed compared to earlier settings. The rate was maximized on 200 m^3/hr, the maximum pressure increase due to injection was taken as ~16 bar and the maximum drawdown as ~ 14 bar to get a less conservative estimate. The values can vary a bit, because in fact absolute values were used and the bottom hole pressure changes slightly with the depth of the top of the inflow section . The outer diameter for all wells is 8.5 inch. The pressure drop inside the wells is not accounted for in these simulations. Only the productivity/injectivity of the reservoir part is estimated. The largest pressure drop is expected for a rate of 200 m^3/hr and temperature of 8°. If the rate is 200 m^3/hr, the pressure drop in the horizontal part of the well (750 m, 7 5/8 inch liner with roughness 2mm) is around 1 bar.

The following well designs were simulated:

- Vertical wells: 850 m distance between injector and producer; ~65 m reservoir section (Figure 4-9)
- Deviated wells: 750 m distance at the top of the reservoir; 65° inclination; ~140 m reservoir (Figure 4-9)
- Sub-horizontal wells with 90° angle: 530 m at the start of the inflow section; 1600 m at the end of the inflow section (Figure 4-10).
- Parallel sub-horizontal wells with 850 m distance (Figure 4-10).
- Parallel sub-horizontal wells with 1250 m distance (Figure 4-10).

Please note that in the simulation the wells are always moved to the center of the gridblock that the well is located in. The length of the inflow area is 750 m for all sub-horizontal well designs. The sub-horizontal wells have an inclination of ~88° and cross the 30 m best performing part of the reservoir. All wells are orientated in the direction of the deeper and thicker part of the reservoir.

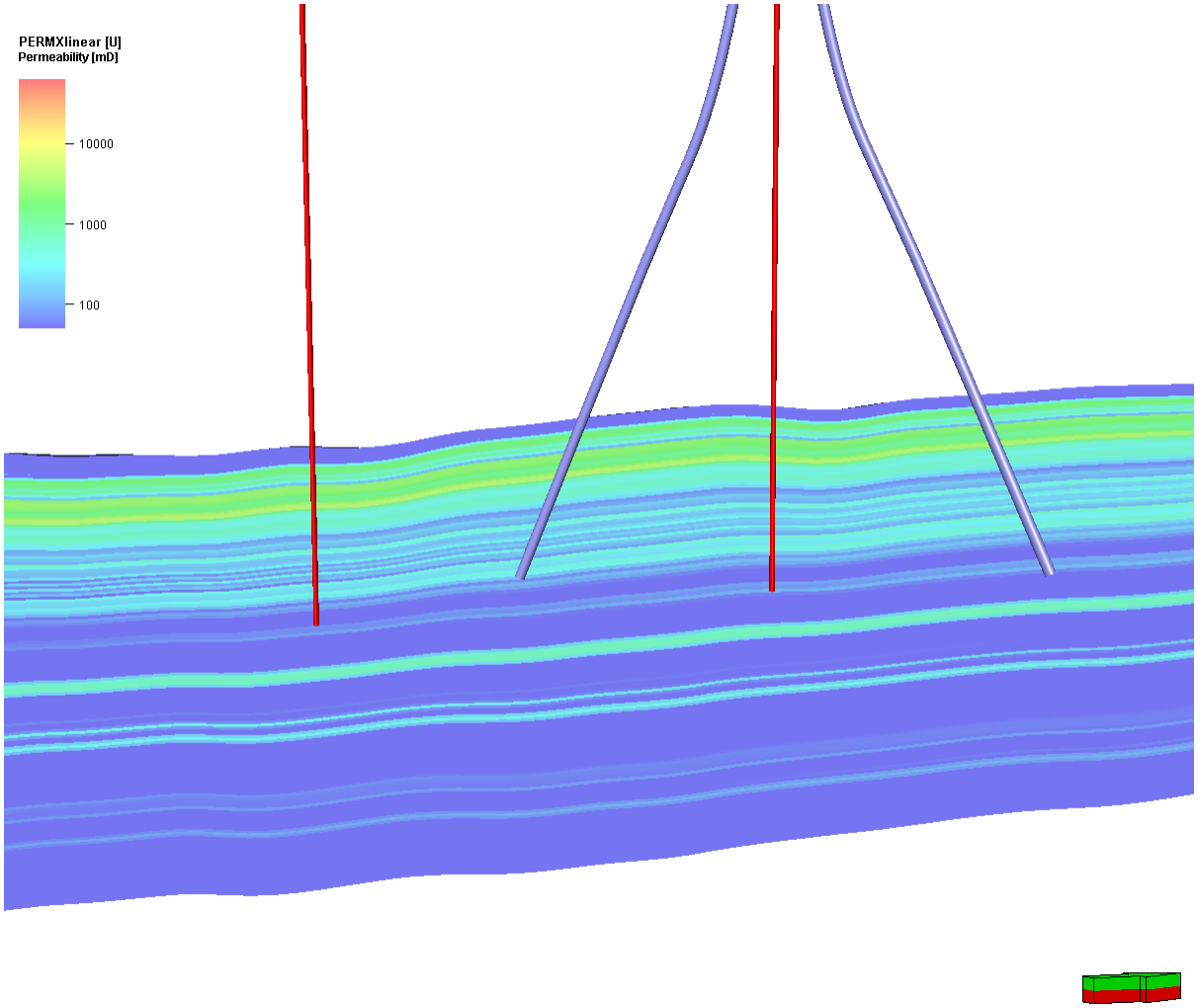

Figure 4-9 Illustration of the vertical and deviated well design (side view, vertical axis x5). Property shown is the base case permeability. In the wells the entire reservoir section is open to flow.

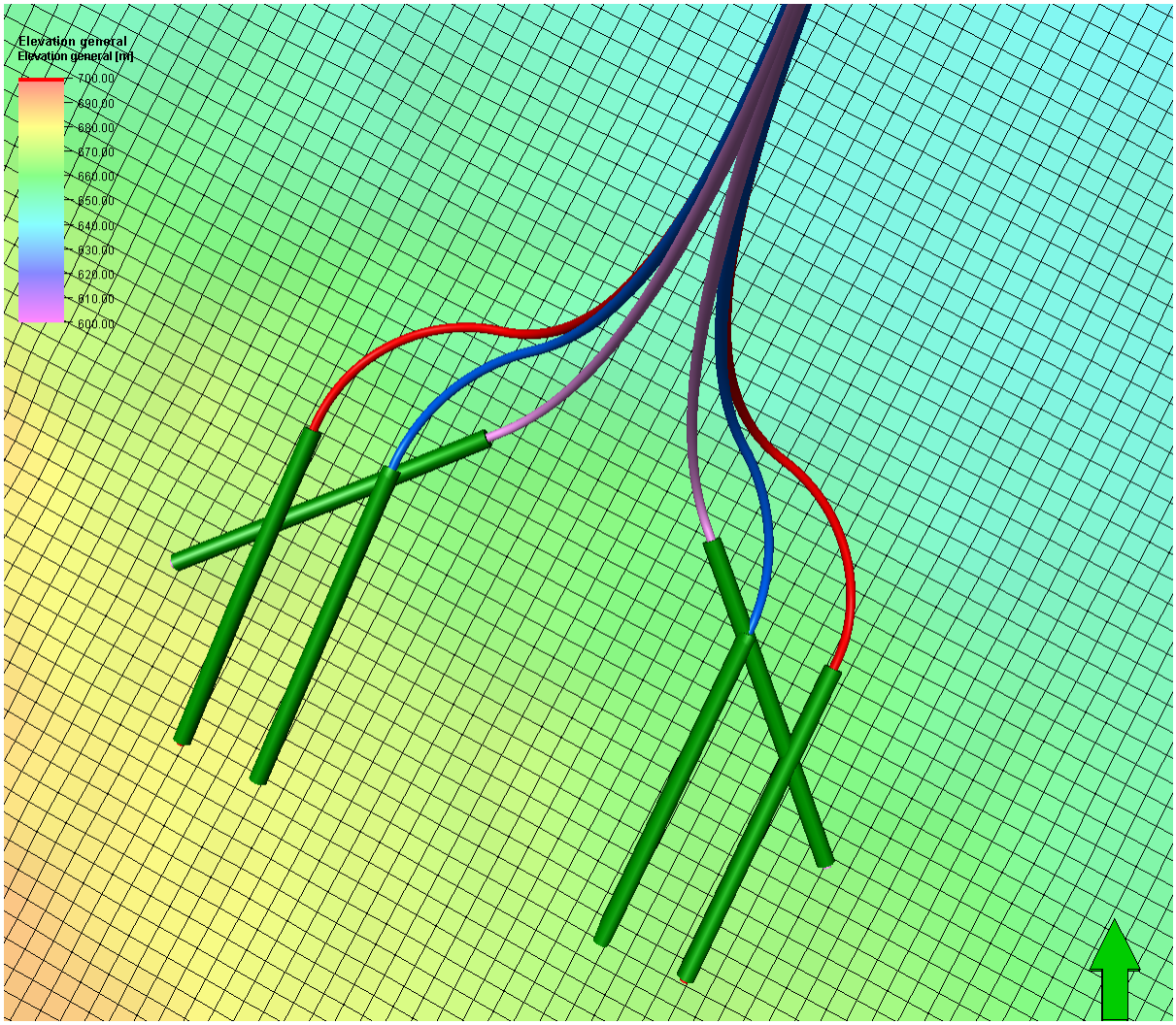

Figure 4-10 Illustration of the sub-horizontal well designs with the grid (top view). Property shown is depth. In green is the location of the inflow sections.

The results are presented in Table 4-4 to Table 4-8. The achieved rate increases with about 30% due to the change from vertical to deviated and with about 57% due to the sub-horizontal wells. The increase is relatively low because the rate is maximized on 200 m^3/hr based for this well design. The PI/II increases more, namely 79 to 118%, so a higher rate could have been achieved if the well design would be adjusted.

The differences between the three sub-horizontal well designs are small: far smaller than the difference due the uncertainty in the permeability and the details of the placement of the well. The three sub-horizontal well designs were also simulated with a simple homogeneous model and the differences in PI/II between the horizontal designs are less than 5%, with the horizontal wells at 850 m distance outperforming the other two designs. This is far smaller than range in performance due to the uncertainty in the reservoir properties and due to the uncertainty due to the details of the placement of the wells. There is some impact on the thermal breakthrough, but that is difficult to quantify, because it depends strongly on the geometry of the high permeability layers. The simple homogeneous model is not suitable for evaluating the thermal breakthrough.

In Section 4.3.2, the uncertainty range due to the vertical permeability only was quantified (Table 4-3). For deviated wells, the uncertainty due to the horizontal permeability is larger than due the vertical

permeability. The standard deviation has more than doubled. For the (sub-)horizontal wells, as expected, the uncertainty in both the vertical and horizontal permeability is approximately equally important. For the vertical wells, the standard deviation is 12% of the average, for the deviated 14% and for the horizontal wells 27% on average. The variation in performance of the (sub-)horizontal wells is larger because they produce from a more limited part of the reservoir in the vertical direction and are thus more sensitive to changes in this part. The variability in horizontal direction is much smaller than that in vertical direction in the current characterization of the uncertainty, which is implemented via the variogram. Changing these assumptions, will also change the variability of the well designs.

On average the producer performs better: ~40% better for most well designs, except for the horizontal wells with 90° angle. On average the producers should be ~50% better due to the difference in viscosity between the production and injection well. The better productivity in the 90° angle wells is probably due to a slightly better placement. For the vertical and deviated well, the difference might also be due to the trend in the permeability resulting from the presence of STR-01 (see Figure 4-7). Since the horizontal wells have the same direction, they are less likely to be affected by a trend. To remove the possible impact of the trend, a second set of simulations is done in which the trend due to STR-01 is removed. These results are presented below Table 4-8.

The focus of these simulations was on the productivity and injectivity of different well designs. However, also temperature was simulated. After 20 years, the deviated wells and the horizontal wells with 850 m distance show the largest temperature drop in the producer: ~3°C. the vertical wells have a smaller rate and smaller temperature drop. Please be reminded that the vertical wells have two well locations, which would not be feasible at this location. It should also be noted that the thermal breakthrough is overestimated because at the top no heat exchange with the overburden was simulated.

Table 4-4 For comparison with the other well designs: vertical wells with 850 m distance. Values after 20 years.

	PI (m^3/hr/bar)	II (m^3/hr/bar) @ 8°C	Rate (m^3/hr)	Prod. Temperature (°C)
Mean	11.3	8.0	120	29.6
Stdev	1.4	0.9	14	0.5
Minimum	8.4	6.0	90	28.8
Maximum	13.6	9.2	138	30.5

Table 4-5 Deviated wells. Values after 20 years.

	PI (m^3/hr/bar)	II (m^3/hr/bar) @ 8°C	Rate (m^3/hr)	Prod. Temperature (°C)
Mean (% increase to vertical)	13.7 (+21%)	9.9 (+23%)	159 (+29%)	27.6
Stdev	1.9	1.3	19	0.8
Minimum	9.2	7.8	135	25.8
Maximum	16.4	12.6	200	28.6

Table 4-6 Horizontal wells at 90° angle . Values after 20 years. Max rate = 200 m^3/hr.

	PI (m^3/hr/bar)	II (m^3/hr/bar) @ 8°C	Rate (m^3/hr)	Prod. Temperature (°C)
Mean	24.6 (+118%)	14.3 (+79%)	188 (+56%)	28.6
Stdev	5.8	4.2	18	1.1

Minimum	17.1	8.8	140	26.1
Maximum	37.1	24.0	200	30.3

Table 4-7 Horizontal wells , parallel, distance 850 m. Values after 20 years. Max rate = 200 m^3/hr.

	PI (m^3/hr/bar)	II (m^3/hr/bar) @ 8°C	Rate (m3/hr)	Prod. Temperature (°C)
Mean	21.1 (+87%)	15.7 (+96%)	192 (+60%)	27.5
Stdev	6.2	3.9	15	0.7
Minimum	14.3	9.8	151	26.6
Maximum	34.4	21.9	200	29.5

Table 4-8 Horizontal wells, parallel, distance 1250 m. Values after 20 years. Max rate = 200 m^3/hr

	PI (m^3/hr/bar)	II (m^3/hr/bar) @ 8°C	Rate (m^3/hr)	Prod. Temperature (°C)
Mean	21.3 (+89%)	14.7 (+84%)	190 (+58%)	30.7
Stdev	7.1	3.5	20	0.2
Minimum	13.8	8.6	128	30.3
Maximum	36.8	21.3	200	31.1

Permeability without STR-01

Because of the possible impact of the trend in the permeability due to the high-permeability, but uncertain well STR-01, a second set of runs was done. The results of this run are more generic because they don't contain the trend in permeability resulting from STR-01. Figure 4-11 shows the net transmissivity without the well STR-01 calculated based on the kriged permeability. In Table 4-9 to Table 4-13 the result for all wells designs is presented. The average ratio PI/II for the vertical and deviated wells is now ~1.5 which is identical to the ratio in viscosity.

Because the best producing well has been removed, overall the rates are decreasing. The decrease ranges from ~20% for the vertical and deviated wells to ~35% for the sub-horizontal wells. For the vertical and deviated doublets, the injectors (which are facing south) decrease more than the producers. The horizontal wells decrease more than the deviated and vertical wells. This is probably because they mainly produce from the ~20 m of the reservoir that has the best performance. This is the part that is affected most by the reduction in permeability from removing well STR-01. From the well logs and simulations, it appears that in the Brussels Sand a few metres with high porosity and not many cemented layers determines whether the overall productivity is only moderate (25-30 Dm or less) or good. Possibly the fact that the horizontal wells were more oriented towards STR-01 could also have impacted the difference, however, the vertical wells also were located quite far south, but had the same decrease as the deviated wells (see Figure 4-9 for the position of wells).

The rate achieved by the sub-horizontal doublets is around 150 m^3/hr on average for the given pressure constraints after 20 years of injection, assuming no decline in productivity or injectivity of the wells except the impact of the cold water viscosity. Compared to the sub-horizontal wells at Zevenbergen, which have an inflow length of around 600 m (Buik and Bakema, 2019), this productivity is a bit poorer. The initial runs, which include the influence of well STR-01, had an estimated productivity higher than at Zevenbergen.

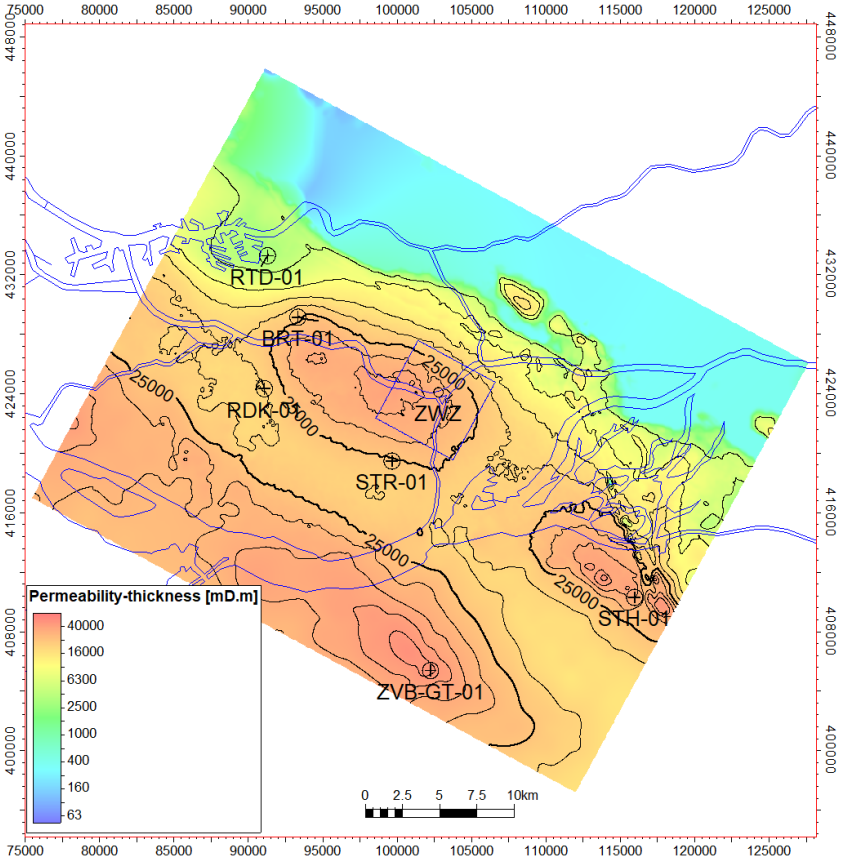

Figure 4-11 Net transmissivity (permeability x net thickness) (KH in mDm) of the regional model including the wells with permeability logs with permeability kriged as a linear property **without** STR-01. Rectangle indicates the model area. Blue lines shows the waterways.

Table 4-9 For comparison with the other well designs: vertical wells with 850 m distance. Values after 20 years. Sensitivity without STR-01.

	PI (m^3/hr/bar)	II (m^3/hr/bar) @ 8°C	Rate (m^3/hr)	Prod. Temperature (°C)
Mean	9.3	6.2	93	30.7
Stdev	1.5	0.8	11	0.3
Minimum	5.9	4.5	67	30.0
Maximum	11.7	7.4	111	31.0

Table 4-10 Deviated wells. Values after 20 years. Sensitivity without STR-01.

	PI (m^3/hr/bar)	II (m^3/hr/bar) @ 8°C	Rate (m^3/hr)	Prod. Temperature (°C)
Mean (% increase to vertical)	11.6 (+25%)	7.5 (+22%)	120 (+29%)	29.3
Stdev	2.2	1.3	21	0.8
Minimum	6.1	5.0	80	27.7
Maximum	14.5	9.8	157	30.5

Table 4-11 Horizontal, 90 angle wells and screen length of 750 m. Values after 20 years.

	PI (m^3/hr/bar)	II (m^3/hr/bar) @ 8°C	Rate (m^3/hr)	Prod. Temperature (°C)

Mean (% increase to vertical)	16.5 (+77%)	10.0 (+63%)	152 (+64%)	29.0
Stdev	4.3	3.1	36	1.7
Minimum	11.8	6.4	101	25.2
Maximum	26.5	16.3	200	31.1

Table 4-12 Horizontal, parallel wells with a distance of 850 m and screen length of 750 m. Values after 20 years.

	PI (m^3/hr/bar)	II (m^3/hr/bar) @ 8°C	Rate (m^3/hr)	Prod. Temperature (°C)
Mean (% increase to vertical)	13.6 (+46%)	10.0 (+62%)	146 (+57%)	29.1
Stdev	4.1	3.2	35	1.1
Minimum	9.3	5.7	87	27.3
Maximum	24.1	17.3	200	30.8

Table 4-13 Horizontal, parallel wells with a distance of 1250 m and screen length of 750 m. Values after 20 years, 13 realizations (1 run failed)

	PI (m^3/hr/bar)	II (m^3/hr/bar) @ 8°C	Rate (m^3/hr)	Prod. Temperature (°C)
Mean (% increase to vertical)	14.0 (+51%)	9.4 (+52%)	139 (+50%)	31.0
Stdev	5.2	2.8	39	0.1
Minimum	9.3	5.3	80	30.8
Maximum	25.5	14.8	200	31.2

4.4 Discussion and conclusions

The productivity/injectivity of different well designs was estimated using a local reservoir model of the Zwijndrecht area. The focus is on how much the formation can deliver for different well designs and pressure drop in the well and any limitations due to possible production of sand or fines have not been included.

Although the uncertainty in the depth and thickness is low and the expected lateral variability is modest, the uncertainty in the expected productivity/injectivity is still considerable. If the petrophysical interpretation of the well STR-01 is correct and this well is a good predictor of the permeability at the location Zwijndrecht, then the productivity of the area is quite good: the deviated wells have an average production rate of around 160 m^3/hr, with a minimum value of around 125 m^3/hr from 14 realizations. Productivity is around 14 m^3/hr/bar. The lifetime of the doublet with deviated wells would be limited though, because of the limited well distance (750 m). After 20 years, already 3 degrees cooling was simulated on average. In reality this is likely to be a bit smaller, because cooling of the overburden was not included. For the sub-horizontal wells, most realizations were able to achieve the maximum rate of 200 m^3/hr for the maximum injection overpressure of 16 bar. The productivity of the horizontal wells (with 750 m inflow length) is ~21 m^3/h/bar (at 30°C) . This includes only the pressure drop in the reservoir though and not the pressure drop inside the well. The differences between the various horizontal designs were not large: the variability due to the uncertainty in the permeability was much larger.

If the well STR-01 is assumed to be overly optimistic and is removed from the simulation, considerably lower productivity is achieved. For the vertical and deviated wells, the productivity decreases ~20%, for the sub-horizontal wells ~35%. The relatively high decrease for the sub-horizontal wells, is probably because mainly the high-permeability zone is reduced in permeability. The average achieved rate for the horizontal well designs decreased to ~145 m^3/hr. The range and standard deviation all decrease with similar percentages. Compared to the productivity at the doublet Zevenbergen, with well STR-01 the productivity is better, without this well the productivity is poorer.

The increase in productivity/injectivity due to the increase in inflow length is relatively limited for the Brussels Sand, because the vertical permeability is small, which is caused by the calcite cemented streaks. The uncertainty on their impact is large however and may not be fully covered by the sensitivity runs done here, since only the lateral extent was varied. For example the permeability of the cemented layers was assumed to be 0.01 mD. And although the selected values and approach were tested for the Zevenbergen doublet and gave good results, they still carry uncertainty. Assuming higher permeability for the cemented layers, will lead to better performance of the horizontal wells. In general, the choices made to characterize the heterogeneity of the permeability will drive the average and variability in the results of the different well designs.

The results in Section 4.2 show that the coarser model with grid layer thickness of around 10 m cannot properly reproduce the behaviour of the fine scale model for all well configurations, probably because of the high vertical variability. The results of the fine scale model are expected to be more accurate. Therefore it is recommended not to use a relatively coarse model for the Brussels Sand, but have a maximum grid block thickness of a few metres for deviated or horizontal wells.

5 Summary and conclusions

A regional geological model was created around the area of Zwijndrecht, which was selected as pilot region in the WarmingUp project Theme 4A on geothermal energy. Near Zwijndrecht, geothermal energy from the Brussels Sand Mb could potentially be a heat source for an urban heat network. The geological model covers an area of 44 by 33 kilometres. For the interpretation of the top and bottom of the Brussels Sand good quality 3D seismic was available, leading to little uncertainty in the depth and thickness of the reservoir. No faults were visible in the seismic data and lateral variability appears to be limited: the defined subunits could be correlated well between wells.

Only a few wells with good quality logs are available in the area, making the property estimation uncertain. In general the best reservoir properties are found in the uppermost unit (S3) and most flow (up to 90%) is expected to come from this unit. The transmissivity KH (product of thickness and permeability) of the 6 wells ranges from 5 Dm for Rotterdam-01 (RTD-01) to 64 Dm for Strijen-01 (STR-01). Well RTD-01 has lower permeability, because it is relatively far to the north and misses part of the best performing unit S3. The range in KH for the other wells is 22 Dm (well Reedijk-01 (RDK-01)) to 64 Dm. No trend could be discerned in the permeability and the variability is probably best interpreted as uncertainty in the petrophysical analysis in particular for the wells with poor log data (STR-01). Analysis of well Strijen West-01 and three wells at Numansdorp might reduce the uncertainty, but this is beyond the scope of this project. The estimated transmissivity for the pilot location Zwijndrecht-Zuid is estimated to be 38 Dm, which is close to the average.

Throughout the Brussels Sand, thin, calcite-cemented layers occur which have low porosity and permeability. The average interval thickness between streaks is about 5 m. The lateral extent of these laterals is uncertain. If they are laterally continuous, they form very effective barriers to vertical flow. But even if the lateral extent is more limited, effective vertical connectivity will be affected.

Productivity/injectivity estimates were made for different well orientations (vertical, deviated and sub-horizontal) for an ensemble of 14 realizations taking into account the variability in the horizontal and vertical permeability. For the vertical permeability, the lateral extent and presence of the calcite-cemented layers were varied. The goal is not an optimized well design for the location of Zwijndrecht, but understanding the well performance for different well orientations. The increase in the average productivity for the sub-horizontal wells with an inflow length of 750 m ranged from 50 to 100% compared to vertical wells depending on the permeability distribution and the position of the well in the reservoir. The range in results for the sub-horizontal wells was larger than that of the vertical or deviated wells. The productivity of the deviated wells (65° inclination) increased 20 to 25% compared to the vertical wells. These results were less sensitive to the details of the permeability distribution.

Upscaled, effective properties for coarser models were difficult to derive due to the high vertical variability. Also, a few thin, high permeability zones contribute a considerable part of the flow (30 to 50%). No single set of upscaled properties could be derived that performed well for all well orientations.

References

Batzle, M., & Z. Wang, 1992. Seismic properties of pore fluids. Geophysics, Vol. 57, 1396-1408.

Blinovs, A. and G. van Og, 2022. Feasibility study. Shallow geothermal well desings. WEP

Buik, N. and Bakema, G., 2019. Geothermie putten in ondiepe fijnzandige formaties. Literatuuronderzoek en ervaringen uit de olie/gas-, drinkwater- en WKO-sector. 65163/RDx/20191218. IF Technology.

Clauser, C. 2011. Thermal Storage and Transport Properties of Rocks, II: Thermal Conductivity and Diffusivity. In: H. Gupta (ed) Encyclopedia of Solid Earth Geophysics. Springer.

Eppelbaum, L. et al., 2014. Applied Geothermics, Lecture Notes in Earth System Sciences, DOI: 10.1007/978-3-642-34023-9_2. Springer-Verlag Berlin Heidelberg.

Geel, C.R. & J. Foeken, 2021. Formation evaluation of the Brussels Sand Member in The Netherlands. WarmingUp report, 47 p.

Geobrothers BV and Visser & Smit Hanab BV, 2020. Aanvraag Instemming Winningsplan Aardwarmte, Zevenbergen II, versie 1.2, 7 April 2020. available via nlog.nl: https://www.nlog.nl/sites/default/files/2021-03/200407_verzoek_tot_instemming_wp_zevenbergen_publiek_gelakt.pdf

Grunberg, L. 1970. Properties of sea water concentrates. 3rd Int. Symp on Fresh Water from the Sea. Vol. 1, p 31-39.

Haan, H. de, J. ten Veen, A. Houben, A. Kruisselbrink, 2020. Mapping of the Brussels Sand Member in The Netherlands. WarmingUp report. https://www.warmingup.info/documenten/report-mapping-brussels-sand_final_v3_22122020.pdf.

Robertson, 1988. Thermal properties of rocks. USGS Open-File Report 88-441.

Vrijlandt, M.A.W., E.L.M. Struijk, L.G. Brunner, J.G. Veldkamp, N. Witmans, D. Maljers, J.D. van Wees. 2019. ThermoGIS update: a renewed view on geothermal potential in the Netherlands. EGC, The Hague, June 2019.

Acknowledgements

Visser & Smit Hanab are gratefully acknowledged for making the data from ZVB-GT-01 available. Henk van Lochem (EBN) and Hilde Coppes (Shell Geothermal) are gratefully acknowledged for reviewing this report.

Appendices

Appendix A: Details of the Petrel model building

Figure A-0-1 – Petrel workflow of the construction of the reservoir model

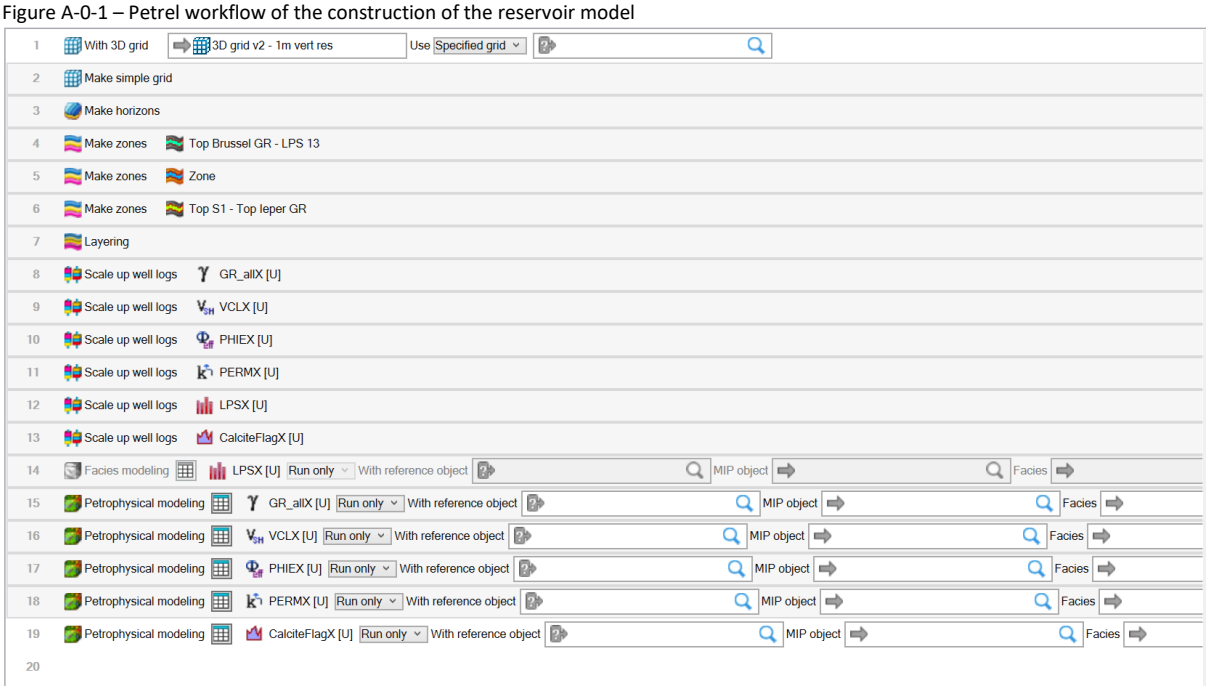

Figure A-0-2 – The “Make Horizons” process in Petrel

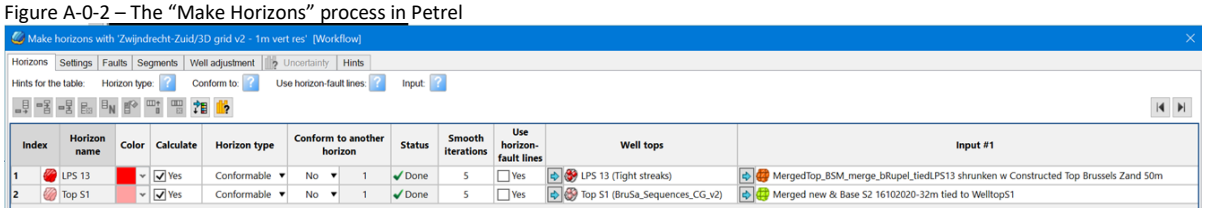

Figure A-0-3 - The “Make Zones” process in Petrel

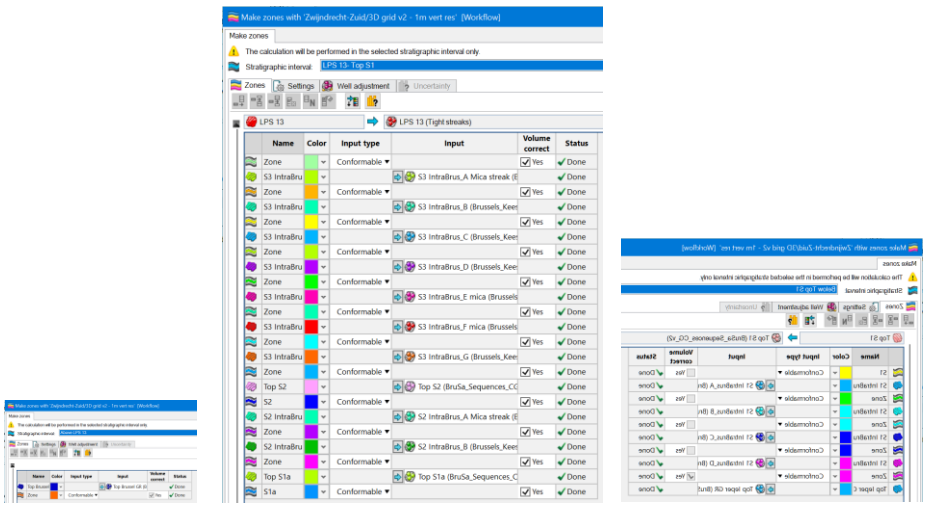

Figure A-0-4 - The “Make Layers” process in Petrel

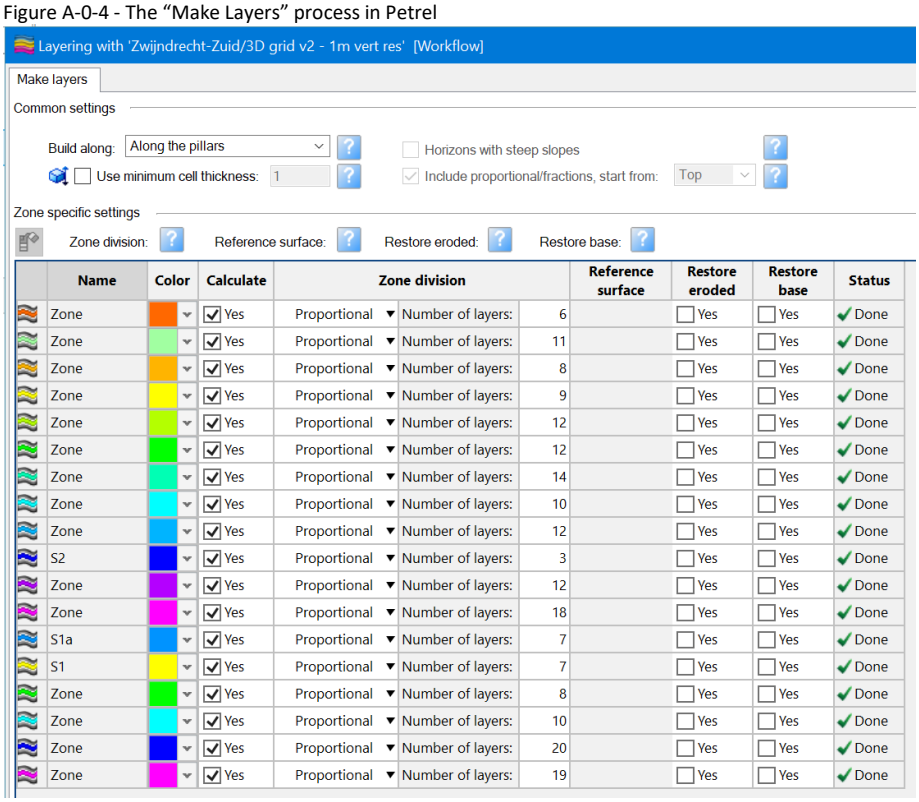

Name	Color	Calculate	Zone division			Reference surface	Restore eroded	Restore base	Status
Zone		Yes	Proportional	Number of layers:	6		Yes	Yes	Done
Zone		Yes	Proportional	Number of layers:	11		Yes	Yes	Done
Zone		Yes	Proportional	Number of layers:	8		Yes	Yes	Done
Zone		Yes	Proportional	Number of layers:	9		Yes	Yes	Done
Zone		Yes	Proportional	Number of layers:	12		Yes	Yes	Done
Zone		Yes	Proportional	Number of layers:	12		Yes	Yes	Done
Zone		Yes	Proportional	Number of layers:	14		Yes	Yes	Done
Zone		Yes	Proportional	Number of layers:	10		Yes	Yes	Done
Zone		Yes	Proportional	Number of layers:	12		Yes	Yes	Done
S2		Yes	Proportional	Number of layers:	3		Yes	Yes	Done
Zone		Yes	Proportional	Number of layers:	12		Yes	Yes	Done
Zone		Yes	Proportional	Number of layers:	18		Yes	Yes	Done
S1a		Yes	Proportional	Number of layers:	7		Yes	Yes	Done
S1		Yes	Proportional	Number of layers:	7		Yes	Yes	Done
Zone		Yes	Proportional	Number of layers:	8		Yes	Yes	Done
Zone		Yes	Proportional	Number of layers:	10		Yes	Yes	Done
Zone		Yes	Proportional	Number of layers:	20		Yes	Yes	Done
Zone		Yes	Proportional	Number of layers:	19		Yes	Yes	Done

Appendix B: Well panels

Figure B-1 - SW-NE Panel, flattened on depth

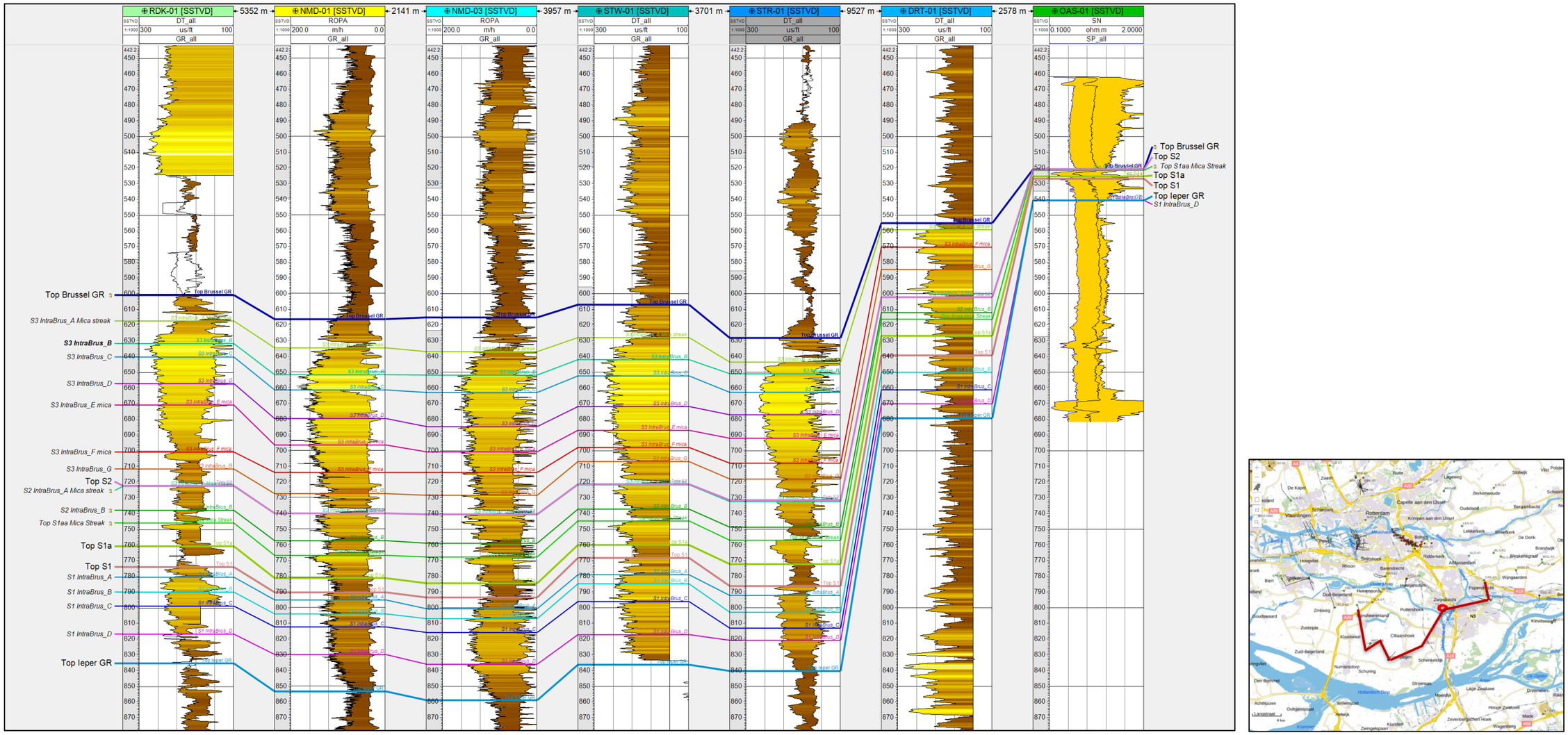

Figure B-2 - SW-NE Panel, flattened on Top S1

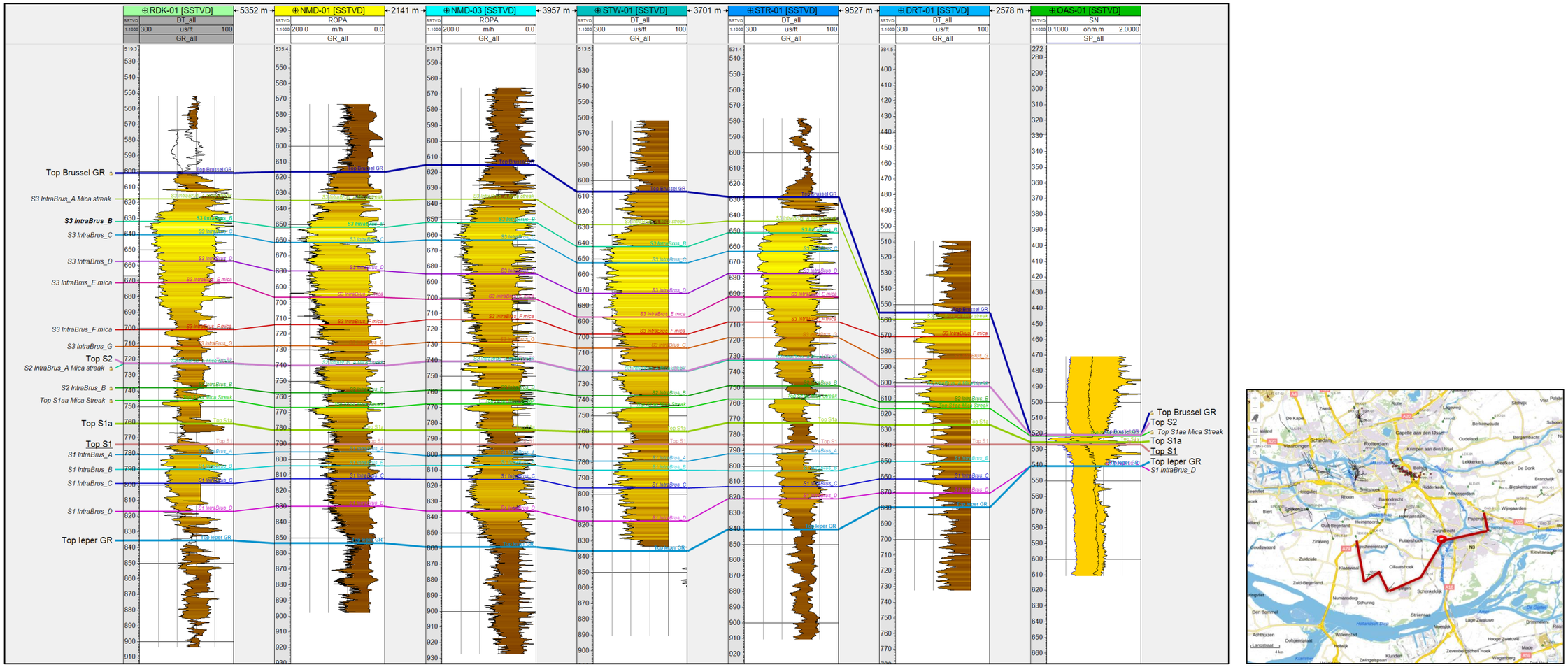

Figure B-3 - N-S Panel, flattened on depth

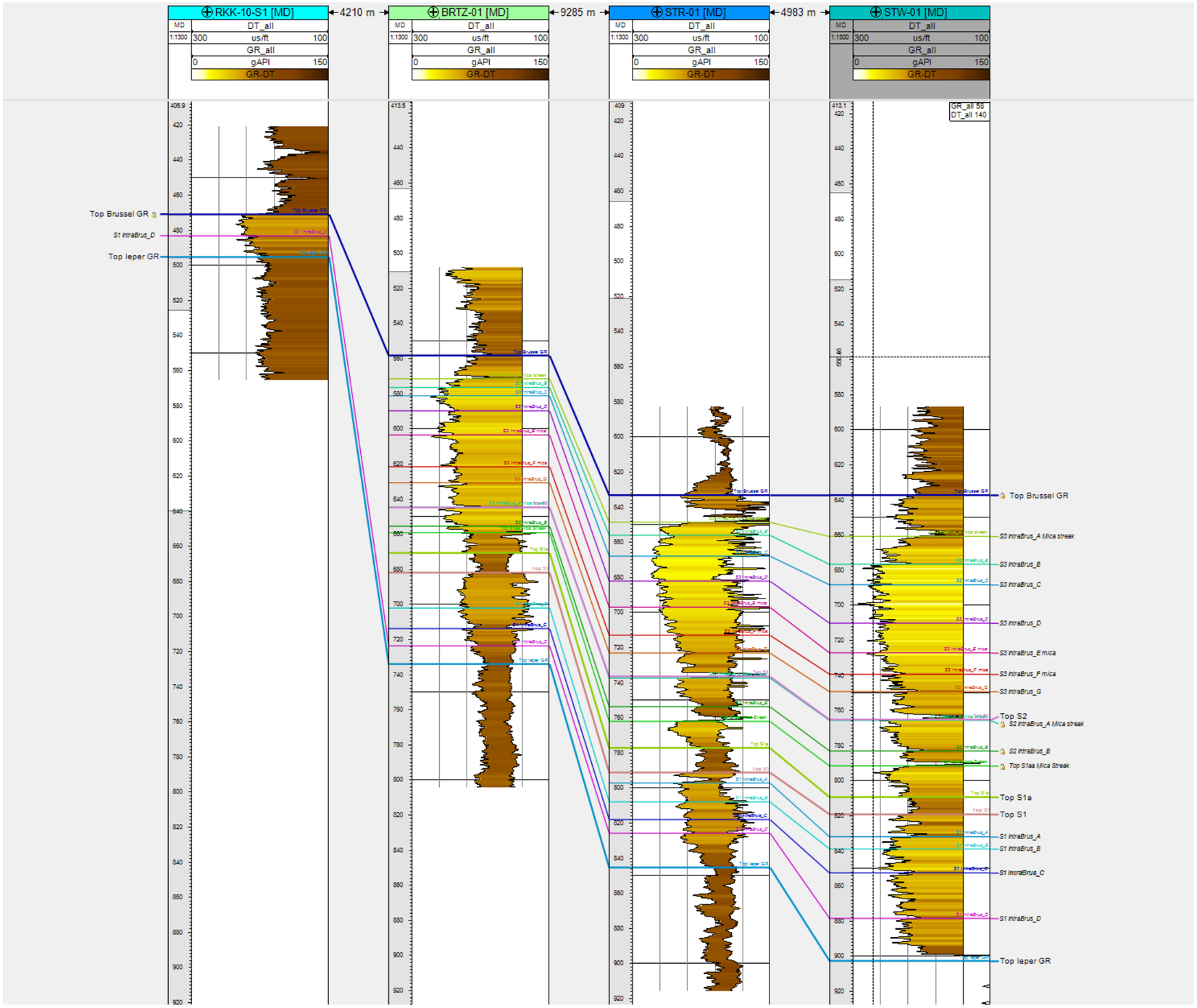

Figure B-4 -N-S Panel, flattened on Top S1

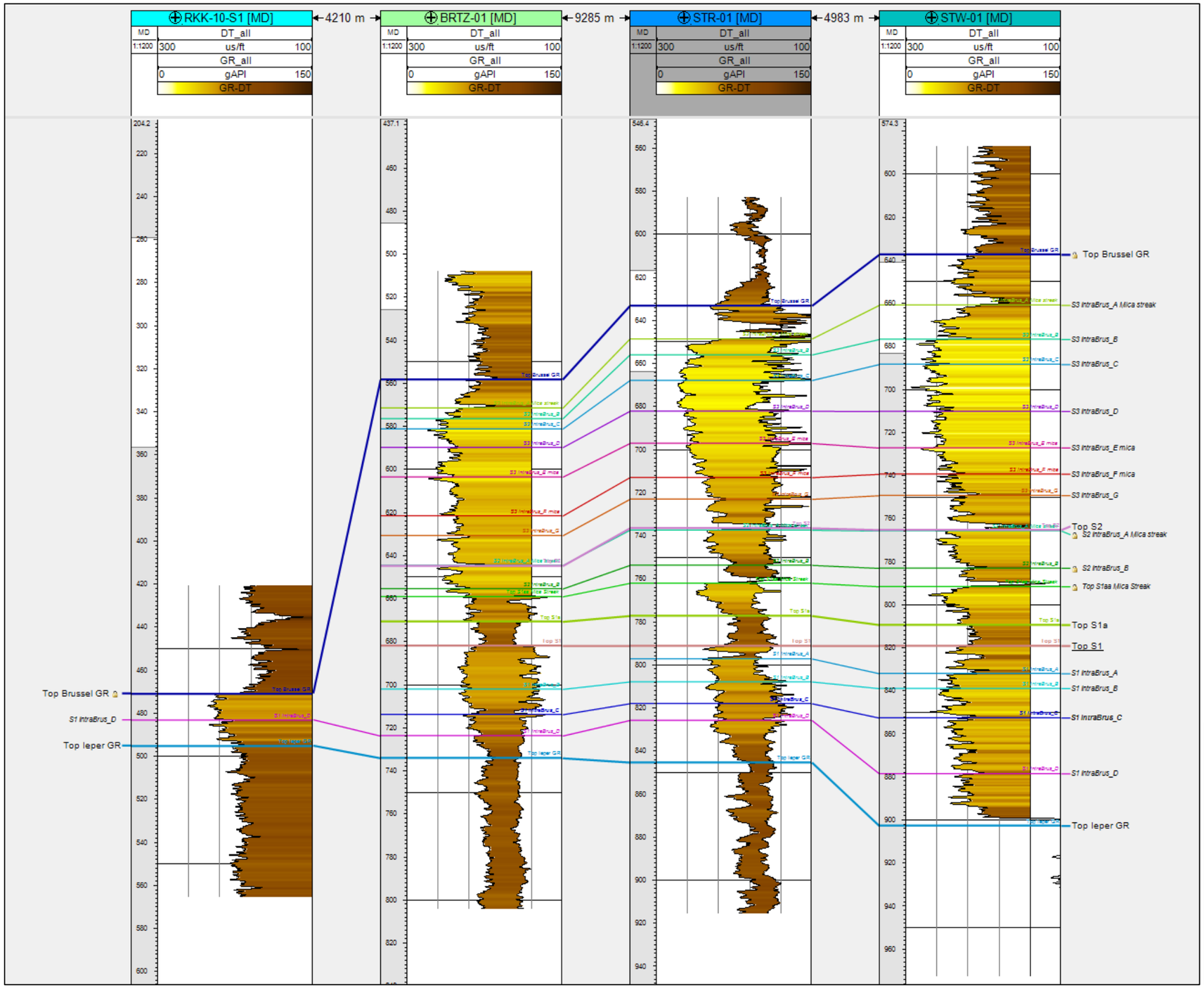

Figure B-5 NW-SE Panel, flattened on depth

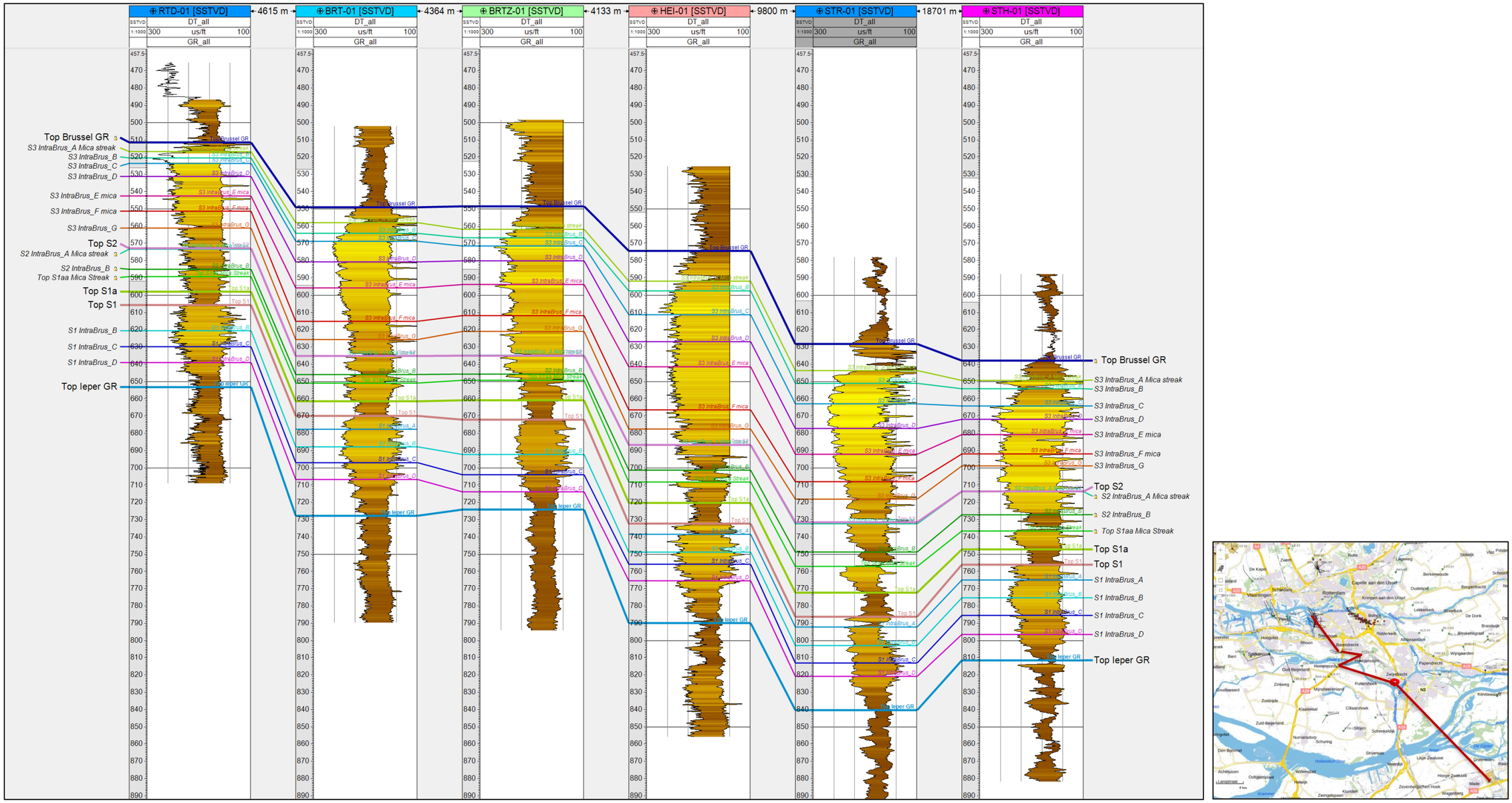

Figure B-6 NW-SE Panel, flattened on Top S1

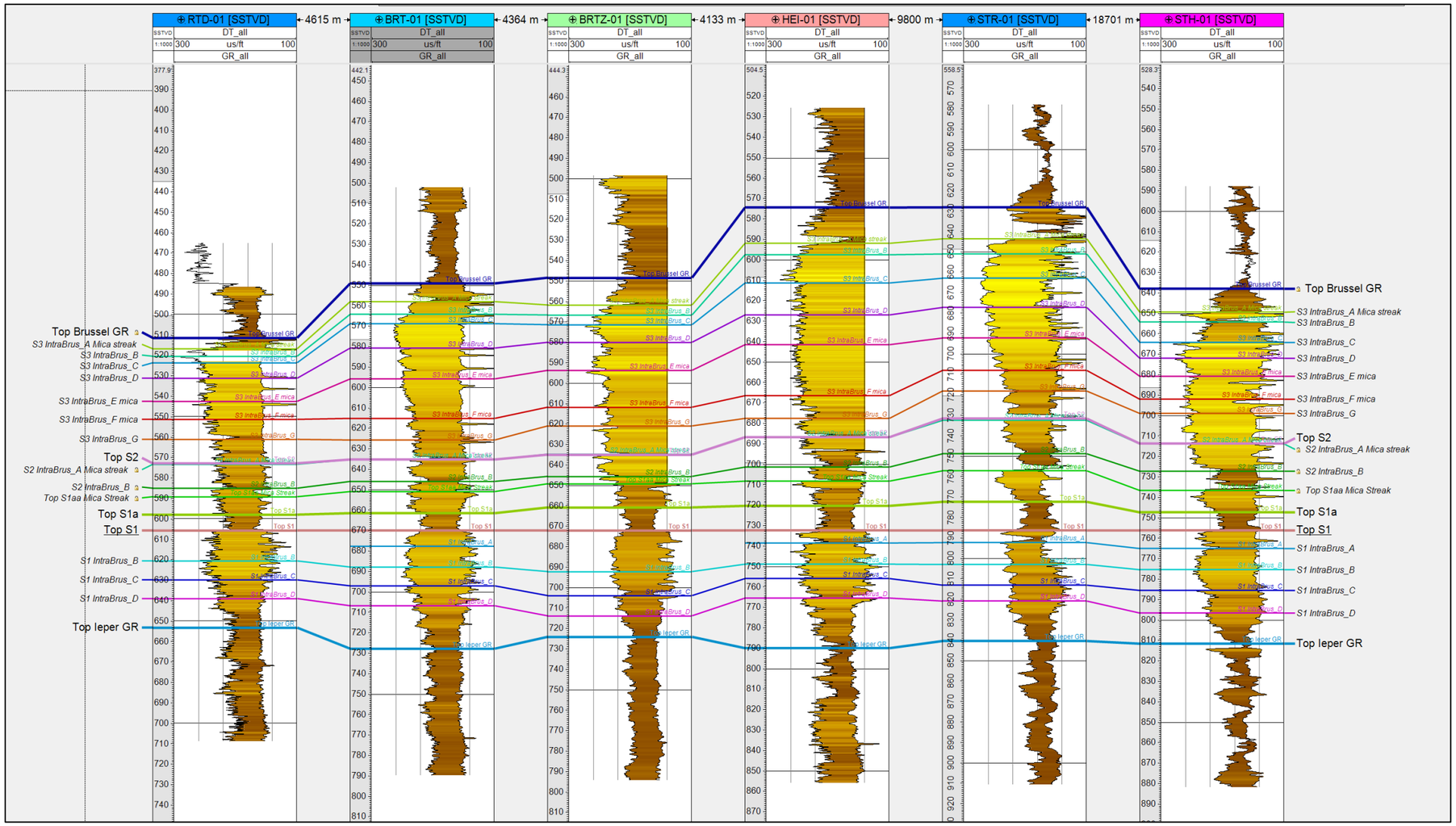

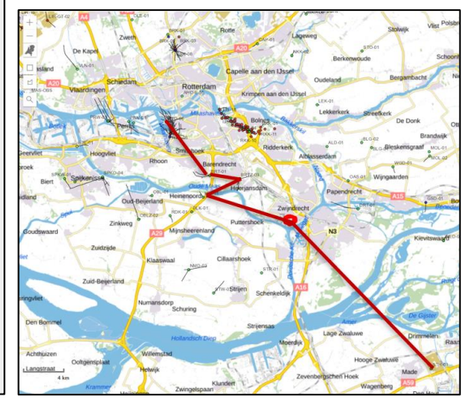

WARMING UP

Innovatief Duurzaam Warmtecollectief

Adres
Princetonlaan 6
3584 CB Utrecht

Postadres
Postbus 80015
3508 TA Utrecht

Telefoon
088 866 42 56

E-mail
contact@warmingup.info

Website
www.warmingup.info

Versie 1.0 25 mei 2022